


Spring 1-1-2018

Energy Management of Microbial Fuel Cells for High Efficiency Wastewater Treatment and Electricity Generation

Fernanda Leite Lobo

University of Colorado at Boulder, lobo.nanda@gmail.com

Follow this and additional works at: https://scholar.colorado.edu/cven_gradetds

 Part of the [Environmental Engineering Commons](#), [Power and Energy Commons](#), and the [Sustainability Commons](#)

Recommended Citation

Leite Lobo, Fernanda, "Energy Management of Microbial Fuel Cells for High Efficiency Wastewater Treatment and Electricity Generation" (2018). *Civil Engineering Graduate Theses & Dissertations*. 372.

https://scholar.colorado.edu/cven_gradetds/372

This Dissertation is brought to you for free and open access by Civil, Environmental, and Architectural Engineering at CU Scholar. It has been accepted for inclusion in Civil Engineering Graduate Theses & Dissertations by an authorized administrator of CU Scholar. For more information, please contact cuscholaradmin@colorado.edu.

ENERGY MANAGEMENT OF MICROBIAL FUEL CELLS FOR HIGH EFFICIENCY
WASTEWATER TREATMENT AND ELECTRICITY GENERATION

by

FERNANDA LEITE LOBO

B.S., Universidade do Estado do Amazonas, 2012

B.S., Universidade Federal do Amazonas, 2013

M.S., University of Colorado Boulder, 2017

A thesis submitted to the
Faculty of the Graduate School of the
University of Colorado in partial fulfillment
of the requirement for the degree of
Doctor of Philosophy
Department of Civil, Environmental, and Architectural Engineering
2018

This thesis entitled:
Energy Management of Microbial Fuel Cells for High Efficiency Wastewater Treatment and
Electricity Generation
written by Fernanda Leite Lobo
has been approved for the Department of Civil, Environmental, and Architectural Engineering

Jae-Do Park, Ph.D.

JoAnn Silverstein, Ph.D.

Mark Hernandez, Ph.D.

Rita Klees, Ph.D.

Zhiyong (Jason) Ren, Ph.D.

Date _____

The final copy of this thesis has been examined by the signatories, and we find that both the content and the form meet acceptable presentation standards of scholarly work in the above mentioned discipline.

Leite Lobo, Fernanda (Ph.D., Environmental Engineering)
Energy Management of Microbial Fuel Cells for High Efficiency Wastewater Treatment and
Electricity Generation
Thesis directed by Associate Professor Zhiyong Jason Ren

Abstract

In order to develop communities in a sustainable manner it is necessary to think about how to provide basic and affordable services including sanitation and electricity. Wastewater has energy embedded in the form biodegradable organic matter, but most of the conventional systems use external energy to treat the wastewater instead of harvest its energy. Microbial fuel cells (MFCs) are unique systems that are capable of converting chemical energy of biodegradable substrates embedded in the waste materials into renewable electricity. Even though the technology showed great progress, the direct electrical energy output from MFC reactors is still very low and the electrical interface with microbial activities is not well understood.

In this work, I investigated the development and deployment of energy management systems to improve energy harvesting of microbial fuel cells during wastewater treatment. The specific studies presented in this dissertation consist of the first AC power generation from microbial fuel cells, the development of harvesting strategies to maximize microbial fuel cell performance in different conditions, and the understanding of microbial community and activities under different harvesting conditions. To enable the application of MFC technology for treating actual wastewaters and providing net electricity output, I also investigated the integration of AC-powered electrocoagulation with granular biochar to treat hydraulic fracturing water, and I used the electricity generated by MFCs to directly power electrocoagulation for oily

wastewater treatment, achieving energy positive wastewater treatment for distributed applications. System scale up and integration will be next steps for technology development.

Acknowledgements

I want to show my gratitude to everyone that helped me along the way.

I would like to thank my advisor Dr. Ren for his guidance and encouragement, I feel very lucky to have had you as my advisor.

Jenny, Rebekah, Heming, Casey, Alex, Tyler, Hadi, Lu, Dianxun and everyone that worked with me in Dr. Ren's group, thank you for all your research and life advices, I am glad that I got to meet all of you.

To all the committee members, Dr. JoAnn Silverstein, Dr. Jae-Do Park, Dr. Rita Klees and Dr. Mark Hernandez, thank you for all your feedback and advice.

This journey has been one of the richest experiences of my life and I am so grateful to have had my husband Ricardo by my side every step of the way, you gave me love and support through the hardest times. I can't find the words to tell you how incredible you are. I could not have done it without. Thank you!

Mother, you are the one that made this all possible. Thank you for all the sacrifices you had to do in order to give me the best opportunities in life. I am really blessed to have you! Lipe, you are as responsible as mom for all of this. Thank you for always have my back big brother.

I also would like to thank my country, Brazil, CAPES, LASPAU, Office of Naval Research, and the program Science without Borders for granting me this opportunity.

CONTENTS

CHAPTER 1	1
INTRODUCTION	1
1.1 Rational	1
1.2 Formal Hypothesis	4
1.3 Dissertation Guideline	4
CHAPTER 2	6
AC POWER GENERATION FROM MICROBIAL FUEL CELLS	6
2.1 Introduction	6
2.2 Materials and Methods	7
2.2.1 MFC construction and operation	7
2.2.2 DC to AC circuit design and control	8
2.2.3 Analyses	9
2.3. Results and discussion	10
2.3.1 Operation of the DC-AC Converter under Different Frequencies	10
2.3.2 AC Power Output without Using Energy Storage Layer (Capacitors).....	12
2.3.3 AC Power Output with Energy Storage Layer (Capacitors)	17
2.3.4 AC Power Quality from MFCs.....	21
2.3.5 The efficiency of the DC-AC converter	24
2.3.6 Discussion.....	25
CHAPTER 3	27
ENERGY HARVESTING INFLUENCES ELECTROCHEMICAL PERFORMANCE OF MICROBIAL FUEL CELLS	27
3.1 Introduction	27
3.2 Materials and Methods	29
3.2.1 MFC construction and operations in 2 stages.....	29
3.2.2 Analyses	31
3.3 Results e Discussion	32
3.3.1 Variations of MFC voltage, current, electrode potentials in different conditions.....	32
3.3.2 Variations in substrate utilization and energy recovery	37
3.3.3 Redox potential shifts in cyclic voltammograms	40
3.3.4 Active harvesting indeed boosted electron transfer and system performance.....	42
CHAPTER 4	44
ACTIVE HARVESTING LEADS TO DISTINCT MICROBIAL COMMUNITY STRUCTURE IN MICROBIAL ELECTROCHEMICAL CELLS	44
4.1 Introduction	44
4.2 Materials and Methods	46
4.2.1 Reactor construction and operation	46
4.2.2 Analyses	49
4.2.3 Bacterial Community Structure Analyses	50
4.3.1 Energy harvesting significantly boosted MFC performance in current and power production	50
4.3.2 Electrochemical responses were different under various energy harvesting scenarios.....	52
4.3.3 Distinct microbial community structures under different conditions.....	54

4.3.4 Statistical analysis shows the correlation matrix between electrochemical activities and microbial community diversity.....	61
CHAPTER 5.....	64
LOW-ENERGY HYDRAULIC FRACTURING WASTEWATER TREATMENT VIA AC POWERED ELECTROCOAGULATION WITH BIOCHAR	64
5.1 Introduction.....	64
5.2 Materials and Methods.....	65
5.3 Results and Discussion.....	67
5.3.1 Produced water treatment performance under different conditions	67
5.3.2 Energy benefits of the AC-EC-Biochar combination.....	72
5.3.3 Future work is needed for optimization and integration	76
CHAPTER 6.....	77
FUTURE RESEARCH.....	77
6.1 Energy Harvesting on a Pilot Scale MFC	77
6.2 Remote Bilge Water Treatment by Electrocoagulation	77
6.3 Preliminary results on MFC energy harvesting and power supply to electrocoagulation for bilge water treatment.....	78
BIBLIOGRAPHY	88
APPENDIX A	96

TABLES

Table 1 Summary of key results obtained in this study.	43
Table 2 Correlation Matrix (Coefficient and Significance Level) between the maximum current, electroactive bacterial activity, anode potential, midpoint potential and anode sample biodiversity (Shannon index H') parameters ^a	62
Table 3 Energy requirement for suspended solids (SS) removal	75

FIGURES

Figure 1 MFC schematic.....	3
Figure 2 (A) Circuit diagram of the DC-AC converter system for MFCs; (B) equivalent circuit diagram when MOSFET M1 is ON and MOSFET M2 is OFF to output the positive part of AC; (C) equivalent circuit diagram when MOSFET M1 is OFF and MOSFET M2 is ON to output the negative part of AC.....	9
Figure 3 Control signals at 1Hz (A), 10Hz (B) and 60Hz (C). The blue curve is the control signal for MOSFET M1 and the magenta curve is the control signal for MOSFET M2.....	12
Figure 4 Input and output voltages without using energy storage layer (capacitors) in the circuit. The DC-AC converter was powered by two MFCs at 1Hz (A), 10Hz (B) and 60 Hz (C) or four MFCs (2 groups of 2 MFCs in series) at 1Hz (D), 10Hz (E) and 60 Hz (F). Blue waves: MFC1; magenta waves: MFC2; green waves: AC output.....	14
Figure 5 Polarization curves of MFC1 and MFC2 without capacitors in the circuit.....	15
Figure 6 Electrode potential changes of MFC1 (A) and MFC2 (B) at frequencies of 1Hz, 10Hz and 60Hz without using capacitors in the circuit.....	17
Figure 7 Input and output voltages when using energy storage layer (capacitors) in the circuit. The DC-AC converter was powered by two MFCs at 1Hz (A), 10Hz (B) and 60 Hz (C) or four MFCs (2 groups of 2 MFCs) in series at 1Hz (D), 10Hz (E) and 60 Hz (F). Blue waves: MFC1; magenta waves: MFC2; green waves: AC output.....	20
Figure 8 Output voltages and the Fast Fourier Transform (FFT) of the output voltages at 60Hz when the DC-AC converter was powered by two MFCs (A) and four MFCs (2 groups of 2 MFCs in series) (B).....	23

Figure 9 Efficiency of the DC-AC converter powered by two or four MFCs (2 groups of 2 MFCs in series) at 1 Hz, 10 Hz and 60 Hz.	25
Figure 10 The power density curve obtained in an MFC operated under a 1000 Ω external resistance. This curve shows the typical Stage I operation and was used to determine different operational points (MPP, MCP, MVP).	30
Figure 11 Time-course profiles of MFC voltage (blue), MFC current (green), anode potential (red) and cathode potential (purple) profiles for (A) MPP-H, (B) MPP-R, (C) MCP-H, (D) MCP-R, and (E) MVP-R.	33
Figure 12 The harvesting circuit controlled MFC voltages for (A) MPP-H and (B) MCP-H.	34
Figure 13 (A) COD removal, (B) Coulombic Efficiency, and (C) Power Production from reactors operated in different conditions. Different durations of batch cycles were used and indicated in the graph to reflect the conversion rate differences among reactors.	37
Figure 14 Cyclic voltammetry profiles of (A) MPP-H, (B), MPP-R, (C) MCP-H, (D) MCP-R, (E) MVP-R in different stages and operational points.	39
Figure 15 Power density profiles obtained by linear sweep voltammetry on day 1, 10, 30, 40, 70, 80 and 90 of reactor running at (A) high current using resistor (CR); (B) high current using energy harvesting circuit (CH); (C) the maximum power using resistor (PR); (D) the maximum power using energy harvesting circuit (PH).	48
Figure 16 (A) Average anode potential, (B) Maximum current output, (C) Coulombic Efficiency and (D) Power output from CR, CH, PR and PH reactors during their peak performance period.	52
Figure 17 Cyclic voltammetry on day 30, 40, 50, 70, 80, and 90 of reactor running at (A) high current using resistor (CR); (B) high current using energy harvesting circuit (CH); (C) the	

maximum power using resistor (PR); (D) the maximum power using energy harvesting circuit (PH).....	54
Figure 18 Weighted Fast UniFrac, Principal Coordinates Analysis (PCoA) of the bacterial communities in MFC reactors on (A) the anode biofilm samples (B) the cathode biofilm samples, and (C) solution samples on the basis of phylogenetic lineages. The characters of “1” and “2” in abbreviations of samples indicate duplicate samples collected on day 60, and “3” and “4” indicate duplicate samples collected on day 90.	56
Figure 19 Taxonomic classification of bacterial DNA sequences at (A) phylum level and (B) the most dominant class level distribution (class level less than 10% is classified as other) A- indicates anode samples, C-indicates cathode samples and S- indicates solution samples..	58
Figure 20 Taxonomic classification of bacterial DNA sequences at the genus level. The genera that are less than 1% of total composition in all libraries were ignored in heat map graph. A- indicates anode samples, C-indicates cathode samples and S- indicates solution samples..	60
Figure 21 Turbidity (A) and TSS (B) removal by the 6 different operational conditions after 30 minutes (with biochar addition) or 50 minutes (without biochar addition). Legends showing process combination matrix, e.g. DC-EC-0 g/L Biochar means DC-powered EC process with 0 g/L biochar addition.....	68
Figure 22 Change of solution conductivity (A) and pH (B), as well as COD removal (C) after 30 minutes (with biochar addition) or 50 minutes (without biochar addition). Legends showing process combination matrix, e.g. DC-EC-0 g/L Biochar means DC-powered EC process with 0 g/L biochar addition.....	69
Figure 23 Turbidity and TSS removal after 30 minutes in biochar-only reactors with a dose of 0.25 g/L or 0.5 g/L biochar.	71

Figure 24 Time-course current profile in DC-EC reactors (A) and AC-EC reactors (B) with different doses of biochar addition.	72
Figure 25 Energy consumption comparison under different conditions.....	74
Figure 26 5L-MFC setup.....	79
Figure 27 Electrical connections of integrated MFC-EC system (EH= Energy Harvesting Circuit, Buck = buck converter, BAT = battery).	80
Figure 28 (A) MFC 1-5 voltage profile, (B) MFC 1-5 current profile, (C) Battery voltage and current profile, (D) 5-L MFC power (Pin), power output from energy harvesting circuits (Pout) and energy stored in the battery in one batch cycle.	82
Figure 29 (A) Battery and electrocoagulation voltage and current profile, (B) oil content and energy consumption during bilge water treatment by electrocoagulation.	84
Figure 30 Energy Flow (Wh) Sankey Diagram of integrated MFC-EC system.....	86

CHAPTER 1

INTRODUCTION

1.1 Rational

In order to develop communities in a sustainable manner it is necessary to think about how to provide basic services including sanitation and electricity. In Brazil, some communities isolated from urban centers do not have access to those services or have them in precarious conditions. In the Amazonas state, the isolated communities population live in poverty conditions, which push them to move to the urban centers looking for better quality of life, which as a result leading to more poverty in big urban centers, because the population is usually without higher education and professional qualification that can assure them a job and stable income¹. In the Amazon region, the communities are dispersed over a large area usually along the rivers, making it very difficult to access due to dense forests and large water bodies. The lack of resources for construction, as well for operation and maintenance of systems makes it very expensive to provide basic services such as sanitation and electricity, especially when using conventional methods.

The conventional methods of electricity generation in these communities is burning fossil fuels, which contributes to climate change with visible implications on the planet². Climate change can be particularly dangerous in developing countries because they often have limited social safety nets, widespread poverty, fragile health care systems, and weak governmental institutions, making it harder for them to adapt or respond to climate change³.

In addition, several environmental problems are associated to the lack of or precarious sanitation, such as: pollution or contamination of water supplying rivers and lakes for instance,

as well as floods among other environmental problems. But, the lack of sanitation also leads to health risks, mainly to the poor population in underdeveloped countries. Data show that 58% of deaths caused by diarrhea are due to inadequate sanitation⁴. The high energy demand for conventional wastewater treatment plays an important role in the lack of sanitation in underdeveloped communities, since it is already difficult to provide electricity for small houses with low energy demand. Hence, in order to improve the quality of life in remote places for developing communities it is necessary to create an integrated sustainable model for sanitation and electricity.

Wastewater has energy embedded in the form of biodegradable organic matter, but most of the conventional systems use external energy to treat the wastewater instead of harvesting its energy. It is estimated that there is up to 9 times more energy embedded in the wastewater than the energy used for treatment. In this context, bioelectrochemical systems (BES) is a unique process that offers a solution for environmental sustainability by simultaneously performing pollutant removal and energy production⁵. These systems are capable of converting the chemical energy of biodegradable substrates, especially those from waste materials, into renewable electricity (microbial fuel cells- MFC) or hydrogen/chemical products (microbial electrolysis cells-MEC)⁶. The key parts of the BES are the anode and cathode that serve as electron acceptor and donor, respectively, to promote oxidation and reduction reactions in one single system⁷.

MFC uses indigenous and self-sustaining microorganisms to oxidize organic and inorganic biodegradable substrates and transfer electrons to the anode electrode, generating electrical current. The current can be captured directly for electricity. The conversion of chemical energy to electrical energy in the anode requires the respiration of the insoluble anode, where a unique group of microbes called electroactive bacteria (EAB) have been used. Such

microorganisms are able to transfer electrons out of their cell membranes to the electrode either directly through nanowires or cytochromes, or they can use self-produced or external mobile electron shuttles⁶. Electrons then flow from the anode to the cathode through an external electrical connection. Protons that are released from organic matter metabolism combine with the electrons and oxygen at the cathode to form water⁸ (Figure 1).

Even though great progress has been made on BES reactor architecture, material and operation optimization⁹⁻¹¹, the direct electrical energy output from MFC reactors is still very low and the electrical interface with microbial activities are not well understood¹². Until now, there is no clear solution to efficiently convert the theoretical potential of microbial fuel cells and practically utilize its power output in a controlled manner. In addition, almost all the studies have been focusing on the design of the feasible circuits and the improvement of the energy harvesting efficiency¹³⁻¹⁵, but the interactions of the bacteria on the anode and cathode of BESs during energy harvesting process has not been investigated yet¹².

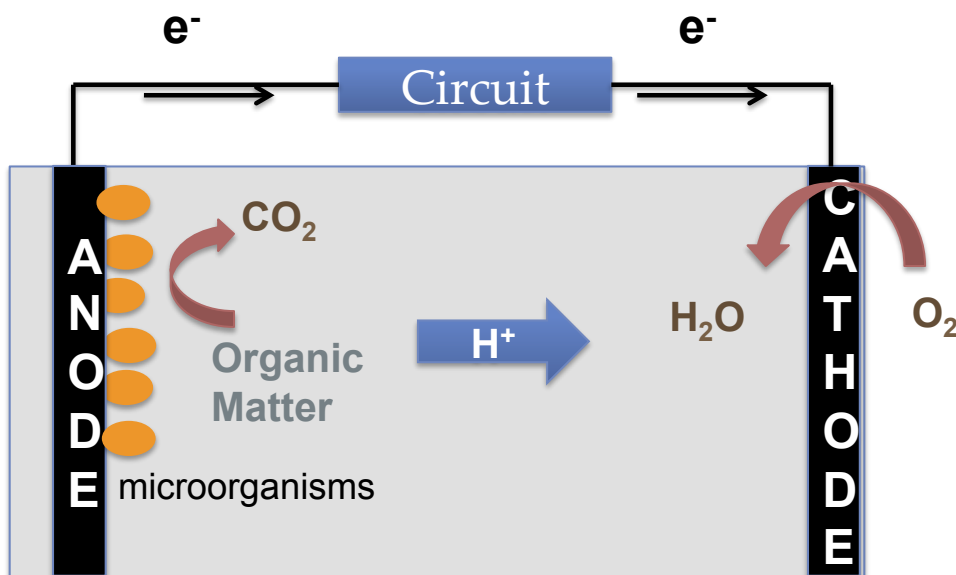


Figure 1 MFC schematic

1.2 Formal Hypothesis

The following hypotheses were developed and challenged to investigate the electrical control methods for microbial fuel cells in order to improve wastewater treatment and at the same time efficiently harvest its energy. In addition, electrical control for electrocoagulation was investigated in conjunction of MFC energy utilization, so efficient energy management can be realized to achieve energy positive sanitation practice in remote areas.

Hypothesis I. In addition to DC power, AC power can be generated from microbial fuel cells (MFCs) with high efficiency.

Hypothesis II. Pulse-shaped high frequency energy harvesting can be realized in MFC systems using power electronics, and such approach can regulate microbial electrochemical reactions and lead to higher performance as compared to traditional passive approach.

Hypothesis III. Active energy harvesting increases microbial fuel cell (MFC) performance by creating a selective pressure on microbial community and activity, leading to microbial community structure change toward higher electron transfer efficiency.

Hypothesis IV. The integration of AC-powered electrocoagulation with granular biochar reduces energy and electrode passivation while achieving high treatment efficiency of hydraulic fracturing wastewater.

1.3 Dissertation Guideline

This dissertation has been written in such that each chapter can be read independently while also addressing the outlined hypotheses. Chapter 2 tested *hypothesis I* that AC power can be generated from microbial fuel cells (MFCs) with high efficiency. The results from chapter 2 were published in *Journal of Power Sources*. Chapter 3 investigated *hypothesis II* that high

frequency pulse-shaped power extraction leads to shifts in microbial electron transfer processes and anode biofilm change, hence different energy harvesting scenarios influence on MFC electrochemical performance and associated microbial activities. Findings from Chapter 3 were published in *Journal of Power Sources*. Chapter 4 covered *hypothesis III* that active energy harvesting increases MFC performance by creating a selective pressure on the electroactive biofilm, which leads to a shift in microbial community structure toward higher efficiency. The results from Chapter 4 are under review in *Water Research*. Chapter 5 evaluated *hypothesis IV* that integration of AC-powered electrocoagulation with granular biochar reduces energy and electrode passivation while achieving high treatment efficiency of hydraulic fracturing wastewater. The results from Chapter 5 were published in *Journal of Hazardous Materials*. Future research directions are covered in Chapter 6, where I evaluate the possibility of integrating electrocoagulation and MFC systems for oily wastewater and domestic treatment seeking energy neutrality for sanitation in remote areas.

CHAPTER 2

AC POWER GENERATION FROM MICROBIAL FUEL CELLS

2.1 Introduction

The microbial fuel cell (MFC) technology has been intensively researched due to its unique capability of converting any biodegradable substrates, especially waste materials, into renewable electricity^{5,6,16}. MFCs carry good potential to transform traditional energy intensive wastewater treatment into energy-neutral or even energy-positive processes, but it requires a quantum change in technological advances in scale, cost, and practicality^{9,11,17,18}. In addition to retrofit existing large-scale wastewater treatment, in the near term, MFCs can be an ideal waste treatment and renewable energy solution for decentralized or remote villages, because it provides both energy and sanitation infrastructures for these communities.

The technology downside is the low power production at current stage. Despite great progress made in reactor configuration, material and operation that improved power output from 1mW m^{-2} to about 19W m^{-2} , the voltage provided by MFCs is still in the order of mV¹⁹. This is why energy harvesting using power electronics is crucial to make MFC application relevant. To date all efforts in MFC energy harvesting have been focusing on direct current (DC) output using DC-DC converters²⁰⁻²², capacitor charging and discharging²³⁻²⁶ and power management systems^{13,27-29}. These systems have been developed to boost the voltage to power small electronic devices such as hydrophones or sensors^{27,28,30,31}, and a recent study provides a comprehensive review of the current status and future need of practical energy harvesting from MFCs¹⁹.

While in many cases DC output is sufficient for MFC-powered sensor applications, alternating current (AC) power generation is needed for community waste treatment and power solutions, because general household electrical appliances require AC power to operate, and the electrical grid distributes the electricity in the form of AC. Other renewable energy source such as Solar also produces DC power, which is then converted to AC power using inverter or DC-AC converter. The DC-AC converters are commercially sold but require an input voltage of at least 12 V³², far beyond MFC voltage output level.

Though AC power generation from MFCs has not been reported so far, it becomes an imminent need for larger scale MFC development to meet real-world requirements. In this study, AC power generation was realized from MFCs through the development of a DC-AC converter system, and AC power in different frequencies with different MFC input voltages were also investigated. In addition, the quality of energy and the efficiency of the converter were also examined. Different frequency and quality investigations are important because unlike DC power, AC power outputs vary among different regions in the world. For example, Europe adopts an AC standard of 220-240 volts at 50 Hz, while North America uses 120 volts at 60 Hz.

2.2 Materials and Methods

2.2.1 MFC construction and operation

Single-chamber MFCs were built by one polycarbonate cube-shaped chamber with an empty volume of 28 mL. A heat-treated graphite brush was used as the anode, and 30% water-proof carbon cloth (7 cm², Fuel Cell Earth) was as the air-cathode, which composed of one carbon base layer, four polytetrafluoroethylene diffusion layers and one catalyst layer (0.5 mg Pt cm⁻²)³³. MFCs were inoculated with anaerobic sludge obtained from the Boulder Water Recourse

Recovery Facility. The growth medium contains (per liter) 1.0 g CH₃COONa, 0.31 g NH₄Cl, 0.13 g KCl, 3.32 g NaH₂PO₄·2H₂O, 10.32 g Na₂HPO₄·12H₂O, 12.5 mL mineral solution, and 5 mL vitamin solution³⁴. Fresh medium was refilled every 24 h. All MFCs were run in duplicate in batch mode at room temperature.

2.2.2 DC to AC circuit design and control

The custom-designed DC-AC converter is able to transform MFC DC power output to AC output (Figure 2). The DC-AC converter consists of MFCs (MFC1 and MFC2) as the DC power sources, capacitors (C1 and C2, 1000 µF) as the intermediate energy storage, and MOSFETs (M1 and M2, NTD4906N) as switches. The switches M1 and M2 were alternately controlled ON/OFF in order to create positive and negative parts of the AC outputs. The control signals to switch ON/OFF were programmed by an Arduino microcontroller (Uno, R2) which was connected to a laptop. A binary value of 1 (5 V) assigned by the Arduino turns on the MOSFET while a binary value of 0 (0V) turns off the MOSFET. Since the control signal is a pulse with a period (T) that is equal to the sum of T_{ON} and T_{OFF} , and the period of a signal is the inverse of the frequency (f) or $T = 1/f$, it can be derived that $T_{ON} = T_{OFF} = 1/2f$. The DC-AC converter was tested in different conditions, including three different frequencies (1 Hz, 10Hz and 60 Hz), absence or presence of energy storage layers (capacitors), and powered by 2 MFCs

or 4 MFCs paired in series. Serial MFC connection provides higher voltages and more power for the DC-AC converter.

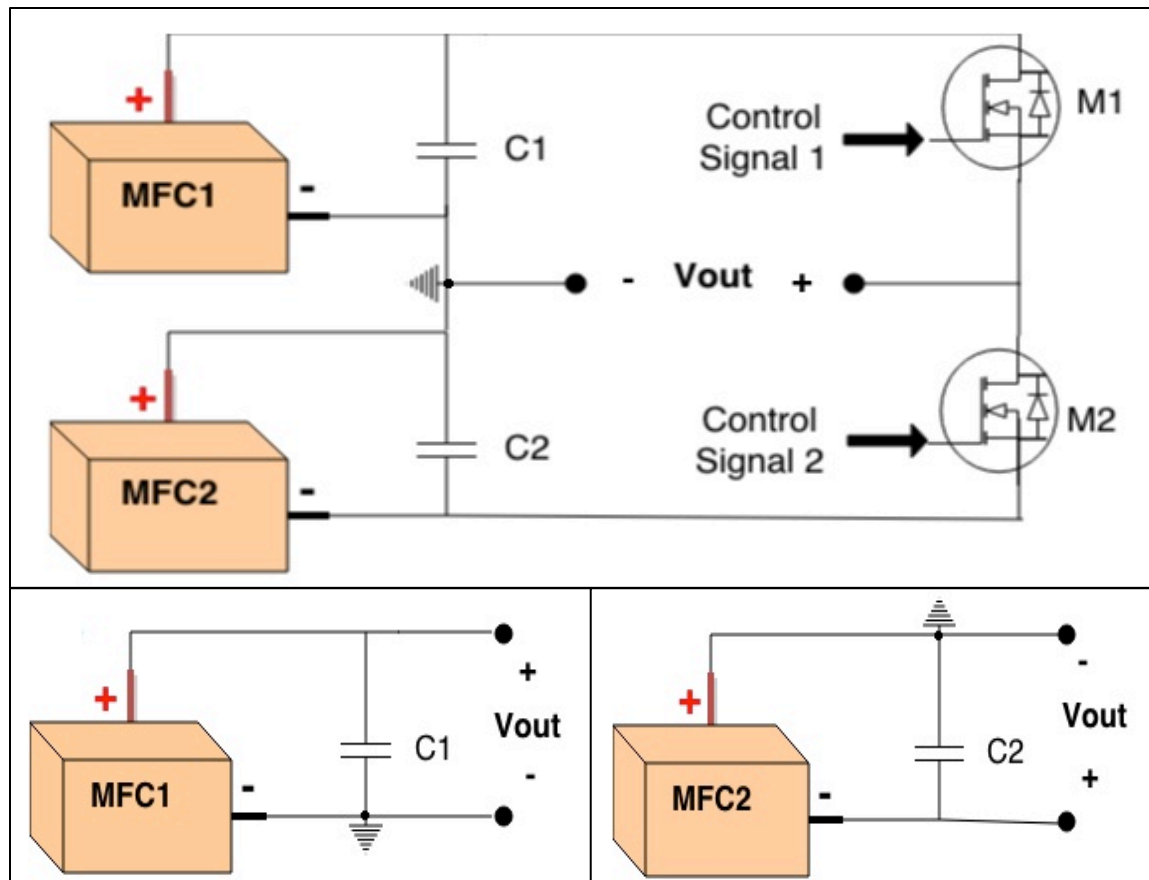


Figure 2 (A) Circuit diagram of the DC-AC converter system for MFCs; (B) equivalent circuit diagram when MOSFET M1 is ON and MOSFET M2 is OFF to output the positive part of AC; (C) equivalent circuit diagram when MOSFET M1 is OFF and MOSFET M2 is ON to output the negative part of AC.

2.2.3 Analyses

The control signals for M1 and M2, the voltages and electrode potentials of the MFCs, the output voltage of the DC-AC converter, and the current in the circuit were all measured using an Oscilloscope (Agilent Technologies, DS01024A). MFC polarization curves were measured by varying external resistors from open circuit to 50 Ω using a resistor box.

To evaluate the efficiency of the DC-AC converter, a 100 kΩ resistor was used as the output load to close the circuit but simulate open circuit condition. The efficiency of the DC-AC converter was calculated by Equation (1):

$$\eta = \frac{V_{output}^2}{R_{output} V_{MFC} I_{MFC}} 100\% \quad (1)$$

where V_{output} is the root mean square (RMS) value of the AC output voltage that represents the usable voltage in AC; R_{output} is the output resistor which equals 100 kΩ; V_{MFC} and I_{MFC} are the voltage and current from the MFC, respectively, and I_{MFC} is the same as the current passing through the output resistor (100 kΩ) (Figure 2B and 2C). Since the output voltage is a square wave, its RMS value is the same as the maximum value³⁵.

2.3. Results and discussion

2.3.1 Operation of the DC-AC Converter under Different Frequencies

The DC-AC converter was operated by an Arduino microcontroller, which generates control signals to turn ON or OFF the MOSFETs at desired frequencies (1 Hz, 10 Hz, or 60 Hz in this study). Figure 2A shows the schematic diagram of the DC-AC converter. When M1 is ON and M2 is OFF, the DC voltage from MFC1 passes through while the DC voltage from MFC2 is cut off, so the MFC1 DC voltage is mirrored as the positive part of the AC voltage (Figure 2B); In contrast, when M1 is OFF and M2 is on, DC voltage in opposite direction is generated from M2 through the converter, which is mirrored as the negative part of the AC voltage (Figure 2C). As a result, the output voltages of the DC-AC converter continuously alternate between positive and negative voltages in periodic cycles, that is, AC voltages.

To test the feasibility of applying different frequencies, control signals for each MOSFET (M1 and M2) were operated at frequencies of 1 Hz, 10 Hz and 60 Hz (Figure 3). The frequency of 60 Hz (Figure 3C) is the primary goal because most electric loads are operated at 60 Hz AC. The frequencies of 1 Hz (Figure 3A) and 10 Hz (Figure 3B) were chosen to demonstrate that the DC-AC converter can work at various frequencies under different MFC performance. All the control signals are periodic square waves with a period of $T = 1/f$, where half of the period (T_{ON}) has a binary value of 1 (5V) and the other half of the period (T_{OFF}) has a binary value of 0 (0V). Since the period of the control signal depends on the frequency, the period decreased from 1 Hz to 60 Hz, as shown in Figure 3A-C.

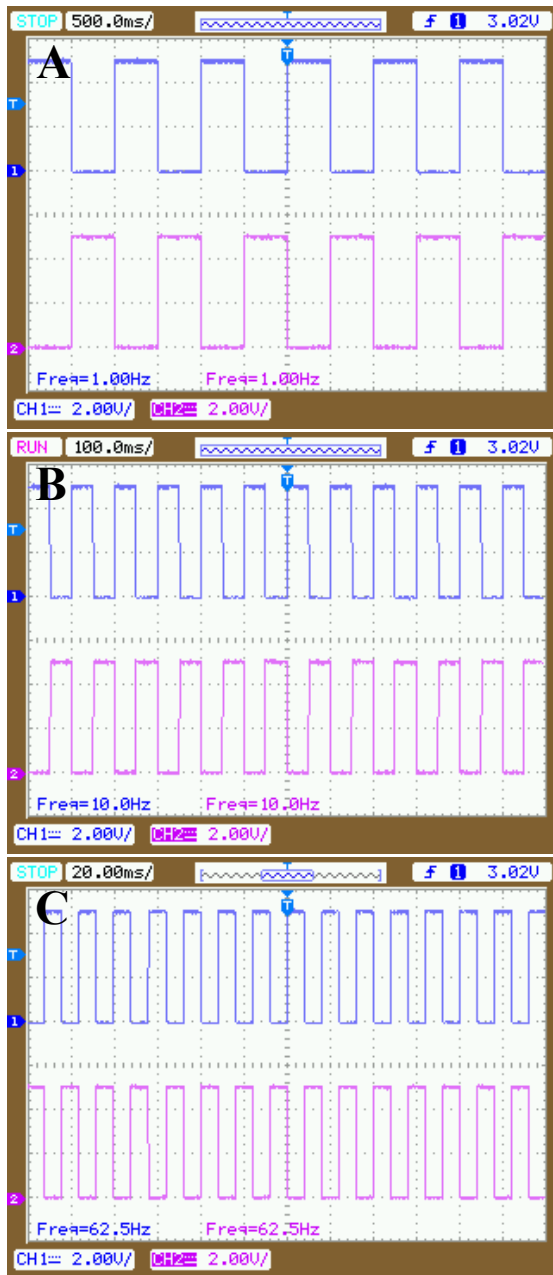


Figure 3 Control signals at 1Hz (A), 10Hz (B) and 60Hz (C). The blue curve is the control signal for MOSFET M1 and the magenta curve is the control signal for MOSFET M2.

2.3.2 AC Power Output without Using Energy Storage Layer (Capacitors)

Most MFC harvesting systems use energy storages, such as capacitors, due to the low direct energy output from MFCs. For this experiment, the energy storage layer was avoided in

order to simplify the circuit and investigate if MFCs can power DC-AC converter directly and effectively (Figure 4). Two MFCs or four MFCs (2 groups of 2 MFCs in series) were used as the direct DC power inputs. Without using capacitors as the energy storage layer, DC power from MFCs was successfully transformed to AC power. The AC voltage outputs kept square-shaped waves at 1 Hz and 10 Hz and only slightly deformed at 60 Hz. The input DC voltages and the output AC voltages both dropped gradually with increasing the frequency from 1 Hz to 60 Hz, but the output AC voltages were always comparable to the input DC voltages. When the DC-AC converter was powered by two MFCs, the positive AC outputs decreased along with the increase of frequency. For example, the AC outputs decreased from 720 mV (1 Hz) to 680 mV (10 Hz) and then to 480 mV (60 Hz), and the absolute values of the negative AC outputs decreased from 600 mV (1 Hz) to 560 mV (10 Hz) and then to 400 mV (60 Hz). Similar trend was observed under 4-MFC conditions, with the positive AC outputs decreased from 1480 mV (1 Hz) to 1280 mV (10 Hz) and 1000 mV (60 Hz), and the absolute values of the negative AC outputs decreased from 1320 mV (1 Hz) to 1160 mV (10 Hz) and 880 mV (60 Hz).

The slope of the linear section on the polarization curve has been widely used to determine the internal resistance of the direct output of an MFC ³⁶. Similar concepts can be adopted in AC condition. Figure 5 shows that the polarization curves under different frequencies can be considered as parallel lines without significant slope changes, which means that the internal resistances of MFC1 and MFC2 kept consistent when energy-harvesting frequencies changed. The internal resistances of MFC1 and MFC2 were estimated as $41.7 \pm 1\Omega$ and $48 \pm 2\Omega$ at the three frequencies, respectively.

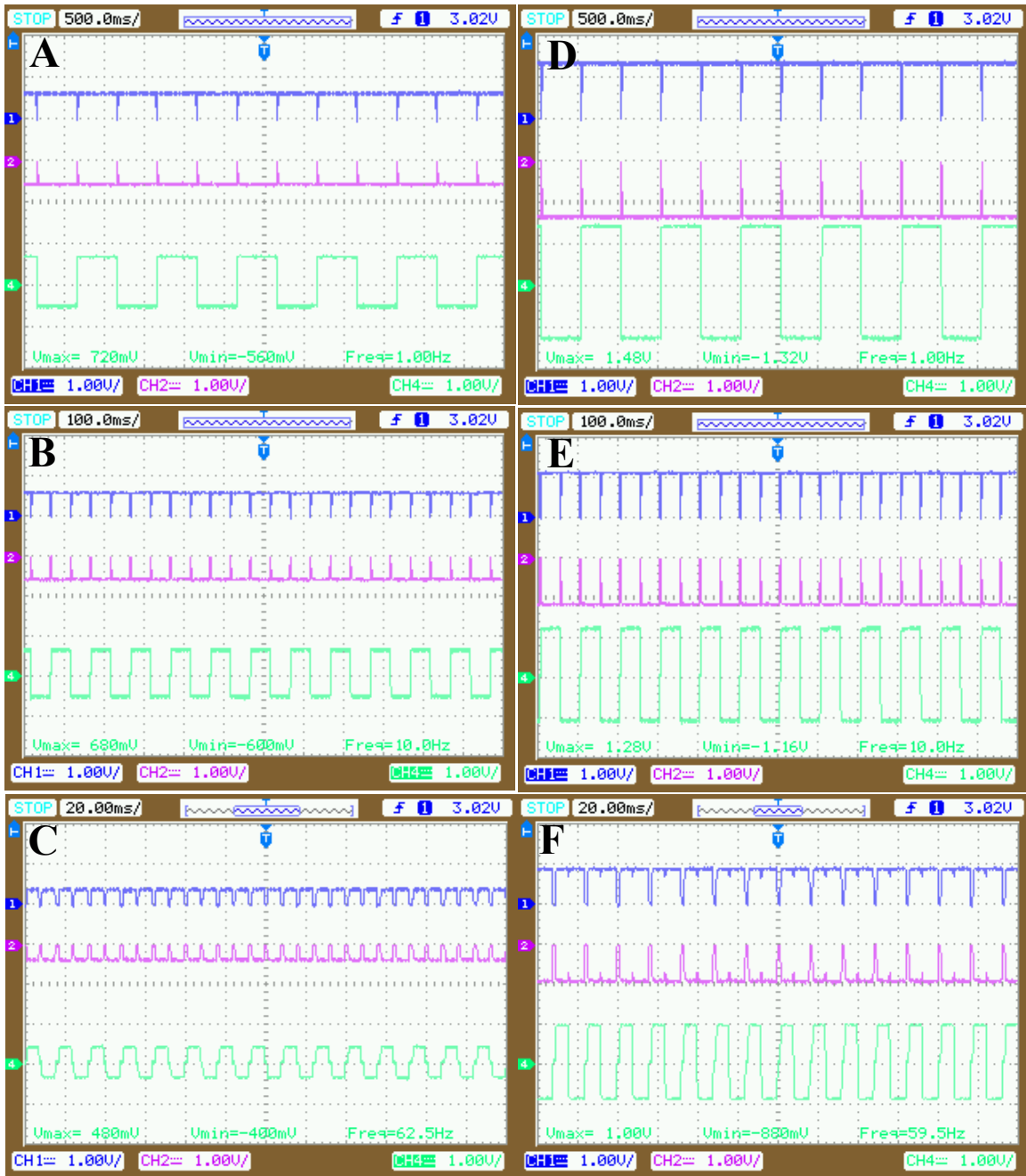


Figure 4 Input and output voltages without using energy storage layer (capacitors) in the circuit. The DC-AC converter was powered by two MFCs at 1Hz (A), 10Hz (B) and 60 Hz (C) or four MFCs (2 groups of 2 MFCs in series) at 1Hz (D), 10Hz (E) and 60 Hz (F). Blue waves: MFC1; magenta waves: MFC2; green waves: AC output.

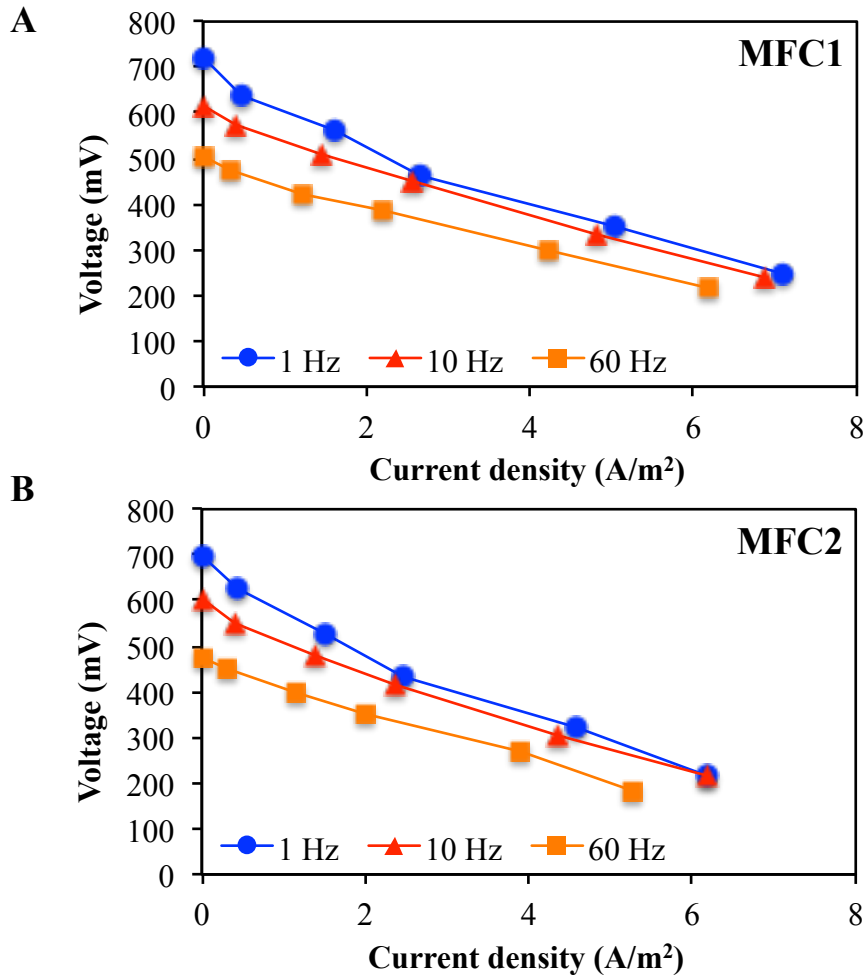
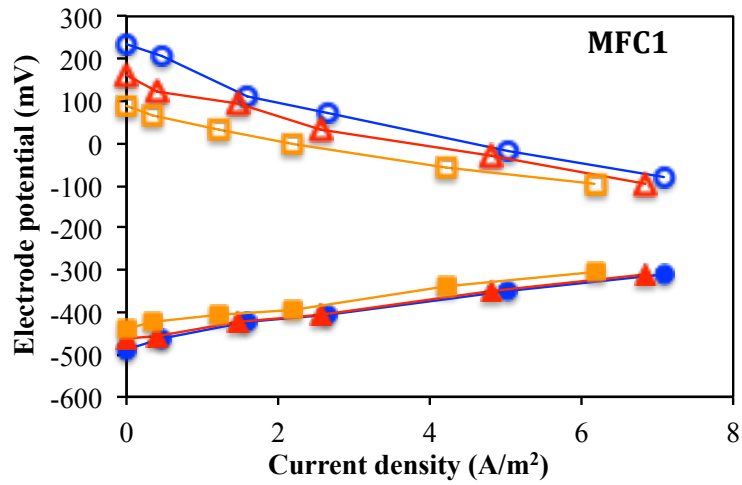


Figure 5 Polarization curves of MFC1 and MFC2 without capacitors in the circuit

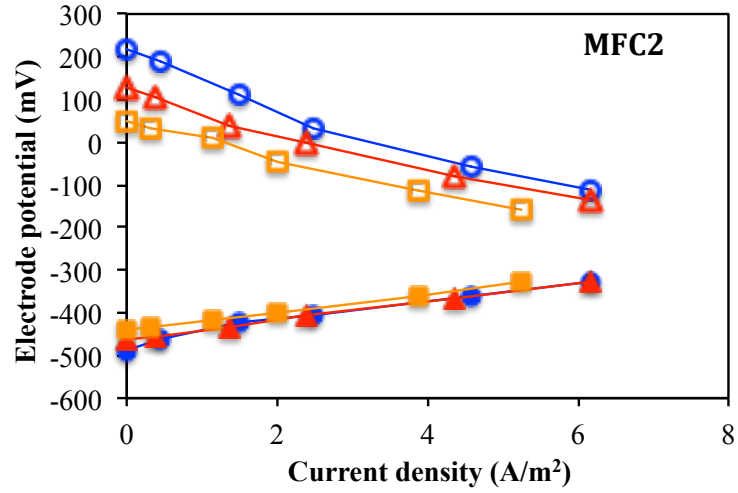
MFC anode and cathode potentials were measured to investigate the influence of frequencies on the MFC voltage. When the frequency increased from 1 Hz to 10 Hz then to 60 Hz, anode potentials were comparable while cathode potentials significantly dropped. The open circuit cathode potentials of MFC1 and MFC2 decreased from 232 mV to 88 mV and from 216 mV to 48 mV, respectively, while the open circuit anode potentials remained at 464 ± 20 mV for all the three frequencies (Figure 6). The comparable anode potentials among different frequencies suggested that enough electrons were available for current generation because of the

capacitive properties of the anodic biofilm ^{37,38}. The decrease of cathode potentials is hypothesized due to local pH increase, which were reported by previous studies that OH⁻ accumulation on the Pt-based air cathode can cause a potential loss up to 0.3V ³⁹. During higher frequency energy-harvesting, the transport of OH⁻ to the bulk electrolyte is slower than lower frequencies because of the smaller T_{ON} and T_{OFF} , which may cause potential drop due to limited mass transfer. No pH change was observed in bulk solution due to the use of buffer solution, but more studies are needed to further investigate the cathode potential drops at different energy-harvesting frequencies with local pH measurements on the electrode surface.

A



B



● 1 Hz Anode Potential ▲ 10 Hz Anode Potential ■ 60 Hz Anode Potential
○ 1 Hz Cathode Potential △ 10 Hz Cathode Potential □ 60 Hz Cathode Potential

Figure 6 Electrode potential changes of MFC1 (A) and MFC2 (B) at frequencies of 1Hz, 10Hz and 60Hz without using capacitors in the circuit.

2.3.3 AC Power Output with Energy Storage Layer (Capacitors)

To compare with the results without using energy storage layer, in following studies we added capacitors in the circuit as temporary energy storage to transform DC power from MFCs to AC power outputs from the converter. Similar MFC connections were used (2 MFCs or 4

MFCs in 2x2 serial connection), but the results in terms of shape and magnitude are very different between the two scenarios with or without capacitors (Figure 4 vs. Figure 7). Compared with regular shaped AC square waves when no capacitors were used, the input and output waves were distorted at even 1 Hz when capacitors were present and the waves became even indistinguishable at 60 Hz. In addition, the input DC voltages and output AC voltages dropped significantly with capacitors in the circuit from 1 Hz to 60 Hz. The positive AC outputs decreased from 680 mV (1 Hz) to 120 mV (60 Hz) when powered by 2 MFCs and from 1160 mV (1 Hz) to -40 mV (60 Hz) when powered by 4 MFCs. The absolute values of the negative AC outputs decreased from 600 mV (1 Hz) to 40 mV (60 Hz) when powered by 2 MFCs and from 1040 mV (1 Hz) to 160 mV (60 Hz) when powered by 4 MFCs.

When comparing the output AC voltages at the same frequency, we found that the AC outputs were much lower when capacitors were used, especially under the conditions of higher frequencies. At 1 Hz, the output voltage decreased only 40 mV (from 720 mV to 680 mV) when the DC-AC converter was powered by 2 MFCs (Figure 4A vs. 7A), and a higher drop was observed (320 mV) when 4 MFCs were used (Figure 4D vs. 7D). At 10 Hz, such drops increased to 320 mV (2 MFCs) and 1000 mV (4 MFCs), respectively (Figure 4B vs. 7B, Figure 4E vs. 7E). Similarly, even bigger drops were observed under 60 Hz, with 360 mV and 1400 mV dropped under the 2-MFC or 4-MFC condition, respectively. (Figure 4C vs. 7C, Figure 4F vs. 7F).

The big drop of output AC voltage when capacitors were added was believed due to the impedance of capacitors at different frequencies. The impedance of a capacitor (X_c) changes according to the frequency (f , Hz) and its capacitance (C , F), with the relationship expressed as

40

$$X_c = \frac{1}{2\pi f C} \quad (2)$$

When the frequency increases from 1 Hz to 10 Hz and 60 Hz, the impedance of the capacitor decreases from $X_{C_{1Hz}} = 160 \Omega$ to $X_{C_{10Hz}} = 16 \Omega$, and then to $X_{C_{60Hz}} = 2.6 \Omega$, based on Equation 2. The capacitor works as a low-pass filter as it cuts the voltage components for the higher frequencies and let only the voltage components of the low frequency pass through⁴⁰. The low-pass filter is a voltage divider between the resistance of the circuit and the impedance of the capacitor. Therefore, the voltage across the capacitor, which is mirrored to the output voltage, drops along the decreasing impedance and increasing frequencies. To avoid this performance drop, the capacitor should be determined according to the desired frequency. For instance, if the desired frequency is 60 Hz, a capacitor with a smaller capacitance of around 20 μF should be chosen to create a greater impedance of around 160 Ω . This study chose a capacitor of 1000 μF , which is more compatible with 1 Hz, and that's why less drop was found under 1 Hz while large drop was found under 60 Hz.

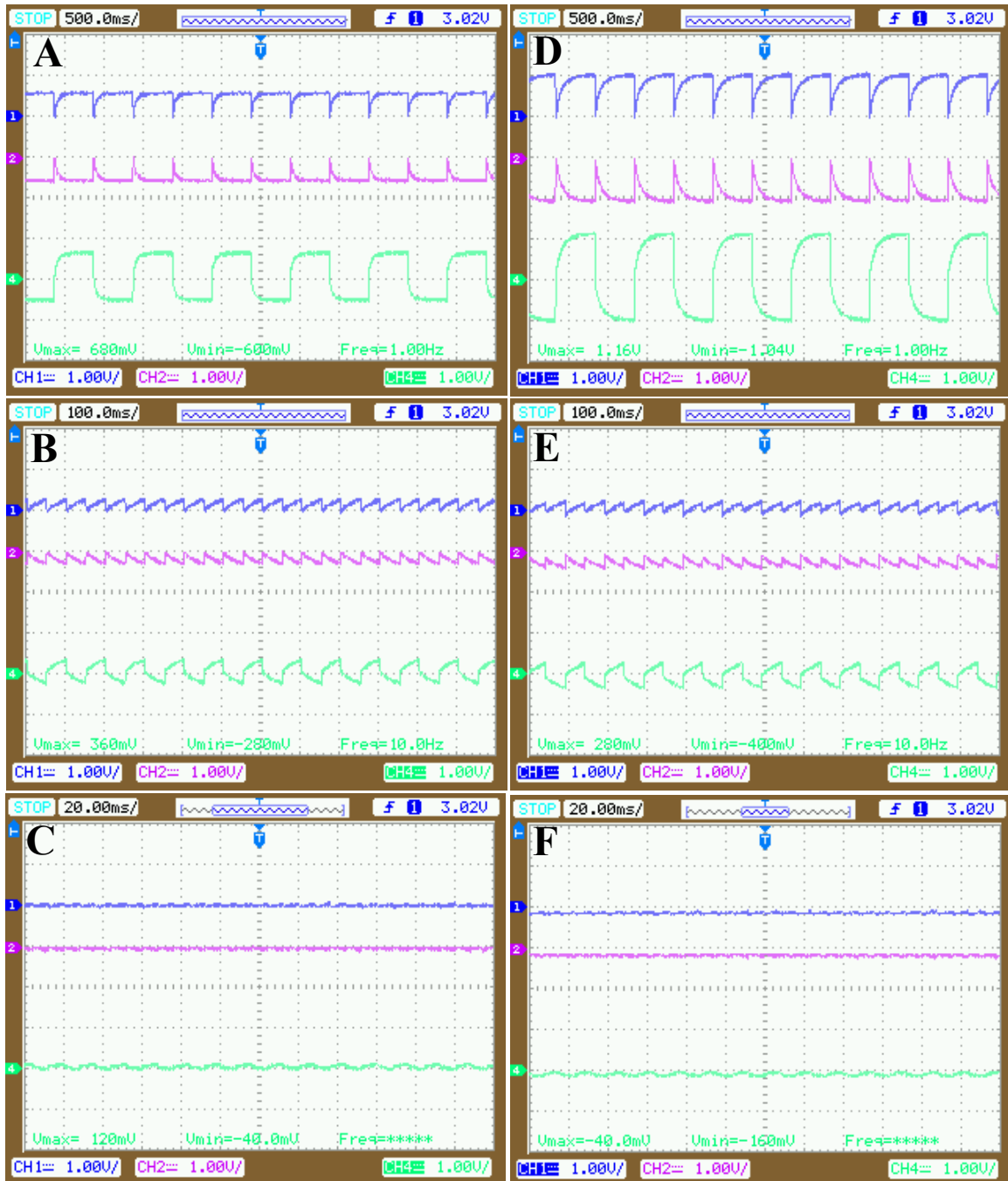


Figure 7 Input and output voltages when using energy storage layer (capacitors) in the circuit. The DC-AC converter was powered by two MFCs at 1Hz (A), 10Hz (B) and 60 Hz (C) or four MFCs (2 groups of 2 MFCs) in series at 1Hz (D), 10Hz (E) and 60 Hz (F). Blue waves: MFC1; magenta waves: MFC2; green waves: AC output.

2.3.4 AC Power Quality from MFCs

In conventional AC electric energy systems, the voltage generated is a sine wave form with a frequency of 60 Hz (U.S.). During the transformation from renewable DC power to AC power, like those from solar panels or MFCs in this study, the power quality, expressed as total harmonic distortion (THD) at 60 Hz, depends on how the AC voltage generated via the DC-AC converter differs from the conventional 60 Hz sine wave voltages. In other words, the power quality is related to the quantity of harmonics in the AC voltage generated via the DC-AC converter. A harmonic is a sinusoidal waveform with a frequency that is an integral multiple of the fundamental frequency of 60 Hz ⁴¹. The THD measures the quantity of harmonics of a wave by using Fourier analysis, via which any periodic waveforms can be described as an infinite sum of sine waves in different frequencies (Supporting Information for more details). Since the output voltage from the DC-AC converter is a periodic waveform with period T , thus it can be described as ³⁵

$$V(t) = \frac{1}{T} \int_0^T V(\tau) d\tau + \sum_{h=1}^{+\infty} [a_h \cos(h\omega t) + b_h \sin(h\omega t)] \quad (3)$$

where h is the harmonic order, ω is the fundamental frequency that is equal to $2\pi/T$ and a_h and b_h are given by

$$a_h = \frac{2}{T} \int_0^T V(\tau) \cos(h\omega\tau) d\tau \quad (4)$$

$$b_h = \frac{2}{T} \int_0^T V(\tau) \sin(h\omega\tau) d\tau \quad (5)$$

The harmonic order is the multiple of the fundamental frequency, for instance, the second harmonic for a fundamental frequency of 60 Hz is at the frequency of 120 Hz.

The Fast Fourier Transform (FFT) is an algorithm that represents the Fourier analysis in the frequency domain, which can easily provide the voltage in each harmonic. The THD is measured by ³⁵

$$THD = \frac{\sqrt{V_2^2 + V_3^2 + V_4^2 + \dots + V_n^2}}{V_1} 100\% \quad (6)$$

where V_1 is the voltage in the fundamental frequency, V_2 is the voltage in the second harmonic, V_3 is the voltage in the third harmonic and so on.

The FFT of the output voltages were measured when the DC-AC converter was powered by 2MFCs (Figure 8A) or 4 MFCs (Figure 8B) at 60 Hz, which is the standard frequency of AC in the electric power grid in the U.S. When the DC-AC converter was powered by 2 MFCs, the most relevant harmonic was the third harmonic, where the frequency (180 Hz) was three times as the fundamental frequency. The corresponding THD of the output voltage was around 30%. When 4 MFCs were used, the most relevant harmonics were the second (120 Hz) and third harmonic (180 Hz), with a relevant THD around 30% as well. The THD standard for grid-tied systems is 8%⁴², but for stand-alone renewable systems the square-wave DC-AC converter with a THD of 30%, like the one developed here, can be used to power linear loads safely³⁵.

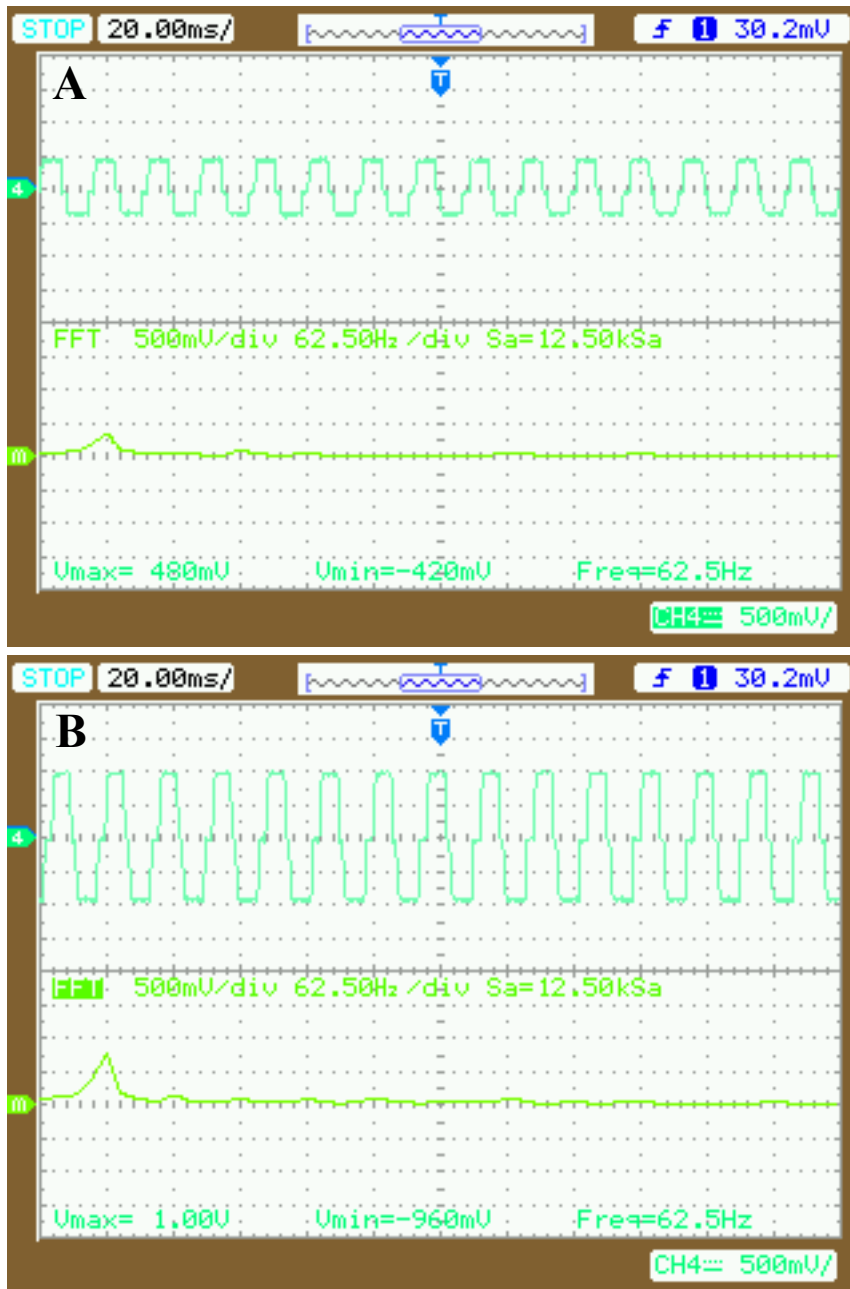


Figure 8 Output voltages and the Fast Fourier Transform (FFT) of the output voltages at 60Hz when the DC-AC converter was powered by two MFCs (A) and four MFCs (2 groups of 2 MFCs in series) (B).

2.3.5 The efficiency of the DC-AC converter

The efficiency of the DC-AC converter was calculated without using the capacitors in the circuit (Figure 9). The custom-designed DC-AC converter was very efficient with the efficiencies reached almost 100% in repeated tests. The efficiencies of the DC-AC converter among various frequencies (1 Hz, 10 Hz, and 60 Hz) were around $97\pm 3\%$, with the limited energy losses mainly due to the MOSFET conduction loss and the switching loss. When the frequencies increased from 1 Hz to 60 Hz, the efficiencies decreased because more energy was lost on the MOSFET switches at the high switching frequency, but the energy loss was still small. When the DC-AC converter was powered by 4 MFCs instead of 2 MFCs, the average efficiencies were slightly higher ($99\pm 1\%$) due to higher voltage and more power provided. This result encourages the potential that if enough MFCs connected in series to provide a DC voltage of 110 V, the energy loss can be manageable. Since the microcontroller was not the focus in this study, the overall efficiency of the circuit including the extra power for Arduino was not investigated.

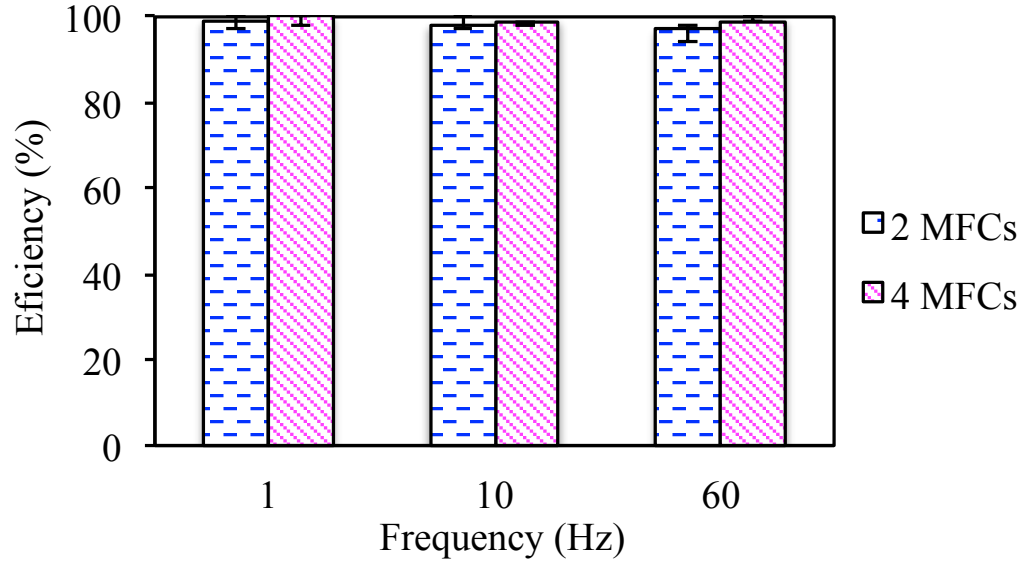


Figure 9 Efficiency of the DC-AC converter powered by two or four MFCs (2 groups of 2 MFCs in series) at 1 Hz, 10 Hz and 60 Hz.

2.3.6 Discussion

This study proves that AC power can be efficiently generated from microbial fuel cells, and different frequencies can be varied depending on the needs of electronic loads. The first DC-AC converter for MFCs has efficiency above 95%, which can assist the development of MFC systems for power and sanitation solutions for decentralized communities. Although the low voltage provided directly from MFCs is not enough to power an electric load, this study shows that MFC stacks may be able to do so without significant energy loss. In addition, transformers can be coupled at the output of the DC-AC converter to boost the voltage to a usable level.

However, many challenges remain before large-scale systems can be developed to power electric loads, such as potential voltage reversal in MFC stacks and more efficiency energy harvesting from MFC reactors. Maximum power point tracking (MPPT) algorithms and many other approaches are being investigated to solve these problems^{14,15,43–46}. In addition, the voltage output in this studied DC-AC converter topology is based on a mirror control of the input voltage

provided by the MFC. By using a different control scheme like modified sine-wave Pulse Width Modulation (PWM), the quality of energy output can be even higher. Also, because MFC DC voltage output can vary constantly due to the change of environmental conditions, a closed loop control in the converter may be applied to improve the output voltage stability.

The information presented in this chapter has been published in a scientific journal; **Lobo, F. L., Wang, H., Forrestal, C. Ren, Z. J.** “AC power generation from microbial fuel cells” *Journal of Power Sources*, **2015**, 297, 252-259.

CHAPTER 3

ENERGY HARVESTING INFLUENCES ELECTROCHEMICAL PERFORMANCE OF MICROBIAL FUEL CELLS

3.1 Introduction

Microbial fuel cells (MFCs) employ electroactive bacteria to produce direct electrical current from biodegradable substrates and demonstrate great potentials for energy-positive wastewater treatment, remote sensing, and environmental remediation^{10,47-50}. Despite great advancements on reactor configurations, materials, and operations, the power density of a single MFC reactor still ranges between mW m^{-2} and W m^{-2} , which is not enough for real-world applications¹². Higher power may be obtained by connecting multiple MFCs in series or parallel, but the operation is challenging and performance is unstable due to voltage reversal and other problems associated with the non-linear nature of biological systems^{13,15,25,37,51}.

Maximum power point (MPP) tracking and power management systems (PMS) have been used for MFC research and development, and reported methods include perturbation and observation⁵², multiunit monolithic system^{44,53}, hysteresis controller, synchronous flyback converter, and transformer^{13-15,43}. Many of these methods reported improved power production especially when using pulsed active energy harvesting approach because they are able to provide real-time energy tracking and capturing and therefore maximize power output. For example, Wang et al. reported that hysteresis controller based MPP circuit was able to harvest 76 times more energy than a charge pump and increase Coulombic Efficiency by 21 times⁴³. New integrated circuits and chips significantly reduced volume and energy consumption of the controller and therefore increased energy harvesting efficiency and enabled self-sustaining operation^{44,50}. However, MPP may not be the best operating point for all applications. For fuel

and chemical productions from microbial electrolysis cells or water desalination from microbial desalination cells, maximum current point (MCP) is generally preferred because higher current can drive faster chemical production or ion separation (Figure 10).^{12,54,55} For MFCs used in wastewater treatment, the primary goal may not be high power output either depending on operation stages, because for efficient organic removal higher current is desired. Therefore, in reality a balance in operation needs to be considered whether to operate the system at the MPP for maximum power output or at the MCP for faster substrate oxidation.

To our best knowledge no study has investigated how active harvesting at different regions (high power, high current, or high voltage) affects MFC electrochemical performance and substrate conversion efficiency, and very limited information is available on comparing system performance under active harvesting or traditional resistor-based operation. Previous studies showed that passive loads did impact the anode biofilm thickness and community structure by influencing the anode potential^{56,57}, but the electrochemical performance such as power production could maintain stable once biofilm reached to a level of electron transfer capability. In contrast, the pulse-shaped power extraction uses power electronic converters with high frequency therefore could lead to swifts in microbial electron transfer processes and anode biofilm change¹². In this study, we investigated extensively how different energy harvesting scenarios including both active harvesting and passive resistor loads affect MFC electrochemical performance and associated microbial activities. System behavior at three operating points including high power, high current, and high voltage were analyzed in different harvesting conditions, and the implications of how harvesting affect MFC operation are discussed.

3.2 Materials and Methods

3.2.1 MFC construction and operations in 2 stages

Cubic single-chamber MFCs were constructed using polycarbonate, and the empty volume of the MFC chamber was 28 mL. Each MFC reactor contained a heat-treated graphite brush as the anode and a carbon cloth air-cathode (7 cm^2 , Fuel Cell Earth) with manufacturing procedure described in previous studies^{58,59}. Diluted brewery wastewater from Avery Brewery (Boulder, CO) was used as the sole substrate during the experiment, and 50 mM phosphate buffer solution (PBS, $\text{NaH}_2\text{PO}_4 \cdot 2\text{H}_2\text{O}$ 3.32 g L^{-1} ; $\text{Na}_2\text{HPO}_4 \cdot 12\text{H}_2\text{O}$ 10.32 g L^{-1} ; NH_4Cl 0.31 g L^{-1} ; KCl 0.13 g L^{-1}) was used for the 1:10 dilution⁶⁰. The final substrate electrolyte used in the study contained $1,800 \text{ mgL}^{-1}$ COD, 938 mgL^{-1} TKN, and $1,860 \text{ mgL}^{-1}$ PO_4^{3-} . All MFCs were run in duplicate in batch mode at room temperature, and fresh medium was refilled at the end of each batch cycle.

The experiment was divided in two stages. In stage I, all 10 reactors were operated under the same condition with an external resistance of 1000Ω . This stage lasted for 2 months until similar performance was obtained which indicate the establishment of a baseline for further research. Using the power density curves derived from linear sweeping voltammetry (LSV) from each MFC reactor at the end of stage I, the key operating points of maximum current points (MCP), maximum voltage points (MVP) and maximum power points (MPP) were identified for phase II operation. In phase II, the reactors were divided in 5 groups. Each group has duplicate reactors and was operated in one of the following scenarios: maximum power with active energy harvesting (MPP-H), maximum current with active energy harvesting (MCP-H), maximum power with passive resistor (MPP-R), maximum current with passive resistor (MCP-R), and maximum voltage with passive resistor (MVP-R) (Figure 10).

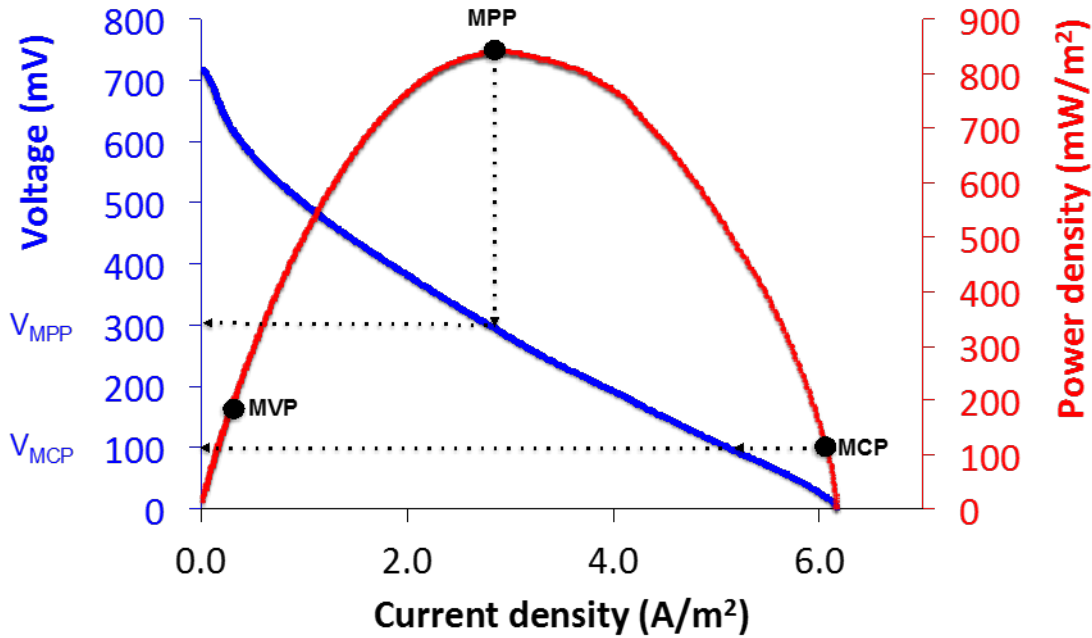


Figure 10 The power density curve obtained in an MFC operated under a 1000Ω external resistance. This curve shows the typical Stage I operation and was used to determine different operational points (MPP, MCP, MVP).

For the passive energy harvesting conditions, the operating resistors were determined by dividing voltage with current at desired points on the power density curve. Specifically, the external resistors used in MVP-R, MPP-R, and MCP-R scenarios were $2.2 \text{ k}\Omega$, 150Ω , and 33Ω , respectively. For active harvesting scenarios, MPP-H and MCP-H circuits were controlled by operating voltages that were determined during phase I operation (Figure 10).

The energy circuit used in this study was the bq25505 (Texas Instruments Inc.), which is an integrated energy harvesting Nano-Power management circuit, specifically designed to efficiently acquire and manage the microwatts (μW) to milliwatts (mW) of power generated from a variety of high output impedance (Hi-Z) DC sources with a highly efficient, pulse-frequency modulated (PFM) boost converter/charger. Embedded in the integrated circuit, a programmable maximum power point tracking (MPPT) keeps sampling the open circuit input voltage every 16 seconds by disabling the boost converter for 256 ms and stores the programmed MPP ratio of the

open circuit voltage on the external reference capacitor at VREF_SAMP. In this study, we adjusted the programmable MPPT to set VREF-SAMP to be at either $V_{MPP} = 300$ mV (MPP-H) or $V_{MCP} = 100$ mV (MCP-H) showed in Figure 10, and this control was able to maintain a constant MFC voltage. Since the maximum current would be given at 0 V, the approximation of $V_{MCP} = 100$ mV was used to give highest current controlled possible by the energy harvester circuit. The energy extracted from each MFC was stored in polymer lithium ion batteries (840mAh, SparkFun Electronics[®]).

3.2.2 Analyses

The individual potential of each anode and cathode was measured each batch using Ag/AgCl reference electrodes (RE-5B, +0.210V versus standard hydrogen electrode, 25 °C). Reactor voltages were recorded using a data acquisition system (Keithley, OH). Cyclic voltammetry (CV) was performed before and after batch operations in different stages. The potential range for CV was determined as -0.7 to 0 V vs. Ag/AgCl according to previous results and the scan rate was 1 mVs^{-1} ⁶¹. First derivative CV (DCV) was derived from turnover CV to determine the changes in each peak value. The main oxidation peak in DCV was fitted to Gaussian function to separate overlapped peaks. LSV tests were performed using the same potentiostat with a scan rate of 1 mVs^{-1} with either the anode or the cathode as the working electrode depending on characterization purposes.

Chemical oxygen demand (COD) before and after each batch was measured using the standard method with a spectrophotometer (DR 3900, Hach Co., Loveland, CO, USA). Coulombic efficiency was determined using Equation (7), where $M = 32$ (molecular weight of

oxygen), F is faraday constant, $b = 4$ is the number of electrons exchanged per mole of oxygen, v_{an} is the liquid volume of anode compartment, and ΔCOD is the change in COD over time^{36,62}.

$$CE = \frac{M \int_0^t I dt}{F b v_{an} \Delta COD} \quad (7)$$

3.3 Results e Discussion

3.3.1 Variations of MFC voltage, current, electrode potentials in different conditions

Figure 11A-E summarizes the profiles of MFCs operated in different stages and different harvesting conditions. Similar profiles were observed across all MFCs in the first 60 days (Stage I), in which all reactors were operated in the same condition of 1000 Ω external resistor. The reactors showed typical batch cycles of 3.5 days with the maximum MFC voltage of ~ 430 mV, the maximum current of ~ 0.43 mA, the lowest anode potential of -460 mV and the maximum cathode potential of 180 mV. The maximum power density achieved ranged from 598 mW m^{-2} to 844 mW m^{-2} (average 739 mW m^{-2}) among 10 reactors.

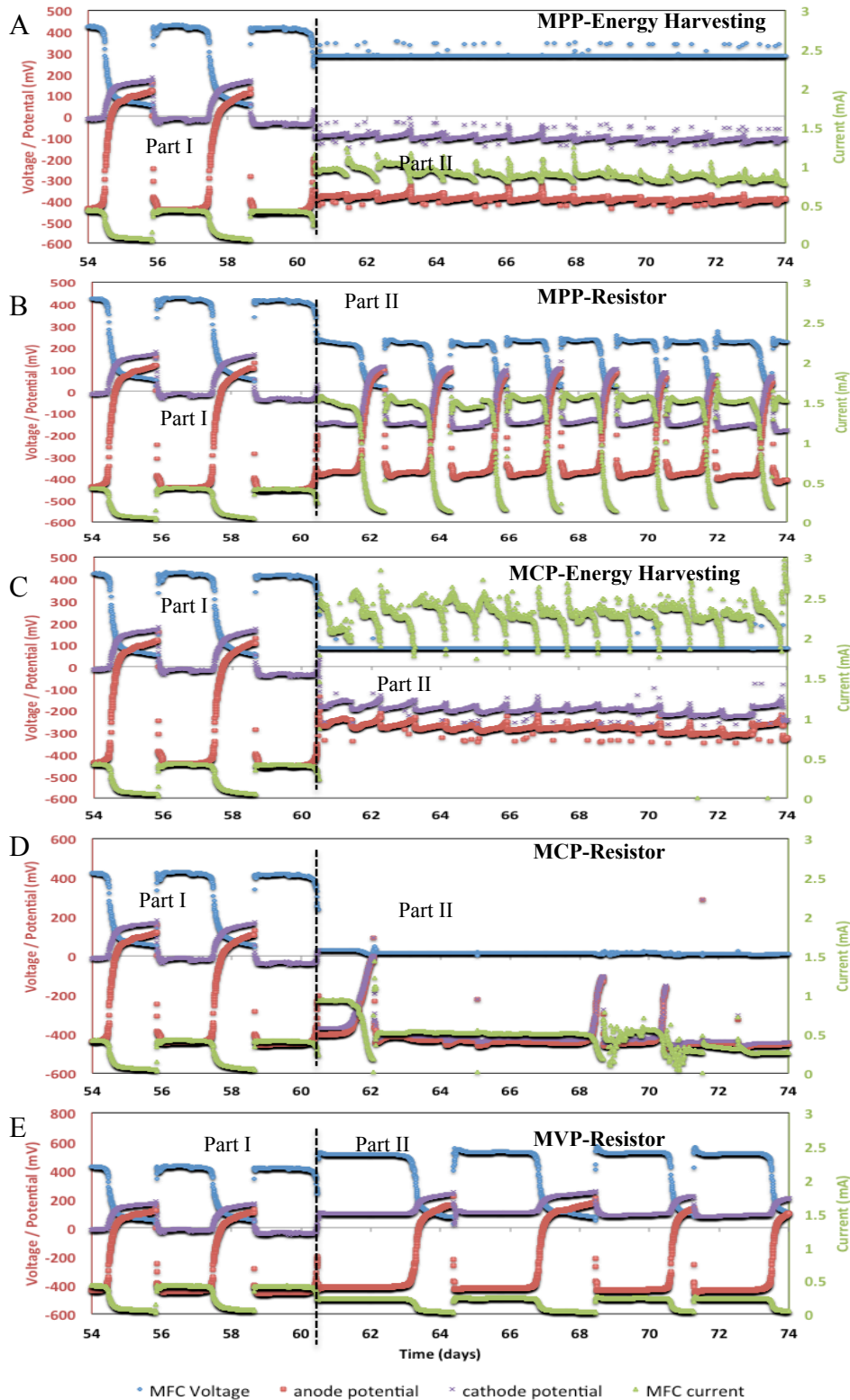


Figure 11 Time-course profiles of MFC voltage (blue), MFC current (green), anode potential (red) and cathode potential (purple) profiles for (A) MPP-H, (B) MPP-R, (C) MCP-H, (D) MCP-R, and (E) MVP-R.

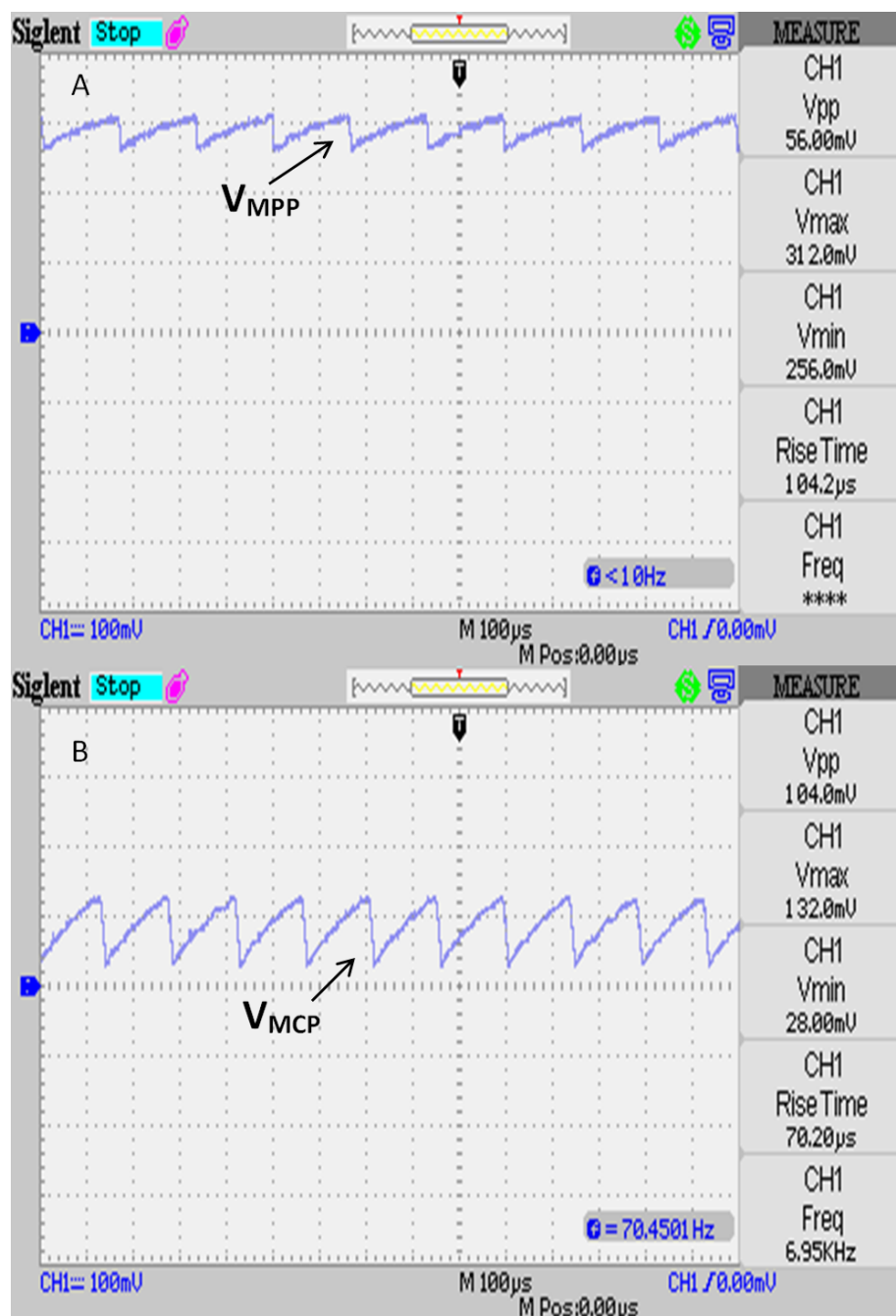


Figure 12 The harvesting circuit controlled MFC voltages for (A) MPP-H and (B) MCP-H.

Starting from day 61, the reactors are divided into 5 groups as aforementioned (MPP-H, MPP-R, MCP-H, MCP-R, and MVP-R), and different profiles in voltage, current, and electrode potentials are shown in Figure 11A-E. For the reactors operated in the maximum power point, stable

voltage, current, and anode and cathode potentials were generated under the MPP-H condition (Figure 11A). This is due to the dynamic control of harvesting voltage around 300 mV by the energy harvesting circuit through pulse frequency modulation. As shown in Figure 12A, under the active control, the MFC voltage was regulated to increase until 312 mV and decrease until 256 mV in high frequency. This harvesting approach enables real time feedback of the MFC's MPP changes during operation and adjusts harvesting condition accordingly. Since the MFC voltage was controlled to be constant, the MFC current was the one indicating the MFC batch cycle, which varied between around 1.3 mA and 0.7 mA. The MPP-H batch cycles were 24 hours each in order to stay in the maximum power area of the power density curve. In contrast, the outputs from MPP-R varied significantly within each batch, with voltage changed from 20 to 280 mV and current fluctuated from 0.1 mA to 1.8 mA. (Figure 11B). While such fluctuation is commonly observed in fed-batch MFC studies, it does reduce energy output and system stability compared with circuit harvesting (Figure 13).

For reactors operated at the maximum current point, similar trends were observed. Figure 11C shows that the MCP-H circuit controlled MFC voltage to stable at around 100 mV, and stable anode and cathode potentials were maintained throughout the operation. The MCP-H MFC current varied between 3.0 mA and 2.0 mA in each 24-hour batch cycle. The difference in redox potentials between the anode and the cathode (100 mV) was much smaller than the MPP-H (300 mV), which is understandable considering the MFC was operated at the highest current and low voltage condition. Figure 12B shows the MFC voltage being controlled in high frequency and varied between 132 mV and 24 mV, indicating a higher ripple than the MPP-H voltage. This is due to the high difficulty in controlling the low voltage by the nanopower harvester circuit. The MCP-R reactors started with a maximum voltage of ~30 mV but the performance dropped

significantly in the following cycles in both reactors. While the anode potentials maintained normal, the air-cathode potentials dropped significantly, led to reactor failure. Cleaning and replacing the cathodes resumed current generation but the voltage output still showed high fluctuation.

The MVP-R reactor was operated at the maximum voltage point (Figure 11E), which serves as a control reactor because such operation is not desired in practical applications due to its low current (slow organic removal) and low power output (low energy generation). The reactor showed stable performance in longer batch cycles (72 hours) due to slow electron transfer. The maximum voltage obtained was 525 mV and the maximum current was 0.25 mA.

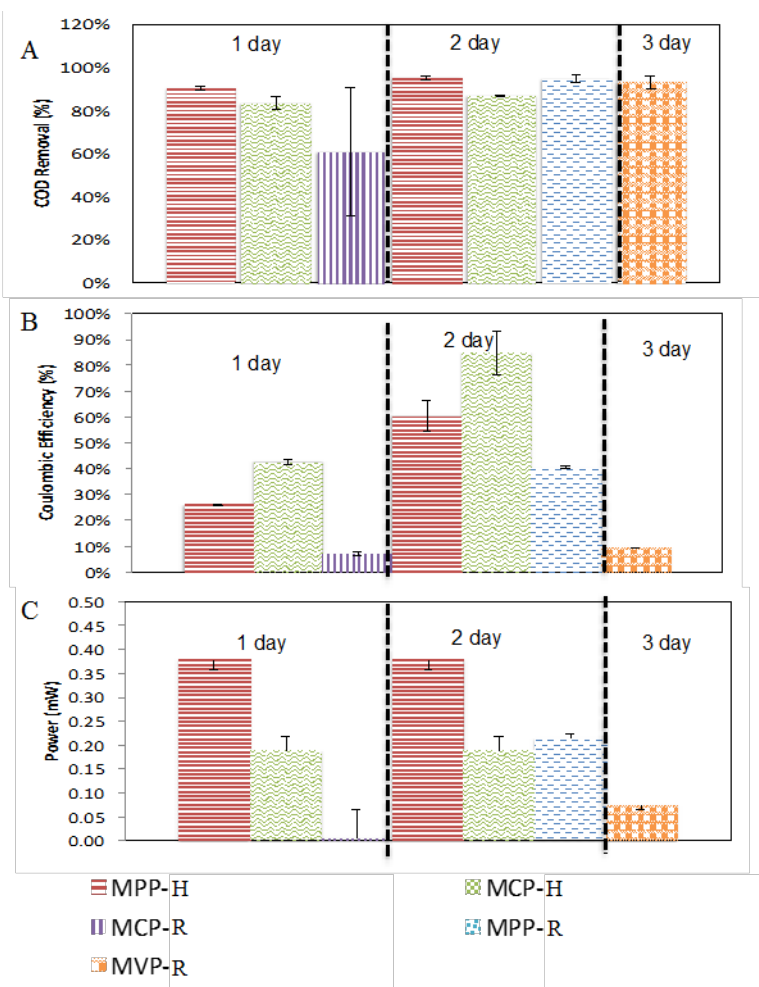


Figure 13 (A) COD removal, (B) Coulombic Efficiency, and (C) Power Production from reactors operated in different conditions. Different durations of batch cycles were used and indicated in the graph to reflect the conversion rate differences among reactors.

3.3.2 Variations in substrate utilization and energy recovery

Figure 13 summarizes the performance of different MFCs in terms of COD removal, Coulombic efficiency, and power generation. Overall reactors with active harvesting showed superior performance than those with resistors, but the differences vary depending on the operation. As a baseline, in stage I the MFCs showed consistent COD removal of $95\% \pm 1\%$, protein removal of $90\% \pm 10\%$, coulombic efficiency of 14% and an average power 108 mW m^{-2} , and each batch cycle lasted for 3.5 days (80 hours).

Because different harvesting scenarios led to various speeds of substrate conversion to currents, different durations of batch tests were conducted to characterize the degradation and energy recovery. The most efficient reactors for the conversion including MPP-H, MCP-H, and MCP-R were tested in 24-hour batch operation, and MPP-H showed higher COD removal (90 %), which was 8% and 32% higher than MCP-H and MCP-R, respectively (Figure 13A). Operated at the high power point, the MPP-H also showed much higher power generation than the other reactors (Figure 13C). On the other hand, the MCP-H showed higher CE than MPP-H and MCP-R, which is consistent with the purpose of high current recovery in MCP operation (Figure 13B). The performance of MCP-R fluctuated significantly as aforementioned, so the data obtained may not reflect the true potential of those reactors.

In 48-h batch tests, the results from the reactors also supported the hypothesized performance. For reactors operated at the maximum power points, both MPP-H and MPP-R showed good COD removal (95 %) (Figure 13A), which was slightly higher than MCP-H. However, because MPP-H extracted more electrons, it showed higher CE than MPP-R, which also resulted in much higher power generation (Figure 13B, 13C). For MCP-H, similar as 24-hour batch test, it recovered much more electrons from COD and therefore achieved the highest CE among the reactors. While similar COD removals were observed in MPP-H and MCP-H reactors in 24-hour and 48-hour batches, the CE obtained in 48-hour operation were approximately doubled compared with the 24-hour batches. Also, compared with the performance obtained in Stage I, MPP-H operation improved CE by 47-77% (average 62%), MCP-H increased CE by 67-88% (average 78%), and MPP-R increased CE by 66%. The MVP-R also achieved 95 % removal but it took much longer operation (72-hour cycle), and the CE and power generation was very low compared with other operations.

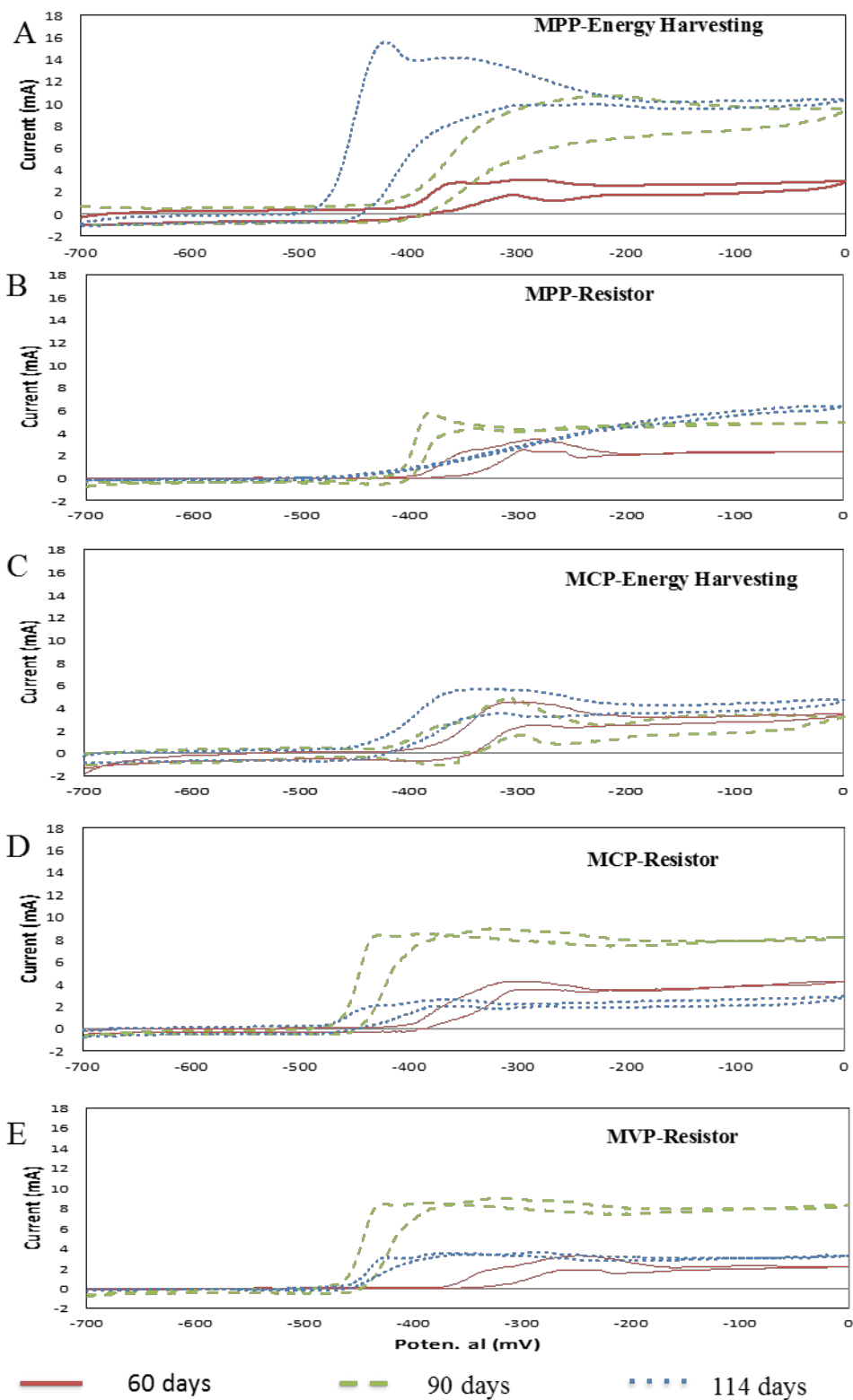


Figure 14 Cyclic voltammety profiles of (A) MPP-H, (B), MPP-R, (C) MCP-H, (D) MCP-R, (E) MVP-R in different stages and operational points.

3.3.3 Redox potential shifts in cyclic voltammograms

Turnover cyclic voltammetry was performed in different stages of MFC operation to reveal the potential changes in microbial electrochemical activities⁶³. Figure 14A-E shows the temporal changes of cyclic voltammograms in each of the operation condition on day 60 (Stage I, all operated under 1000 Ω), day 90 (30 days after shifted to respective harvesting regimes in stage II), and day 114 (54 days after shifted to respective harvesting regimes in stage II).

All curves in stage I are similar with midpoint potentials at 380 ± 20 mV and currents at 3.5 ± 0.5 mA. The peaks mean the highest electron transfer rate. The duplicate reactors showed similar profiles so only one profile is shown in Figure 13. Figures A1-5 (appendix) show the first derivative of CVs (DCVs) for all the scenarios, which indicates more clearly the midpoint potentials. The midpoint potential on the oxidation curve indicates the redox reaction and electron transfer occurred at the anode at that potential.

When the reactors were switched to different harvesting regimes, the redox reaction profiles changed very differently. The MPP-H reactors showed the highest power output among all reactors, and its midpoint potential shifted negatively from -380 mV to -400 mV by day 90 and further down to -450 mV by day 114. The corresponding peak current almost tripled from increased 3.5 mA in stage I to 9.8 mA on day 90, and it further increased to 15 mA by day 114. This trend indicates a clear increase in electron transfer rate which is supported by other results as well.

Current increase was also observed in MPP-R reactors but to a lesser scale. The peak current increased from 3.2 mA to 5.5 mA, which was accompanied by the shift of midpoint potential from -380 mV to -400 mV. Interestingly, the CV profile at day 114 showed the limited current never reached a plateau, indicating a midpoint potential could not be identified. This has been

reported before and was hypothesized due to the mix of electroactive cytochromes with different midpoint potentials involved in electron transfers especially in mixed culture biofilms. Other studies also suggested if the dominant species is *Shewanella*, the electron transfer may happen at the midpoint potential higher than the scan range⁶⁴. However, it is unlikely that *Shewanella* was the dominant species in this study, because even though microbial community was not analyzed, the same inoculum was used in our recent study and *Geobacter spp.* was found to be the main electroactive bacterial species⁶¹.

For MCP-H, higher anode midpoint oxidation potential was observed, which is consistent with reference electrode measurement. The current in Stage II was higher than stage I but not significant as compared with MPP-H. For MCP-R and MVP-R the midpoint potential shifted negatively at the beginning of stage II (from -400 mV to -450 mV), but it kept stable since after. However, the current decreased in both cases, indicating slower electron transfer by the biofilm. For MCP- R the CV did show higher current (8.2 mA) at a similar midpoint potential, because the resistor was changed from 1000 Ω to 33 Ω . Similar results were reported in DCVs by previous studies⁶⁵ when reactors were acclimated with high resistance but switched to lower resistance. For MVP-R, it was not clear why the initial current increased after the resistor changed from 1000 Ω to 2200 Ω , but after stabilization the end point current dropped to a similar point as the one in Stage I. The narrower and more negative midpoint potentials presented in MVP-R (2200 Ω) DCVs were also observed in DVCs in our previous study when using high external resistors (Figure A5B and A5C).⁶⁵

The MPP-H condition showed very high current peaks over a narrow anode potential range (-500 mV to -400 mV). This is because the anode potential in MPP-H was maintained between -400 mV and -380 mV by the harvesting circuit. Similarly, MCP-H peak was over broader and

positive anode potential range (-473 mV to -330 mV) than MPP-H, with the circuit controlling the anode potential between -220 mV to -340 mV. These voltammogram profiles are very similar as the CV graphs shown by Commault, et al.,⁶⁶ when they fixed the anode potential at -0.25 V. The control of MFC voltage via energy harvesting generates a mechanism to stabilize the redox potentials closer to the set anode potentials and therefore resulted in narrower fluctuation as compared with the self-regulated resistor scenarios.

3.3.4 Active harvesting indeed boosted electron transfer and system performance

Table 1 summarizes the average performance data of different reactors operated in various harvesting conditions. It is clear that active harvesting approach significantly increased system output no matter which operational point was desired. For reactors operated at MPP, the MPP-H showed the highest power of 0.38 mW, which was 81 % higher than MPP-R and up to 375 % higher than other reactors. This is partially reflected by the lower anode potential obtained at MPP reactors. All reactors showed higher than 94% organic removal as brewery wastewater is a easily biodegradable substrate, but the removal rates ranged from 24 to 72 hours as shown in Figure 13. The MCP-H reactor obtained the highest CE of $85 \pm 10\%$ as hypothesized, because higher conversion was gained from organics to current. The MCP-R didn't show higher CE due to the failure of the cathode. The MPP reactors showed lower CE than MCP due to their different operational goal, but MPP-H showed higher CE than MPP-R presumably due to the higher electron transfer rate regulated by the active harvesting circuit. The MVP reactor showed the lowest CE due to the low current. The CV data also confirm that active harvesting increased the biofilm electron transfer activities compared with passive resistors when operated at the same polarization point.

Table 1 Summary of key results obtained in this study.

Scenario	Power (mW)	Anode Potential (mV)	COD removal (%)	CE (%)
MPP-H	0.38	-390	94±1	60±10
MCP-H	0.19	-277	94±0.5	85 ±10
MPP-R	0.21	-429	95±1	41±2
MCP-R	0.09	-160	95±3	27±5
MVP-R	0.08	-290	95±2	10±1

This study demonstrates that the active harvesting approach is very effective in maximizing the performance of MFCs at different operational points. This expands the knowledge from focusing on MPP operation to broader applications of MFCs such as MCP operation for accelerated organic removal, chemical production and desalination. More studies are needed to reveal the potential community structure changes during different operations. Pure culture studies will also be very helpful to elucidate the exact electron transfer mechanism shifts during different harvesting scenarios. While active harvesting showed much higher performance in MFCs, more work on system integration and scale up are needed to realize the potentials for operating practical scale systems.

The information presented in this chapter has been published in a scientific journal; **Lobo, F. L., Wang, X., Ren, Z. J.** “Energy harvesting influences electrochemical performance of microbial fuel cells” *Journal of Power Sources*, **2017**, 356, 356-364.

CHAPTER 4

ACTIVE HARVESTING LEADS TO DISTINCT MICROBIAL COMMUNITY STRUCTURE IN MICROBIAL ELECTROCHEMICAL CELLS

4.1 Introduction

The economic, environmental and social impacts of fossil fuel exploration, production and consumption are driving the development of renewable energy alternatives, but to replace fossil fuels a variety of energy sources are needed to meet different needs. The microbial electrochemical technology (MET) has been intensively researched in recent years as a clean, distributed and renewable energy source, because it offers a simple and direct method for converting the chemical energy of embedded in biomass (such as wastewater and sediments) into electricity or fuels while at the same time achieving environmental cleanup goals^{6,67,68}. The core uniqueness of MET process comes from the electroactive bacteria used in these systems. Such microbes are capable of catalyzing the conversion of chemical energy that is stored in biodegradable substrates into direct current via anaerobic respiration of the anode^{8,10,69}. Despite recent advancements on materials, reactor configurations and operations, the energy output of MET systems is still low², which is not sufficient for real world applications^{12,70}.

A microbial fuel cell (MFC) is a classic MET reactor, and it directly harvests electrons to generate electricity from the substrate. An MFC's power output is directly related to the electron transfer rate catalyzed by electroactive bacteria on the MFC anode, but very limited information is available on how energy harvesting influences microbial community structure and metabolisms. Previous studies showed that proper enrichment of electroactive bacteria improved MFC current generation, and energy harvesting systems using capacitors, charge pumps, and

boost converters enabled energy storage and utilization¹². These passive loads showed impacts on anode biofilm thickness and community structure by influencing the anode potential^{56,71}, but the electrochemical performance reached to a plateau once biofilm reached to a level of electron transfer rate. However, because an MFC is a dynamic system that its internal resistance and power density curve vary constantly with changes of microbial activities and operational parameters, pulse-shaped harvesting using maximum power point tracking (MPPT) techniques showed much higher efficacy by tracking the MPP and maintaining energy harvesting at the peak level in real-time^{20,43,46}. Compared with traditional circuits that passively receiving electrons from the reactor, such process actively extracts energy from the MFC at any operating point, especially at the peak power point to maximize energy production and therefore extracts higher energy by an order magnitude^{15,68}.

More importantly, though no study has proved it, such dynamic energy harvesting approach is hypothesized to dramatically shape microbial ecology and metabolisms, because it creates a selective pressure on the microbial community to regulate respiratory pathways for more efficient electron transfer and ATP synthesis. The microbial electrogenic activities and metabolisms may be significantly changed, as bacteria shift to more efficient extracellular electron transfer pathways to accommodate the higher demand of electrons⁸. Mixed culture community structure may evolve that those microbes with the most efficient extracellular electron transfer mechanisms become dominant, and more efficient microbial consortiums maybe formed for more efficient respiration of substrates^{68,72}. In the meantime, the feedbacks of external energy harvesting on biocatalysts activity needs to be characterized and a balanced approach needs to be conducted to maintain a stable reactor performance and sustainable power production.

In this study, we characterized for the first time how MFC electrochemical performance was changed and microbial community structure was shifted under different energy harvesting scenarios, even though the same substrate and microbial inoculum were used. Both active harvesting and passive resistor loads were used to provide high power or high current conditions, and comprehensive analysis on microbial ecology was performed to reveal the unique distribution of microbial communities under active harvesting conditions compared with traditional passive approaches.

4.2 Materials and Methods

4.2.1 Reactor construction and operation

Cubic single-chamber MFCs were constructed using polycarbonate, and the empty volume of each MFC chamber was 28 mL. Each MFC reactor contained a heat-treated graphite brush as the anode and a carbon cloth air-cathode (7 cm², Fuel Cell Earth) with manufacturing procedure described in previous studies^{13,58}. Diluted (1:10) brewery wastewater from a local brewery (Boulder, CO) was used as the sole substrate during the experiment, and 50 mM phosphate buffer solution (PBS, NaH₂PO₄·2H₂O 3.32 g/L; Na₂HPO₄·12H₂O 10.32 g/L; NH₄Cl 0.31 g/L; KCl 0.13 g/L) was used to amend the pH⁶⁰. The final substrate electrolyte used in the study contained 1,800 mg/L COD, 938 mgL⁻¹ TKN, and 1,860 mgL⁻¹ PO₄³⁻. All MFCs were operated in duplicate in batch mode at room temperature, and fresh medium was refilled at the end of each batch cycle.

All reactors were operated in the same condition at the beginning till repeatable voltage profiles were obtained. After that, linear sweeping voltammetry (LSV) with a 1 mV/s scan rate was performed on each reactor to determine the key operating points of maximum current points

and maximum power points³⁷. The reactors were then divided into 4 groups, with each group containing duplicate reactors operated in 1 of the 4 following scenarios: maximum power with active energy harvesting (PH), maximum current with active energy harvesting (CH), maximum power with passive resistor (PR), and maximum current with passive resistor (CR). The scenarios can be further divided into 2 groups: active, where the MFC was connected to an energy harvesting circuit being controlled to track maximum power (PH) or current (CH) and the MFC energy was used to charge a battery, and passive, where resistor with values that would achieve maximum power (PR) or current (CR) were connected in parallel with the MFC, dissipating the MFC energy as heat.

For active harvesting scenarios, the circuits were controlled to track maximum power (PH) or current (CH) by operating voltages that were determined using the LSV results shown in Figure 15. The LSV results were used to identify the maximum power point and correlate this point with a voltage, V_{MPP} (maximum power point voltage). Hence, the MFCs running on PH mode would be controlled to have a constant voltage at V_{MPP} using an integrated energy harvesting nano-power management circuit with pulse-frequency modulated (PFM) boost converter/charger (bq25505, Texas Instruments Inc.)⁷³.

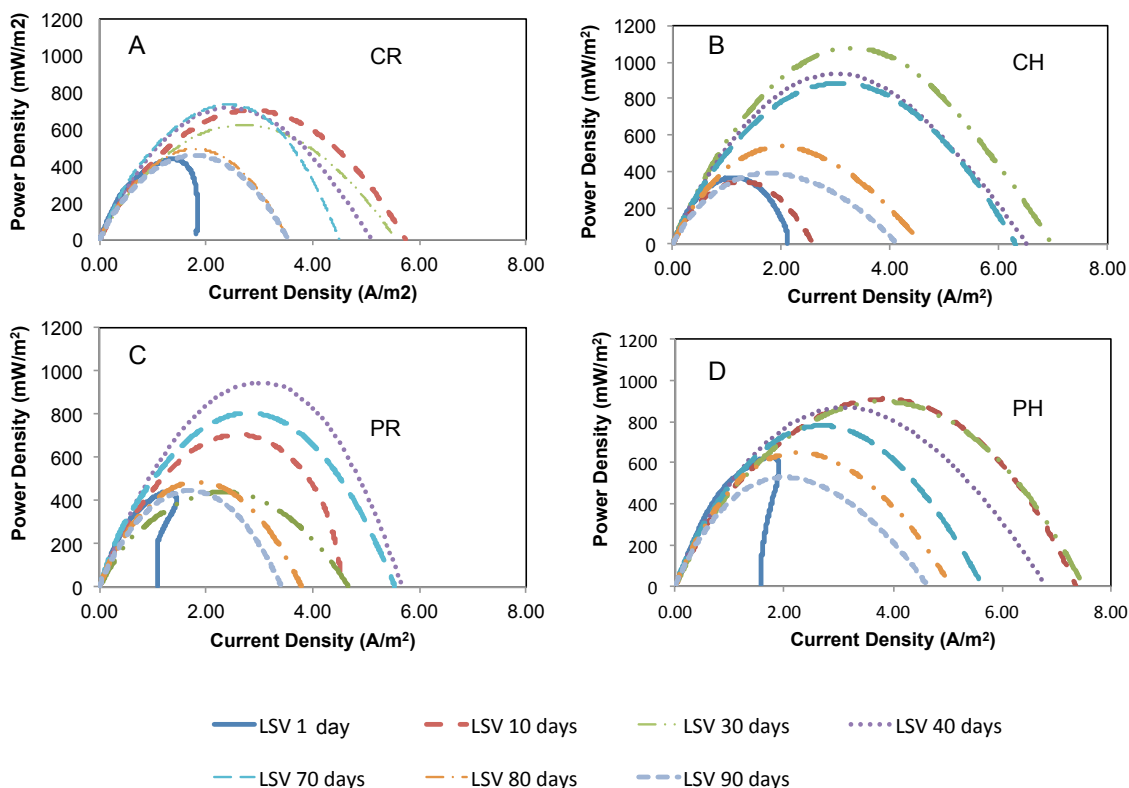


Figure 15 Power density profiles obtained by linear sweep voltammetry on day 1, 10, 30, 40, 70, 80 and 90 of reactor running at (A) high current using resistor (CR); (B) high current using energy harvesting circuit (CH); (C) the maximum power using resistor (PR); (D) the maximum power using energy harvesting circuit (PH).

Since the maximum current would be given at 0 V, an approximation of V_{MCP} (maximum current point voltage) between 80 mV to 100 mV was used to give the highest possible controlled current by the circuit, which was 85% of the short circuit current. A programmable maximum power point tracking (MPPT) unit is embedded in the circuit and keeps sampling the open circuit input voltage every 16 seconds and calculates V_{MPP} as 50% or 80% of the open circuit voltage. In this study, because on MFCs, the open circuit voltage takes more than a few seconds to reach its real value, the programmable MPPT was set using a reference voltage at either V_{MPP} or V_{MCP} from LSV results, and this control was able to maintain a constant MFC voltage on the desired

point of the power density curve. The energy extracted from each MFC was stored in polymer lithium ion batteries (840mAh, SparkFun Electronics[®]).

For the passive energy harvesting conditions, the LSV results were used to identify the maximum power point and correlate this point with a voltage (V_{MPP}) and current (I_{MPP}), so the resistor value could be calculated ($R_{MPP}=V_{MPP}/I_{MPP}$). The maximum current point was determined to be at 85% of the short circuit current to be comparable to CH scenario, and the resistor value was calculated using the maximum current point voltage (V_{MCP}) and current (I_{MCP}).

4.2.2 Analyses

The individual potential of each anode and cathode was measured at each batch using Ag/AgCl reference electrodes (RE-5B, +0.210V versus standard hydrogen electrode, 25 °C). Reactor voltages were recorded using a data acquisition system (Keithley, OH). Cyclic voltammetry (CV) was performed before and after batch operations in different stages. The potential range for CV was determined as -0.7 to 0 V vs. Ag/AgCl with a scan rate 1 mV/s based on previous results⁶¹. First derivative CV (DCV) was derived from turnover CV to determine the changes in each peak value. The main oxidation peak in DCV was fitted to Gaussian function to separate overlapped peaks. LSV tests were performed using the same potentiostat with a scan rate of 1 mV/s with either the anode or the cathode as the working electrode, depending on characterization purposes. Chemical oxygen demand (COD) before and after each batch was measured using the standard method with a spectrophotometer (DR 3900, Hach Co., Loveland, CO, USA). Coulombic efficiency (CE) was determined using Equation (7) (Chapter 3), where $M = 32$ (molecular weight of oxygen), F is faraday constant, $b = 4$ is the number of electrons

exchanged per mole of oxygen, v_{an} is the liquid volume of anode compartment, and ΔCOD is the change in COD over time^{36,62}.

4.2.3 Bacterial Community Structure Analyses

The bacterial community structure was analyzed by using high-throughput 454 GS-FLX pyrosequencing of the 16S rRNA. Biofilms of the anode and cathode as well as suspension samples were collected from the reactors after 60 and 90 days of operation. Total genomic DNA was extracted using a PowerSoil DNA Isolation Kit (MoBio Laboratories, Inc., Carlsbad, CA) according to the manufacturer's instructions. The pyrosequencing and bioinformatics analysis were carried out according to previously described methods⁷⁴⁻⁷⁶.

4.3 Results and Discussion

4.3.1 Energy harvesting significantly boosted MFC performance in current and power production

Figure 15 shows the evolution of power density profiles overtime under 4 different operational scenarios. Overall the reactors operated under active harvesting (CH and PH) showed much higher current and power output as compared with those run under passive resistors (CR and PR). When operated at high current mode, the maximum current density and power density obtained at CH was 6.95 A/m² (day 40) and 1078 mW/m² (day 40), respectively. These numbers were 23% and 47% higher than those obtained at CR reactors (Figure 15A, 15B). Similarly, the PH reactors showed 32% higher maximum current density (7.48 A/m², day 30) than PR reactors (5.68 A/m²). Similar maximum power output (947 mW/m² vs 909 mW/m²) was observed in PH and PR reactors during stable operation, which is understandable as the harvesting circuit controlling PH

reactors tracks and operates the reactor at MPP in real time, so during stable conditions, similar MPP were obtained in all reactors. However, because PH was operated constantly under active MPP control, the overall electrons harvested in PH was much higher than PR (195 Coulombs vs 110 Coulombs), and the PH reactor showed more stable performance as well. (Figure A6-7). Plus, no real energy was stored in PR or CR reactors as it was dissipated as heat on the resistor, rather PH and CH reactors stored the electrical energy in rechargeable batteries. Time course profiles show the reactors took different times to start but almost all reactors reached to the peak performance at around 30-40 days (Figure A6-7). Performance declined after reaching to the peak, primarily due to cathode fouling observed in most reactors. This phenomenon was reported when real wastewater was used in air-cathode MFCs, and periodic physical cathode cleaning was performed every 30 days⁷⁷. Microbial biofilm samples were taken by cutting a few carbon fibers from anode after 60 days, which also caused reactor performance decline.

Figure 16 compares the average anode potential, maximum current, Coulombic efficiency, and power outputs for reactors operated in 4 different conditions. While PR and CR showed similar average anode potential (-164 ± 1 mV and -161 ± 9 mV, respectively), reactors under active energy harvesting showed much lower anode potential, with PH at -423 ± 2 mV and CH at -238 ± 13 mV, respectively. These results indicate that active harvesting improved anode biofilm electron transfer, which in turn decreased anode potential and therefore led to higher power output (Figure 16A). Reactors operated under active harvesting conditions (CH and PH) showed higher current output than those operated in external resistors mode, in which energy harvesting improved current production by 50% (Figure 16B). Similarly, active harvesting mode led to much higher Coulombic efficiency (CH and PH). The CH reactor obtained the highest Coulombic efficiency $77 \pm 29\%$, which is followed by PH ($52 \pm 5\%$), while CR and PR only

obtained efficiencies ranged from 26-32%. This is exciting as higher current means higher conversion efficiency from organic substrate to electrical circuit as well as faster wastewater treatment. In terms of power output, PH stands out by producing a highest power of 0.66 mW, which is multiple times higher than other operational conditions. This is consistent with previous findings that when MFC is operated in the maximum power mode by active harvesting, much higher power was obtained compared with other passive approaches⁷⁸.

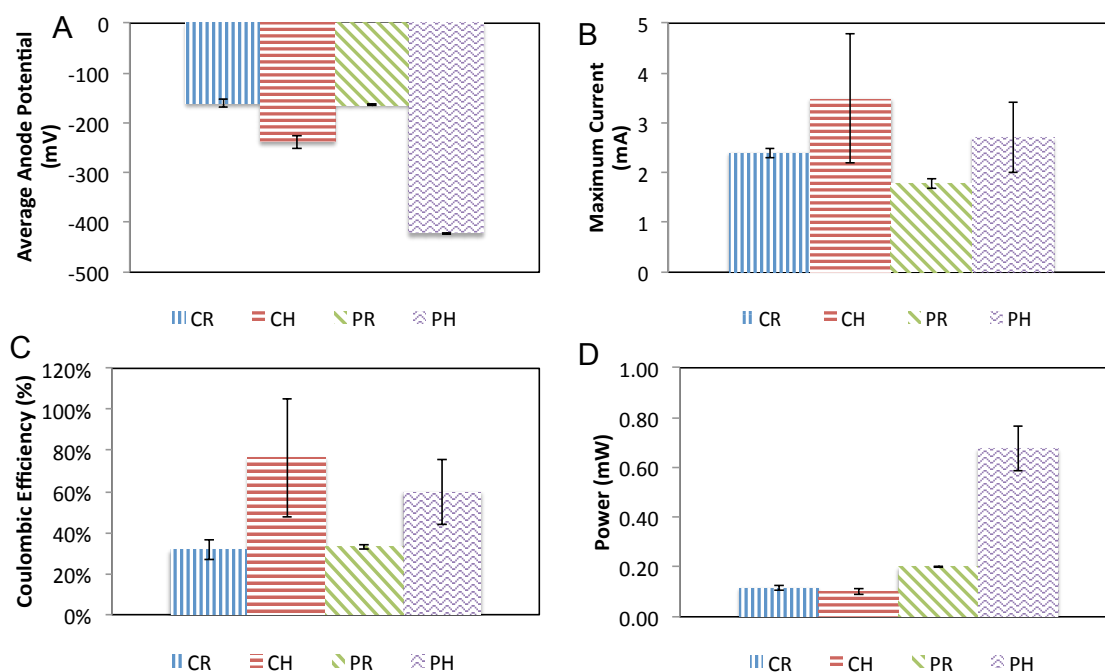


Figure 16 (A) Average anode potential, (B) Maximum current output, (C) Coulombic Efficiency and (D) Power output from CR, CH, PR and PH reactors during their peak performance period.

4.3.2 Electrochemical responses were different under various energy harvesting scenarios

Figure 17 shows the profiles of cyclic voltammetry of the reactors operated under four scenarios on day 30, 40, 50, 70, 80, and 90. The CH reactors demonstrate the highest current or electron transfer rate of 12.48 mA, which is nearly double the current obtained in PR reactors (6.75 mA) (Figure 17B, 17C). This is expected as CH operation is designed to extract more

electrons to the anode. The reactor midpoint potentials did not shift over the 90-day of operation, but a current drop was observed after microbial sampling at day 60. Reactor midpoint potentials in energy harvesting reactors (PH and CH) were similar and low (~ -414 mV vs. Ag/AgCl). Because a mixed culture of microorganisms was used, the electroactive cytochromes involved in extracellular electron transfer were mixed and difficult to be identified, but this low midpoint potential was discussed in previous studies similar as multiple cytochromes *OmcZ*, *OmcS* and *OmcB*⁷⁹. The CR reactor showed a midpoint potential of -367 mV, which is close to the potential of *PpcA* cytochromes⁷⁹. In contrast, PR operation led to the highest midpoint potential of -281 mV, which was rather close to the potential of some known electron shuttles like ACQN quinones (-281 mV) and pycyanine phenazines (-310 mV)⁸⁰. Again, even though the results show an interesting trend, it is difficult to directly connect the midpoint potentials and CV profiles with specific microbial communities and electron transfer pathways as a mixed culture was used.

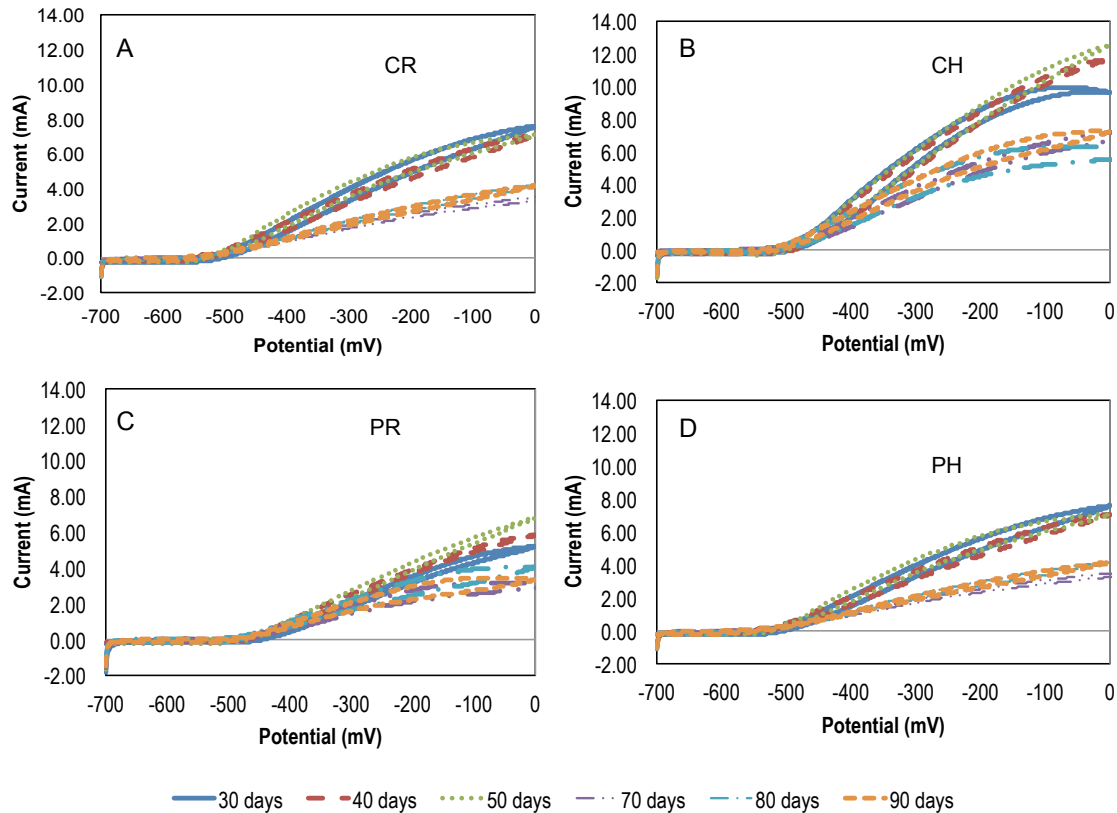


Figure 17 Cyclic voltammetry on day 30, 40, 50, 70, 80, and 90 of reactor running at (A) high current using resistor (CR); (B) high current using energy harvesting circuit (CH); (C) the maximum power using resistor (PR); (D) the maximum power using energy harvesting circuit (PH).

4.3.3 Distinct microbial community structures under different conditions

The most interesting findings in this study involve the distinct microbial community distribution found in reactors operated under different energy harvesting conditions. Using high-throughput culture-independent 454 GS-FLX pyrosequencing, different bacterial communities were identified on the anode, cathode and the in the solution of MFCs. From 48 generated libraries, a total of 1,785,703 high-quality 16S rRNA gene sequences with an average length of 464 bp were obtained. These sequences were assigned into 619 OTUs. The Good's Coverage estimators indicate that the sizes of libraries were sufficient to cover 99.7–99.9% of the bacterial

communities. Multiple samples were taken in each reactor in different stages of operation (60 days and 90 days). The samples taken from each duplicate reactor on day 60 were marked as sample 1 and 2, and those taken on day 90 were marked as sample 3 and 4. Therefore for each operation condition, the samples are marked as CH/PH/CR/PR 1-4.

Very interestingly, distinct clusters of anode bacterial communities were found under different energy harvesting conditions by Weighted Fast UniFrac Principal Coordinates Analysis (PCoA) (Figure 18A). The anode biofilm samples are distributed into four distinct and separated clusters based on each harvesting scenario as shown in Figure 17A. The bacterial community structure associated with CH (green) is very distant from the communities in other scenarios. This is related to the results that CH operation showed the far highest current production and Coulombic efficiency. PH (blue) and CR (red) are close to each other, and they also showed comparable current outputs (2.7 ± 0.7 mA and 2.4 ± 0.1 mA, respectively) (Figure 15B). However, both scenarios showed great difference in the anode potential, which have been reported before as criteria to select bacteria in microbial fuel cells⁸¹. The community structure associated with the PR (orange) is dispersed and distant from other scenarios, and correspondingly the PR reactors had the lowest current production and Coulombic efficiency. These findings demonstrate that even using the same substrate and microbial inoculum, the bacterial community drastically diverged under different energy harvesting operations.

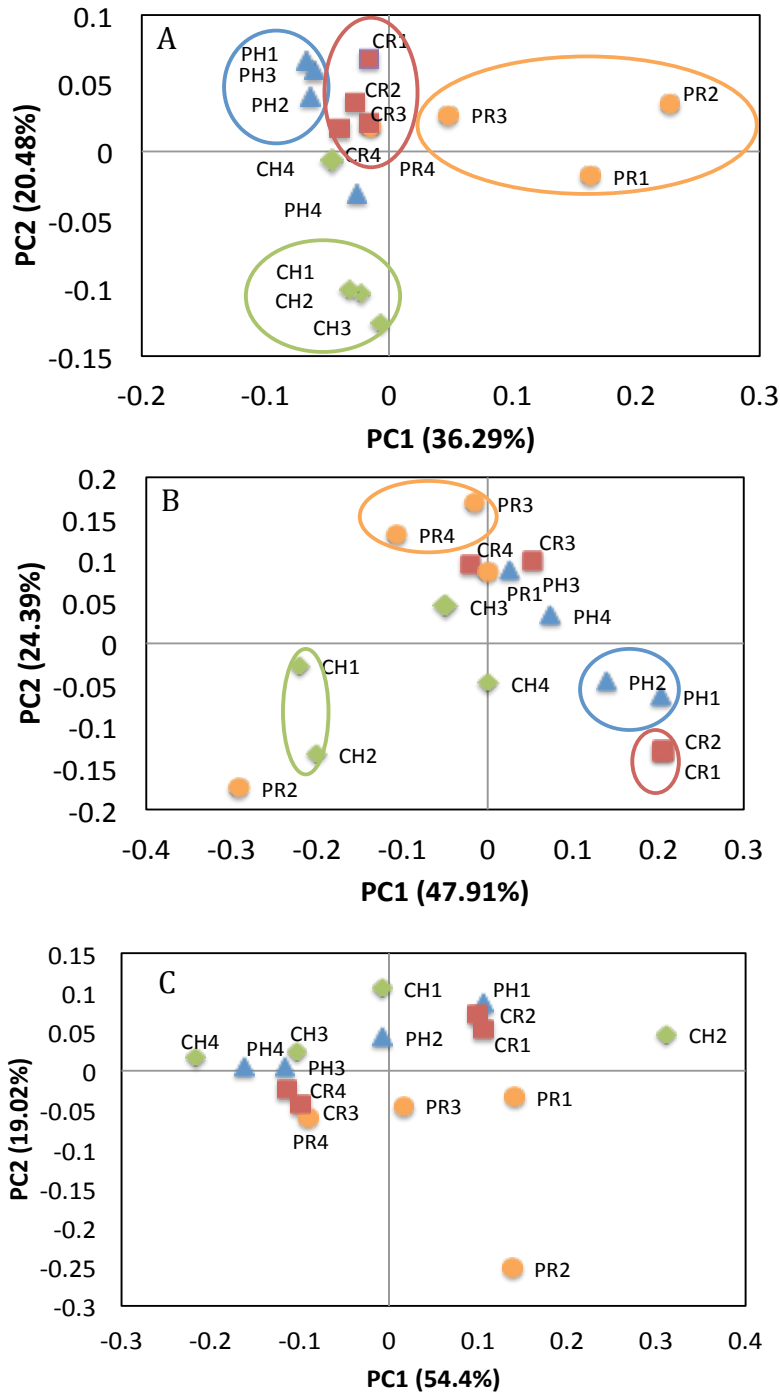


Figure 18 Weighted Fast UniFrac, Principal Coordinates Analysis (PCoA) of the bacterial communities in MFC reactors on (A) the anode biofilm samples (B) the cathode biofilm samples, and (C) solution samples on the basis of phylogenetic lineages. The characters of “1” and “2” in abbreviations of samples indicate duplicate samples collected on day 60, and “3” and “4” indicate duplicate samples collected on day 90.

In contrast, less clear distribution is found in cathode and solution communities. Four clusters could be identified based on each harvesting scenario a) CH1 and CH2; b) PH1 and PH2; c) CR1 and CR2; and d) PR3 and PR4, but because the cathodes were periodically cleaned to reduce air-cathode fouling, the community was significantly affected by these manual operations. The microbial community in solution samples are all mixed together without an identifiable trend (Fig. 17C). This is expected as fermentative bacteria dominated in all reactors with a presumable role of breaking down sugars into carboxylic acids and other fermentation products.

Nine bacterial phyla were observed from twelve libraries (Figure 19A). The most dominant sequences on the anode belonged to *Bacteroidetes* (28-42%), *Firmicutes* (13-37%) and *Proteobacteria* (13-54%). The cathode samples mainly consisted of *Bacteroidetes* (22-37%) and *Proteobacteria* (39-73%). The solution samples contained relative abundance of 27-33% in *Bacteroidetes* and 41-51% in *Proteobacteria*. This microbial distribution is similar as previous MFC studies in treating brewery wastewater^{82,83}. Other minor bacterial phyla include *Actinobacteria*, *Elusimicrobia*, *Euryarchaeota*, and *Synergistetes*. Compared with other scenarios, the best performing CH reactors in terms of electrochemical activities showed higher percentage of *Firmicutes* (37%) and lower percentage of *Proteobacteria* (13%). This is believed to be related to the fermentative substrate used in this study, because the high current generated in such reactors demanded faster conversion of sugars into commonly desired carboxylic acids and alcohols by electroactive bacteria^{84,85}.

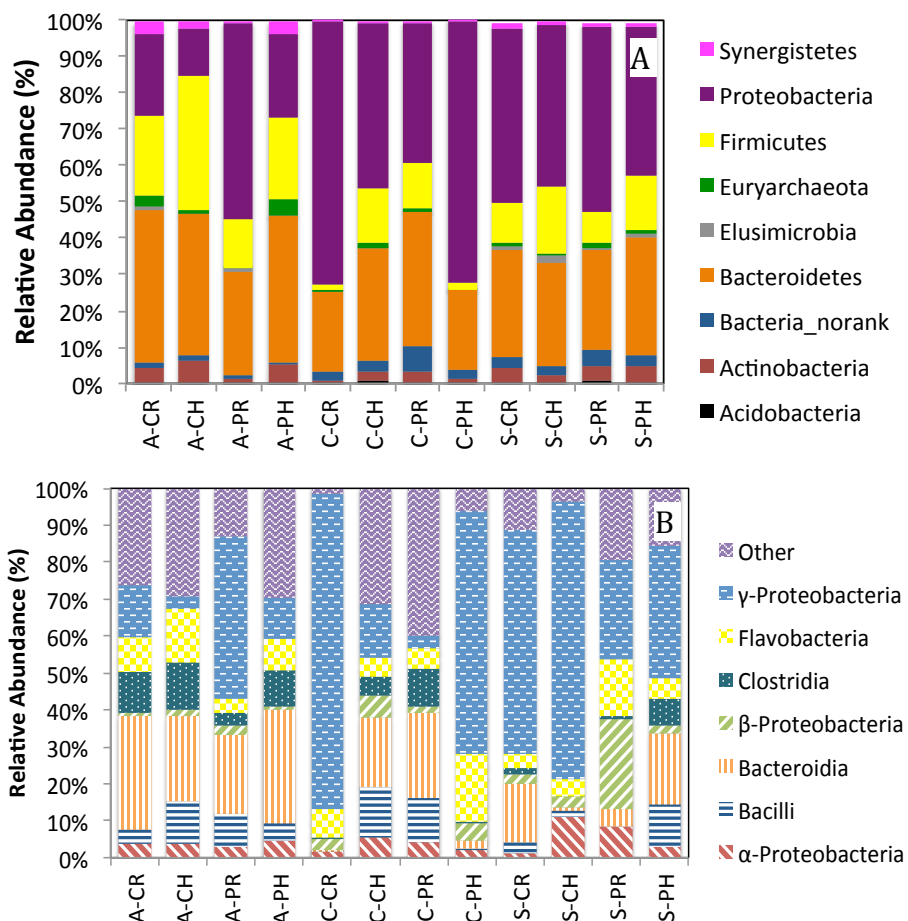


Figure 19 Taxonomic classification of bacterial DNA sequences at (A) phylum level and (B) the most dominant class level distribution (class level less than 10% is classified as other) A- indicates anode samples, C-indicates cathode samples and S- indicates solution samples.

At the class level (Figure 19B), the sample distribution includes *Gamma-Proteobacteria* (3-85%), *Alfa-Proteobacteria* (3-11%), *Beta-Proteobacteria* (1-24%), *Bacilli* (0-14%), *Clostridia* (0-13%), *Bacteroidia* (0-31%) and *Flavobacteria* (4-18%). On the anode samples, the best performing scenario (CH) showed a class distribution of 23% *Bacteroidia*, 15% *Flavobacteria*, 13% *Clostridia* and 11% *Bacilli*, while the worst performing scenario (PR) showed much higher distribution of *Gamma-Proteobacteria* (44%), *Bacteroidia* (21%), and *Bacilli* (9%). The scenarios of CR and PH, which presented similar performance in terms of current and efficiency, also showed similar class distribution which was dominated by *Bacteroidia* (31%), *Gamma-*

Proteobacteria (11-14%), and *Clostridia* (10-11%). On the cathode, the scenarios CR and PH were dominated by *Gamma-Proteobacteria* (66-85%) and Flavobacteria (9-18%), while CH reactors contained well-distributed community among *Gamma-Proteobacteria* (15%), *Bacteroidia* (19%) and *Bacilli* (14%). For solution samples, *Gamma-Proteobacteria* dominated in the reactors designed for high current scenarios CR and CH (60-75%). This is hypothesized to relate to the anoxic condition due to faster current flow and is discussed at the genus level shown in Figure 20.

The genus level characterization further illustrates the differences and diversity of the functional communities. Figure 20 presents a heat map that shows the relative abundance of different bacteria genera found in different samples. *Bacteroides* and *Dysgonomonas* were found abundant in all anode samples, which is understandable as it is an important fermenter known for sugar catabolism with major products of hydrogen and lower fatty acids such as acetate and succinate⁸⁶. In addition, for reactors operated under active harvesting scenarios (CH, PH), the abundance of *Lactococcus* and *Clostridium* were also higher on the anode than those operated using resistors. This is consistent with class level findings and indicates that energy harvesting circuits posed a selective pressure on the anode community as compared with passive resistors. Plus, these reactors showed higher maximum current and Coulombic efficiency (Figure 16), which supports the hypothesis that active harvesting facilitated electron transfer from substrates to the electrode catalyzed by electroactive bacteria. Because almost all known electroactive bacteria utilize simple volatile fatty acids or alcohols as their substrates, it is reasonable to hypothesize the quick consumption of these fermentation products facilitated fermentation process of brewery wastewater and therefore led to higher abundance of fermentative bacteria in these reactors.

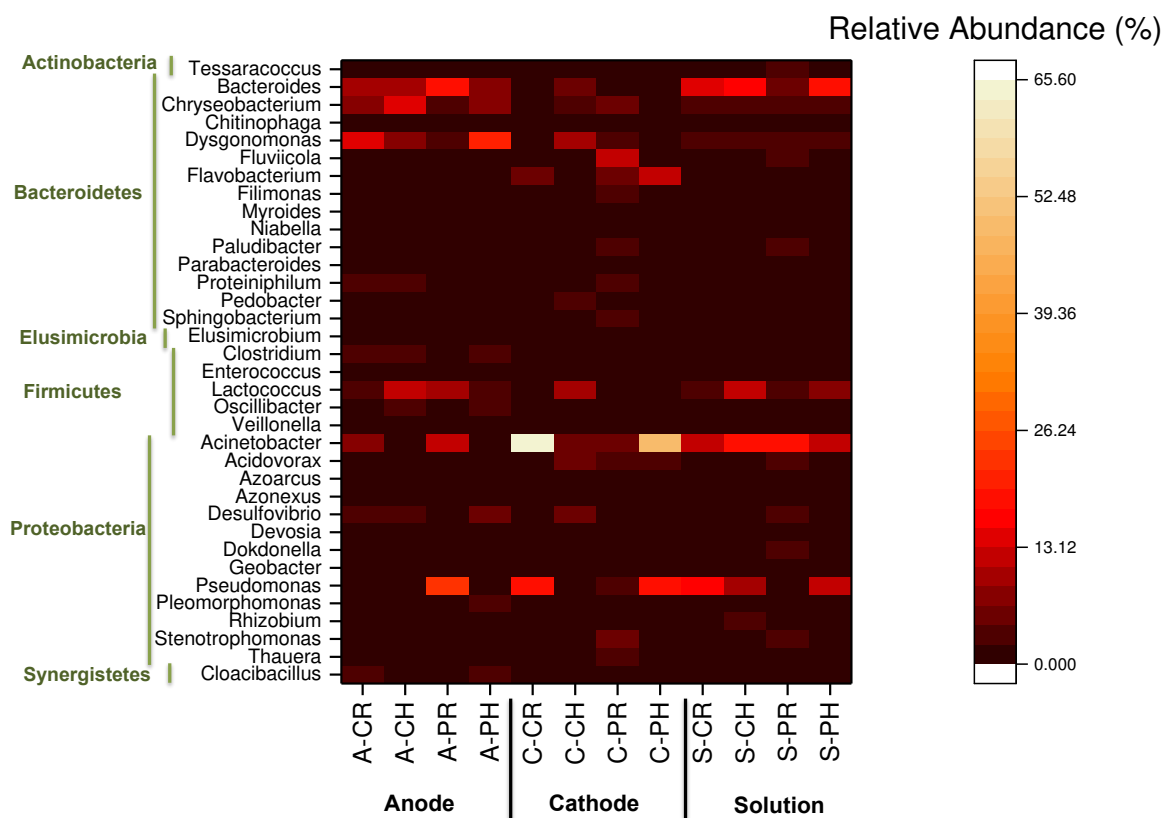


Figure 20 Taxonomic classification of bacterial DNA sequences at the genus level. The genera that are less than 1% of total composition in all libraries were ignored in heat map graph. A- indicates anode samples, C- indicates cathode samples and S- indicates solution samples.

On the other hand, the harvesting reactors (CH, PH) showed relatively higher abundance of *Desulfovibrio* while lower abundance of facultative bacteria *Pseudomonas* and *Acinetobacter* (Figure 20). This correlates with the lower anode potentials of CH and PH reactors observed in Figure 16 and Figure 17. *Desulfovibrio spp.* such as *Desulfovibrio desulfuricans* are anaerobes that possess several low potential cytochrome c proteins, all of which are membrane-bound and have been reported involved in direct extracellular electron transfer to the anode⁸⁷⁻⁸⁹. One study even reported that the electron transfer via cytochrome c of *D. desulfuricans* was more effective than that of *G. sulfurreducens*⁸⁸. In contrast, *Pseudomonas* are facultative and known of performing extracellular electron transfer via excreted mediators such as phenazines^{8,90-92} at

relatively higher redox potential, which supports well the higher midpoint potentials observed in PR and CR reactors. The *Acinetobacter* species are also facultative and have been reported in MFCs with the involvement in oxidation of organic compounds and electricity generation⁹³. It is also interesting that *Geobacter* spp. was not found dominant in any of the reactors, rather it only showed a relative abundance less than 2% in all samples. Many studies found that *Geobacter* was dominant in MFC reactors using non-fermentable substrates^{8,49}, while some studies reported the absence of *Geobacter* when using fermentative substrates⁹⁴. This may be associated with the lack of *Geobacter* in the inoculum and the fermentation nature of the substrate used in this study, but it should not conclude that *Geobacter* didn't play a role in these reactors, because the numerical abundance of microorganism in biofilms cannot be necessarily assumed a priori to correlate to their capacities of extracellular electron transfer⁹⁵.

4.3.4 Statistical analysis shows the correlation matrix between electrochemical activities and microbial community diversity

Table 2 shows a correlation matrix (coefficient and significance level) between the maximum current, electroactive bacterial activity (anodic current showing on the CV), anode potential, midpoint potential and anode biodiversity (Shannon index, H'). It can be seen that the electroactive bacterial activity is positively correlated with the maximum current ($P < 0.01$) but negatively correlated with midpoint potential ($P < 0.001$). On the other hand, midpoint potential was negatively correlated to the maximum current and electrochemical activity ($P < 0.001$). In addition, anode samples diversity H' index was negatively correlated with midpoint potential of CV ($P < 0.001$) but showed no correlation with the anode potential, which is consistent with previous findings⁸¹. The Shannon diversity index (H') indicates the information of richness and distribution of each microbial species. Overall, the diversity index shows the anode samples had

the highest biodiversity (average $H' = 4.04$ for CR, $H' = 3.71$ for CH, $H' = 3.85$ for PR and $H' = 3.83$ for PH) compared with cathode and solution samples. Because raw brewery wastewater was used as the sole substrate, fermentation was a major reaction during organic degradation, which contributes to the diversity on the anodes and in the solution (average $H' = 3.57$ for CR, $H' = 3.07$ for CH, $H' = 3.68$ for PR and $H' = 3.52$ for PH). Cathode samples showed lower diversity with *Acinetobacter* the dominate species on most cathodes.

Table 2- Correlation Matrix (Coefficient and Significance Level) between the maximum current, electroactive bacterial activity, anode potential, midpoint potential and anode sample biodiversity (Shannon index H') parameters ^a

	Maximum current	Electroactive bacterial Activity	Anode potential	Midpoint potential	Anode diversity
Maximum Current	-	0.99 0.006 ^b	-0.07 0.005 ^b	-0.68 0.000 ^c	0.04 0.145
Electrochemical performance	-	-	-0.03 0.004 ^b	-0.61 0.000 ^c	-0.07 0.010 ^b
Anode potential	-	-	-	0.64 0.128	0.09 0.004 ^b
Midpoint potential	-	-	-	-	-0.38 0.000 ^c

^aCorrelation: Strong (positive, 0.5 to 0.1 or negative, -1.0 to -0.5), Medium (positive, 0.3 to 0.5 or negative, -0.5 to -0.3), Small (positive, 0.1 to 0.3 or negative, -0.3 to -0.1, None (positive, 0.0 to 0.1 or negative, -0.1 to 0). Sample number = 48. ^b $P < 0.01$. ^c $P < 0.001$.

This study reveals that active energy harvesting not only improved MFC performance in terms of current production and Coulombic efficiency, it greatly shaped the anode microbial community by creating a selective pressure to facilitate substrate conversation and electron transfer to the anode. The anaerobic microbial consortia of fermentative bacteria and electroactive bacteria

were found dominant in best performing reactors with energy harvesting circuit, and the relatively low abundance of known electroactive bacteria compared with fermentative bacteria in these reactors suggest that anode electron transfer may not be the rate limiting process, rather the overall conversion rate involving both fermentation and respiration determines system performance. This confirms the hypothesis that the cooperation of differential functional bacteria is a key to convert complex organics in brewery wastewater into electrons on the anode, and active harvesting helped shape the community distribution. While this study demonstrates the critical role harvesting plays in improving MFC performance and influence microbial community, the interactions among different functional species need to be further investigated. Metagenomic tools and microbial physiology tools will help address some key questions such as the mechanisms of interspecies electron transfer, the interactions between microbial cells and the electrodes, as well as levels of gene expressions that are related to the syntrophy among the different functional groups.

CHAPTER 5

LOW-ENERGY HYDRAULIC FRACTURING WASTEWATER TREATMENT VIA AC POWERED ELECTROCOAGULATION WITH BIOCHAR

5.1 Introduction

Produced and flowback waters are the largest byproducts associated with oil and gas exploration and production. Approximately 21 billion barrels of produced water is generated each year from about 900,000 wells in the United States alone ⁹⁶, and more than 90% of the water is currently deep-well injected. Technologies are being developed and implemented to treat and reuse this type of wastewater onsite, so the negative effects of seismic activity, traffic congestion, increased water demands, and potential contamination resulting from underground injection can be alleviated, and operational cost can be reduced. Electrocoagulation (EC) is among these technologies that are being used to remove suspended solids especially emulsified oil particles from water so it can be reused for re-fracking. Compared with traditional chemical coagulation, EC is more attractive due to the lack of chemical required, less sludge production, and simpler operation needs ⁹⁷⁻¹⁰⁰. However, traditional EC process consumes 0.5 to 6.25 kWh/m³ of electricity depending on water conductivity and other factors, and the conversion from AC to DC at high current condition is expensive ¹⁰¹. For example, a pilot study showed a 1 m³/h EC reactor required 2.25 kWh/m³ to reduce oil concentration from 478 mg/L to 20 mg/L from produced water with conductivity of 1000 mS/m ¹⁰². In addition, the current EC process suffers an electrode passivation problem, leading to short operation time and high cost ¹⁰¹. Such challenges are especially difficult when EC is used in produced water treatment, because the availability of electricity is limited and system maintenance is expensive.

This study presents a new method of EC operation to significantly reduce energy consumption and electrode passivation by introducing alternating current (AC) and low-cost granular biochar. Recent studies compared the energy consumption between DC and AC powered EC for cadmium, copper, iron, fluoride and arsenate removal¹⁰³⁻¹⁰⁷, and it was found that AC powered EC used 10-66% less energy. Studies also found that AC delayed cathode passivation and anode deterioration¹⁰⁸. The addition of adsorptive particles such as granular activated carbon (GAC) can scour the electrode surface to reduce electrode fouling, and the adsorptive nature will improve the removal of particulate and dissolved contaminants¹⁰⁹⁻¹¹¹. The downside of using GAC is the high material cost, considering the price of GAC ranges from 800–2500 US\$/ton. To maximize the energy saving while reducing cost, we integrated the AC-EC process with granular biochar as adsorptive material. The recently developed biochar is derived from local waste biomass from agricultural and forestry residues, and its pyrolysis manufacturing process is much easier than GAC, so the cost is nearly ten times lower than GAC, in the range of 51 to 381 US\$/ton¹¹². Biochar has been shown as an effective adsorption media for heavy metal and organic carbon removal^{113,114} but has not been widely used in produced water treatment. The system efficacy and energy consumption for treating produced water were compared in DC-EC and AC-EC systems, and the effects of granular biochar were characterized under different doses at 0 g/L, 0.25 g/L and 0.5 g/L.

5.2 Materials and Methods

The produced water samples were collected from a hydraulic fracturing site located in the Denver-Julesburg basin. The characteristics of the water were: pH = 7.6, Turbidity = 400±44 NTU, Total suspended solids (TSS) = 514±47 mg/L; COD = 3,631±69 mg/L, Conductivity =

46.1 mS/cm. The biochar was made using lodgepole pine wood that was thermally converted in a top-lit up-draft (TLUD) gasifier at a highest heat temperature of 1000 °C at a ramp rate of 17°C/min. Detailed biochar carbonization process was described in previous studies by Huggins, et al ^{112,115}. After carbonization the biochar material was crushed and sieved using a 12x40 sieve without any chemical modification, and the sample was washed with distilled water and dried in an oven for 2 hours at 100 °C before use. Based on Brunauer–Emmett–Teller (BET) tests, the biochar has a surface area of 428.6 cm²/g, a total area of 0.52 m², and an average pore diameter of 37.6 Å. The cost of biochar was estimated approximately 0.000504 US\$/m² based on previous studies. An electron scanning microscope image of the biochar is presented in the appendix (Figure A8) ¹¹².

The electrocoagulation system has a working volume of 200 mL and used two 28.16 cm² aluminum electrodes that are 3 mm apart. The experiment was carried out in six different conditions: DC-EC with 0 g/L biochar, DC-EC with 0.25 g/L biochar, DC-EC with 0.5 g/L biochar, AC-EC with 0 g/L biochar, AC-EC with 0.25 g/L biochar, and AC-EC with 0.5 g/L biochar, respectively. Biochar adsorption control without current was performed under 0.25 g/L and 0.5 g/L as well. The experiments were conducted under a fixed voltage of 1.2 V and variable currents using a 3644A DC power supply 0-18V/0-5A. The frequency used in AC-EC process was 3.33 mHz with polarity changed every 5 minutes. The duration of the electrocoagulation operation varied from 30 to 50 minutes in order to achieve 99% turbidity removal, which was the target for produced water treatment. Water samples were settled for 60 minutes before analyzed for pH, conductivity, turbidity, TSS and COD. The pH was measured using a pH meter (Thermo Scientific, Orion™ Star A216); conductivity was measured using a conductivity meter (Hach, HQ440d); turbidity was measured using a turbidimeter (Hach, 2100N); and TSS and COD were

measured using a standard photometric and colorimetric method (Hach Company, CO), respectively. Each experiment was done in triplicate, and no statistical difference was found, so the results were averaged. The residual Alum concentration was calculated according to the Faraday's Law,

$$m = \frac{ItM}{ZF} \quad (8)$$

where I is the electrical current (A), t is the electrolysis time (s), M is the molecular weight (g/mol), Z is the number of electrons and F is the faraday constant (96485.3 C/mol).

5.3 Results and Discussion

5.3.1 Produced water treatment performance under different conditions

Figure 21 shows that the electrocoagulation system was able to remove around 99% of the turbidity and TSS under all six operational conditions (DC or AC powered EC, with or without biochar). This is consistent with previous findings that EC can be an effective process for suspended solids removal. However, the addition of biochar significantly reduced the time it took to achieve a 99% reduction in turbidity and TSS. That is the addition of 0.25 g/L of biochar required only a 30 minute reaction time, while the same conditions without biochar took 50 minutes. For the EC systems with 0 gram biochar addition, the turbidity removal after 30 minutes was around 85%. The pH and conductivity measured at the end of the experiments in each condition showed no significant changes compared to the feed water (Figure 22A, 22B). In the six operational conditions pH ranged from 6.5 (DC-EC with 0.25 g/L biochar) to 7.5 (AC-EC with 0 g/L biochar) and conductivity ranged from 42.8 mS/cm (DC-EC with 0 g/L biochar) to 45.6 mS/cm (DC-EC with 0.25 g/L biochar and AC-EC with 0 g/L biochar). The average COD

removal ranged from 5-14% after 30 min (with biochar) and 50 min (without biochar), respectively.

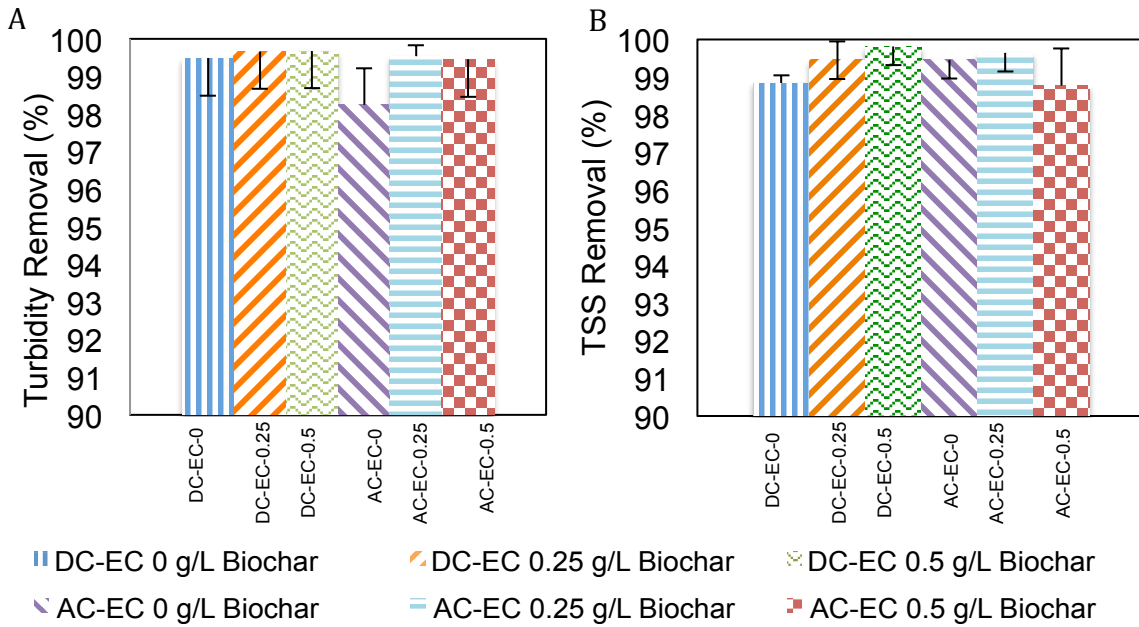


Figure 21 Turbidity (A) and TSS (B) removal by the 6 different operational conditions after 30 minutes (with biochar addition) or 50 minutes (without biochar addition). Legends showing process combination matrix, e.g. DC-EC-0 g/L Biochar means DC-powered EC process with 0 g/L biochar addition.

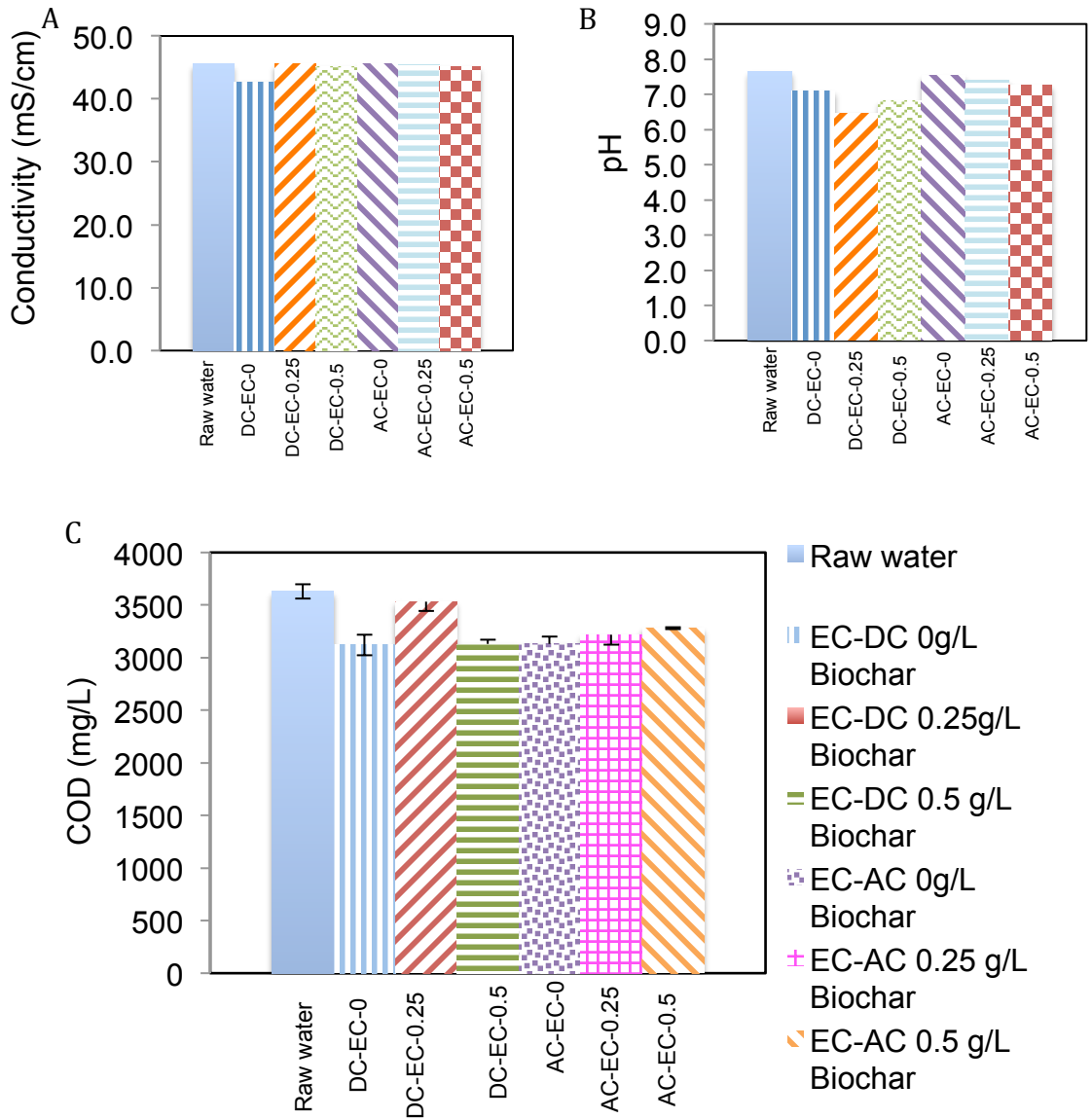


Figure 22 Change of solution conductivity (A) and pH (B), as well as COD removal (C) after 30 minutes (with biochar addition) or 50 minutes (without biochar addition). Legends showing process combination matrix, e.g. DC-EC-0 g/L Biochar means DC-powered EC process with 0 g/L biochar addition.

Due to the long settling time before chemical measurements and limited water volume, we were not able to obtain time-course data similar to the AC/DC current profile (Figure 24), instead 99% removal of turbidity or TSS was set as a treatment goal to be consistent with general industry practice (personal communication). The 30 and 50 minutes reaction times for different

conditions were examined during pre-testing to determine an approximate timeframe for 99% turbidity removal. This was done so energy calculations could be performed from a uniform baseline.

The removals of turbidity and TSS in biochar control without EC reactor are shown in Figure 23. After 30-minute adsorption, 5% of turbidity and 3% of TSS were removed when 0.25 g/L biochar was added. The removal increased to 15% for turbidity and 9% for TSS when biochar dosage increased to 0.5 g/L. These data show that a higher suspended solids removal was observed when combining EC and biochar in one system (>99%) compared to the individual contribution by each process, suggesting a synergy existed in the EC-biochar operation. It is hypothesized that suspended solids coalesce with biochar into larger and lighter particles due to the low density and porous structure of biochar. With electrolytic microbubbles rising during the EC process, faster removal was accomplished for such particles as compared with regular flocs¹⁰². While this study focused on feasibility and energy savings, further studies are needed to understand these synergistic removal mechanisms.

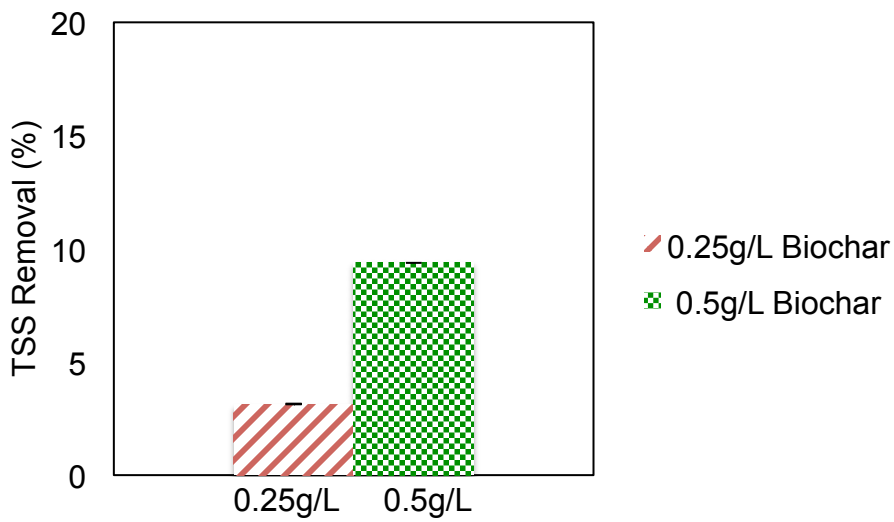
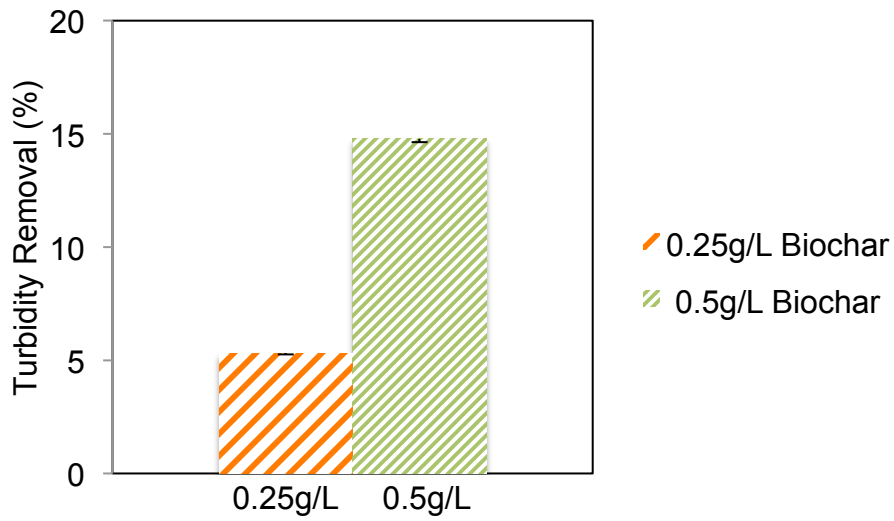


Figure 23 Turbidity and TSS removal after 30 minutes in biochar-only reactors with a dose of 0.25 g/L or 0.5 g/L biochar.

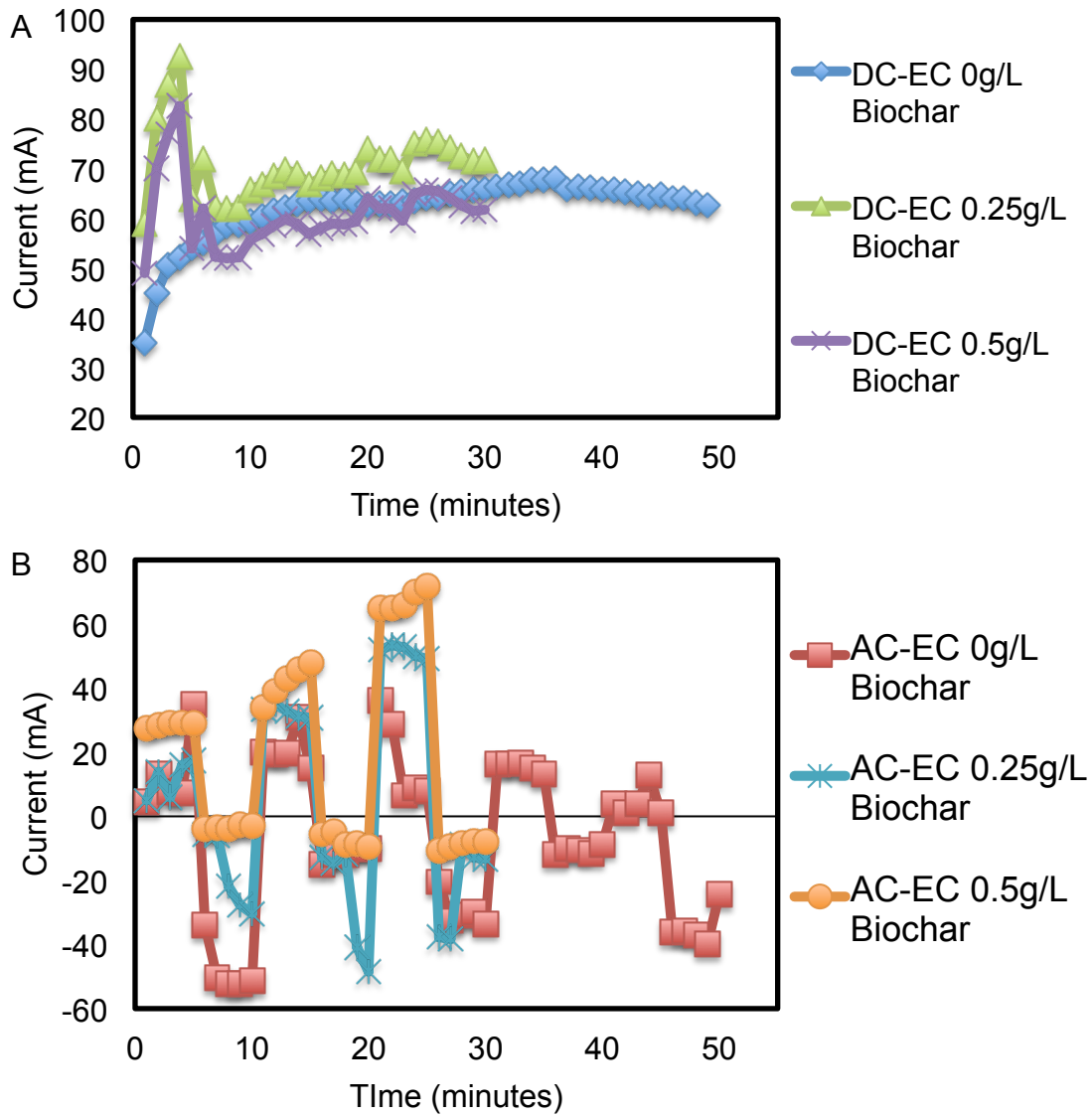


Figure 24 Time-course current profile in DC-EC reactors (A) and AC-EC reactors (B) with different doses of biochar addition.

5.3.2 Energy benefits of the AC-EC-Biochar combination

Figure 24 shows the current profiles under different conditions. During DC-EC operation, when no biochar was used, the average current was 62.1 mA, giving an average current density of 22 A/m² (Figure 24A). Adding biochar significantly boosted the current during the first 4-5

minutes, but the current then dropped quickly and maintained at a comparable level to the DC-EC condition without biochar. The average current was 70.9 mA (25.2 A/m^2) for 0.25 g/L biochar, and the current was 60.9 mA (21.5 A/m^2) for 0.5 g/L biochar. The current fluctuation at the beginning is hypothesized to relate to the highly conductive nature of biochar in the solution, which was facilitated with the electron transfer. When the biochar settled with the flocs, the current dropped to non-biochar levels, supporting the above hypothesis.

For the AC-EC system without biochar, the average positive current was 14.4 mA (5.12 A/m^2), while the average negative current was 26.9 mA (9.6 A/m^2) (Figure 24B). The addition of biochar significantly shifted the current profile to the more positive region. When 0.25 g/L biochar was added, the average positive current more than doubled to 31.9 mA (11.3 A/m^2), while the negative current decreased to 19 mA (6.7 A/m^2). Higher shifts were observed when 0.5 g/L was added, with positive current increased to 46 mA (16.3 A/m^2) and negative current dropped to 6.55 mA (2.3 A/m^2). The increase in the current is a result of the decrease of system resistance based on Ohm's law $R=V/I$, because the voltage is at a fixed 1.2 V for all experiments. As shown in Figure 22, the conductivity of the solution remained stable, which indicates its inverse, or solution resistance, was stable. Also, since the distance between the two electrodes was kept the same, the change of electrode resistance due to scarification and passivation is believed to be the main reason for the current shift.

The energy consumption of all EC systems is shown in Figure 25. It is clear that overall the AC-powered EC consumed less energy than the DC-powered EC, and the amount of biochar added positively correlates with energy savings. The energy consumption of the DC-EC systems were of 0.263 kWh/m^3 (0 g/L biochar), 0.213 kWh/m^3 (0.25 g/L biochar), and 0.183 kWh/m^3 (0.5 g/L), respectively. The energy consumption of the AC-EC systems were 0.103 kWh/m^3 (0

g/L biochar), 0.081 kWh/m³ (0.25 g/L biochar), and 0.079 kWh/m³ (0.5 g/L biochar), respectively. When comparing with the DC-EC without biochar, the AC-EC reduced energy consumption by 61% yet achieved a similar turbidity and TSS removal, indicating switching DC to AC as EC's power source can lead to significant energy saving. The examination of electrode surface showed an impermeable oxide film formed on the DC-EC cathode, which requires higher current to maintain the reaction. The AC-EC system slowed such cathode passivation process and anode deterioration by inverting the polarity of the electrodes and creating a self-cleaning mechanism. Previous studies using scanning electron microscope (SEM) showed when AC-EC was used, the electrode surface presented a smooth microstructure of aluminum, suggesting the aluminum electrodes were dissolved uniformly during the electrolysis. When DC-EC was used the electrode surface presented disordered pores formed with dents.¹⁰³ It is also known that AC electric fields can induce dipole-dipole interactions in a system with no spherical charged particles, therefore disrupting their stability¹⁰⁸.

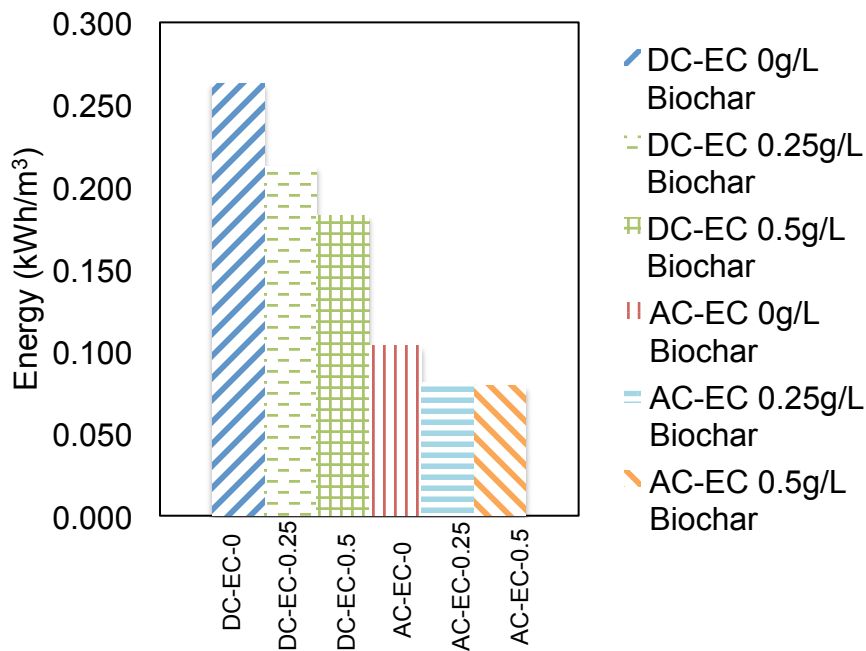


Figure 25 Energy consumption comparison under different conditions.

A similar energy saving benefit was shown in biochar enhanced EC process for identical treatment goals. By adding 0.25 g/L biochar, the energy consumption in the DC-EC and AC-EC was reduced by 19%, and 21%, respectively. This saving further increased to 33% and 23%, respectively, when 0.5 g/L biochar was added. Overall, for achieving a similar 99% turbidity and TSS removal, the combination of AC-EC and biochar saved up to 70% of energy (AC-EC plus 0.5 g/L biochar vs. DC-EC without biochar). This translates to an energy consumption of 0.15 kWh/kg TSS, among the lowest energy expenditure in EC studies. Table 1 shows that previous studies reported 0.83-23.34 kWh of energy was used for every kg TSS removed in different EC systems, and the AC-EC-Biochar combination showed 35-99% energy reduction compared with previous studies using EC systems for wastewater treatment.

Table 3. Energy requirement for suspended solids (SS) removal

Reference	kWh/kg SS	Details
116	23.34	DC EC, artificial wastewater
117	20.62	DC EC, Automotive wastewater
118	18.04	DC EC, egg processing wastewater
119	4.60	AC EC, superfund site remediation
120	3.91	DC EC, oily bilge water
121	0.83	DC EC, almond industry wastewater
122	0.23	DC EC, tannery wastewater
Our study	0.15	AC EC+biochar, produced water

5.3.3 Future work is needed for optimization and integration

Despite the excellent energy savings and suspended solids removal capability, the EC systems used in this study showed limited removal for COD and TDS (Figure 22). While this is consistent with general findings that EC is not effective for COD or TDS removal, the combination of EC with other technologies has been reported for more advanced produced water treatment, including softening with EC ¹²³, or EC combined with reverse osmosis ¹²⁴. Membrane based organic removal and desalination processes have been reported as EC post-treatment options, but they are energy intensive, consuming 10-600 kWh/m³, depending on the technology used ¹²⁵. In this context, new technologies such as microbial capacitive deionization (MCD) could have a good synergistic relationship with an EC process ¹²⁶. This is the result of MCDs ability to remove COD and TDS, while generating electricity that can be used to power EC reactor, thus providing a pre-treatment step prior to MCD ¹²⁷. Though current MCDs have a low power output, recent developments in system scale-up and DC-AC converter shows the feasibility of system integration ¹²⁸. Other systems such as forward osmosis and membrane distillation may also be coupled with EC for the complete treatment and reuse of produced water, and more studies are needed to characterize and optimize these possible system integrations.

The information presented in this chapter has been published in a scientific journal; **Lobo, F. L.**, Wang, H., Huggins, T. M., Rosenblum, J., Linden, K. G., Ren, Z. J. “Low-energy hydraulic wastewater treatment via AC powered electrocoagulation with biochar” *Journal of Hazardous Materials*, **2016**, 309, 180-184.

CHAPTER 6

FUTURE RESEARCH

6.1 Energy Harvesting on a Pilot Scale MFC

In order to bring MFC into practical applications, MFC must be scaled up to a certain extent to treat meaningful amount of wastewater in continuous basis. However, studies revealed that as the dimension of an individual MFC enlarged, the power density declines due to increase of volumetric ohmic resistance and inactive reactor volume, leading to low power generation of scaled-up MFC. Combining multiple small MFC modules to form a larger stack may be a more feasible and efficient strategy to scale up MFC ¹²⁹. In addition, several energy harvesting systems have been developed for MFC applications ^{15,43,128}, but most studies show energy harvesting and power applications for small MFCs (28 mL cubic reactors) ⁷³ as shown in chapters 2-4. Energy harvesting on pilot scale MFCs can facilitate practical application of MFC power. In this study, I investigated the possibility of using MFC generated power to support electrocoagulation process so oily bilge water generated from Navy ships can be effectively treated.

6.2 Remote Bilge Water Treatment by Electrocoagulation

Bilge water is a complex and corrosive shipboard wastewater produced from machinery leakage and fresh water wash downs. Bilge water contains lubricating oils, hydrocarbons, fuel, hydraulic oils, and cleaning agents ¹³⁰. Because of the high oil content in bilge water and its harmful effects on sea ecology, the International Maritime Organization (IMO) prohibited the direct bilge water discharge since 1973 to protect marine environments. To meet the IMO regulations the bilge water is either treated en route, in an oil separation system before being discharged to the sea or deposited at reception facilities on land. The treatment is difficult due to

its mixed content of chemicals in the water ¹³¹. Electrocoagulation is a robust and economical technology that has been popular in oily wastewater treatment over the last decade ¹³². The high conductivity of bilge water makes it appropriate electrocoagulation treatment considering the advantages of low energy consumption and less chemical usage ¹³³. A small power supply can be used on a ship in order to power electrocoagulation to treat bilge water on-site. But in this study, we take advantage of the wastewater generated on the ship by using MFCs to produce electricity, which can be used directly for powering the electrocoagulation process and therefore facilitating bilge water treatment.

6.3 Preliminary results on MFC energy harvesting and power supply to electrocoagulation for bilge water treatment

Initially, four identical two-chamber MFCs were built and assembled together as stacked system. For each MFC, granular activated carbon and carbon felt were used as electrode in both anode and cathode, and the two chambers were separated by a cation exchange membrane. Another two-chamber MFC was built with carbon felt as electrode in both anode and cathode, and a cation exchange membrane was used to separate the two. The 5 MFCs were hydraulically connected in parallel. The effective liquid volume of anode or cathode is about 5L. Figure 26 shows MFCs setup. The MFC ran in batch mode, replacing solution after depletion of substrate (3-4 days). The solution media contained 1.5 g/L sodium acetate and 50mM Phosphate Buffer Solution.



Figure 26 5L-MFC setup

An integrated energy harvesting nano-power management circuit with pulse-frequency modulated (PFM) boost converter/charger (bq25505, Texas Instruments Inc.) was connected in parallel with each MFC module in order to extract its energy. MFC 1-4 was set to 80% of the open circuit voltage and MFC 5 was set 50% of the open circuit voltage (closest to maximum power point voltage), then the energy extracted was stored in a polymer lithium ion battery (2.7Wh, 850mAh, SparkFun Electronics ®). After charging the battery for one batch cycle, the battery was connected to buck converter (MCP 1603, evaluation board, Microchip ®), set to 1.2

V output voltage to power the electrocoagulation system. The electrical connections and electronics configuration is shown in Figure 27.

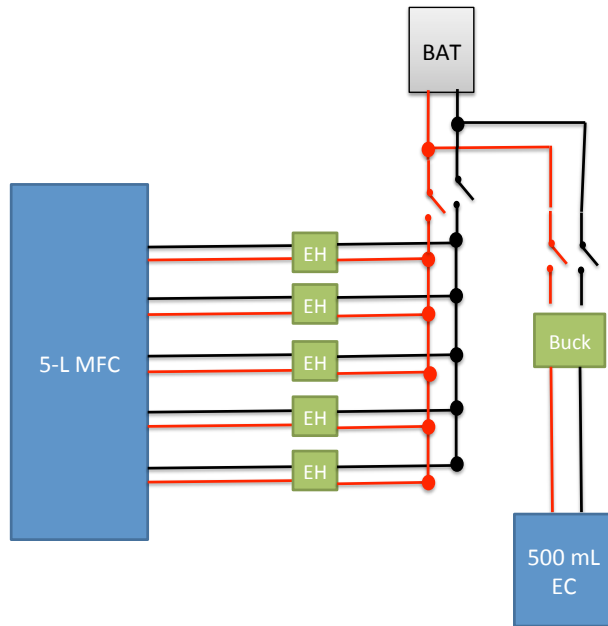


Figure 27 Electrical connections of integrated MFC-EC system (EH= Energy Harvesting Circuit, Buck = buck converter, BAT = battery).

During one batch cycle of the 5-L MFC the COD was depleted from 1170 to 27 mg/L and coulombic efficiency was 47%. Figure 28A shows the voltage profile of the 5-L MFC. MFCs 1-4 are the 4 stack module and MFC 5 is the separate module. MFC 5 presents a much lower voltage and current production than the 4 stacked module. The GAC in anode and cathode of MFC 1-4 improves power production and helps to sustain it for a longer time due to the adsorption of COD. Since MFC 5 anode and cathode do not possess this advantage of GAC, current drops much faster as it can be seen in Figure 28B. Figure 28C shows the voltage and current profile of the battery. The increase in voltage shows that the battery is being charged, according with the datasheet, the battery voltage ranges between 2.8V when discharged and 4.2V

when completely charged. Figure 28D shows the power produced by the 5-L MFC and the power delivered to the battery (output power from energy harvesting circuit). The efficiency of the energy harvesting circuit was 71%, the maximum power produced by 5-L MFC was 0.07W while the maximum power delivered to the battery was 0.05W. The energy stored in the battery during one batch cycle was 1.6 Wh, which is 60% of its capacity.

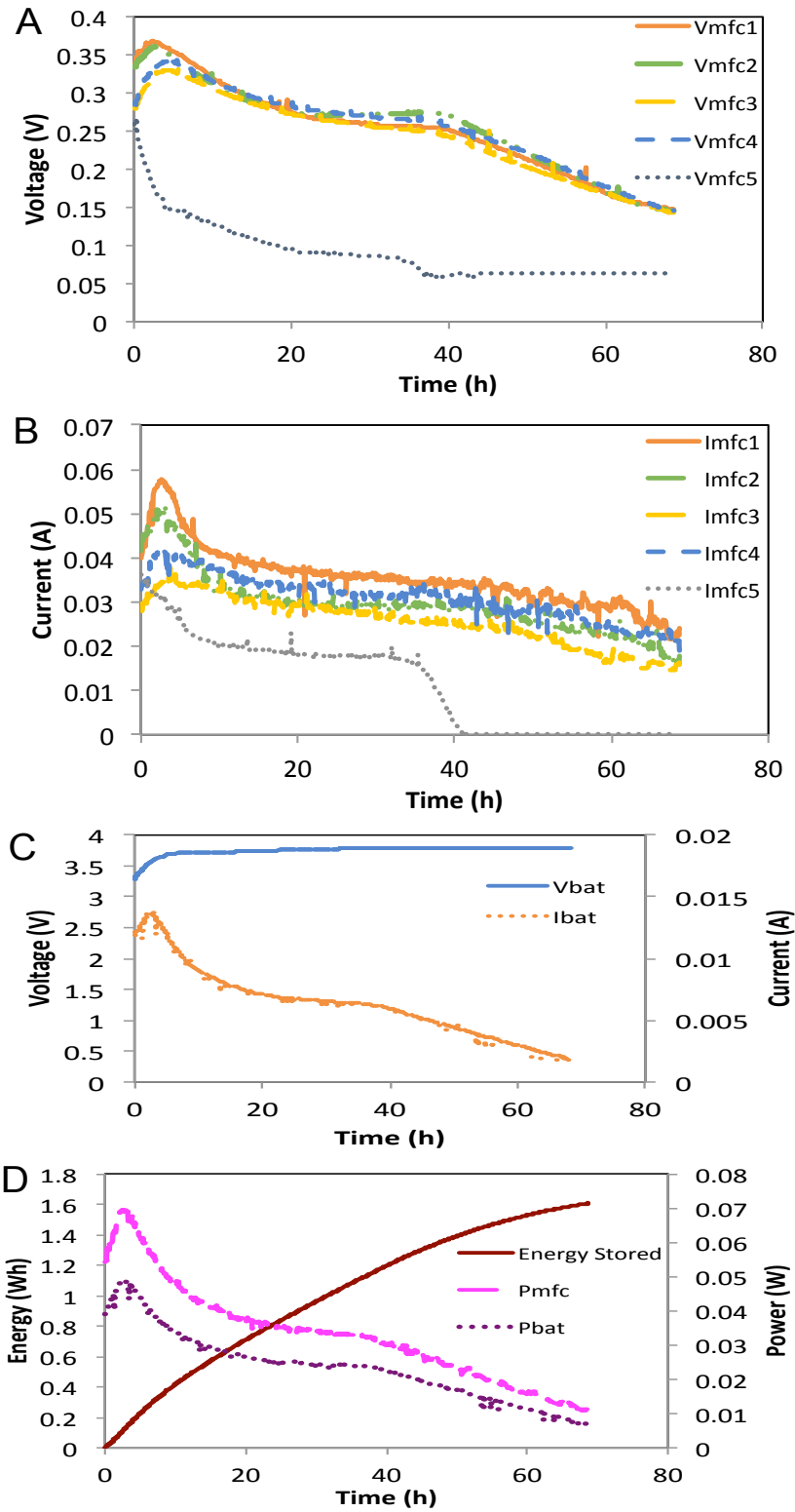


Figure 28 (A) MFC 1-5 voltage profile, (B) MFC 1-5 current profile, (C) Battery voltage and current profile, (D) 5-L MFC power (P_{mfc}), power output from energy harvesting circuits (P_{bat}) and energy stored in the battery in one batch cycle.

The bilge water samples were provided by The Carderock Division of the Naval Surface Warfare Center in Maryland. The water had an oil content of 1824 ppm. A working volume of 500 mL was considered for the entire experiments. Six pairs of aluminum plates of thickness 0.4 cm were used as electrodes (both anode and cathode) and were placed vertically in the working volume. The total electrode effective area was 84 cm². All the reactor setup was kept above a magnetic stirrer for giving proper agitation and a constant speed of 300 rpm that was kept during the whole electrocoagulation process. An aliquot of 5 ml from the middle of the EC cell was collected using pipette for every 5 min up to 120 min. Then the sample was allowed to settle for 60 min. After settling time the sample was analyzed for oil content using oil in water analyzer (Model TD-3100, Turner Designs).

The battery was charged by the 5-L MFC then it was used as power supply for the electrocoagulation system that lasted for 120 min. A buck converter was used to discharge the battery and control the voltage output at 1.2 V for electrocoagulation. Figure 29A shows the voltage and current profiles of the battery and the electrocoagulation system (buck converter output). The decrease of battery voltage shows the battery discharging during the EC treatment of bilge water. The discharge current was around 70-80 mA for the first hour, and then started to increase as the battery voltage decrease. Maximum current on EC was 196 mA, which corresponds to a current density (electrode area) of 23 A/m², while the voltage was kept constant at 1.2 V throughout the experiment. The buck converter showed an 80% efficiency.

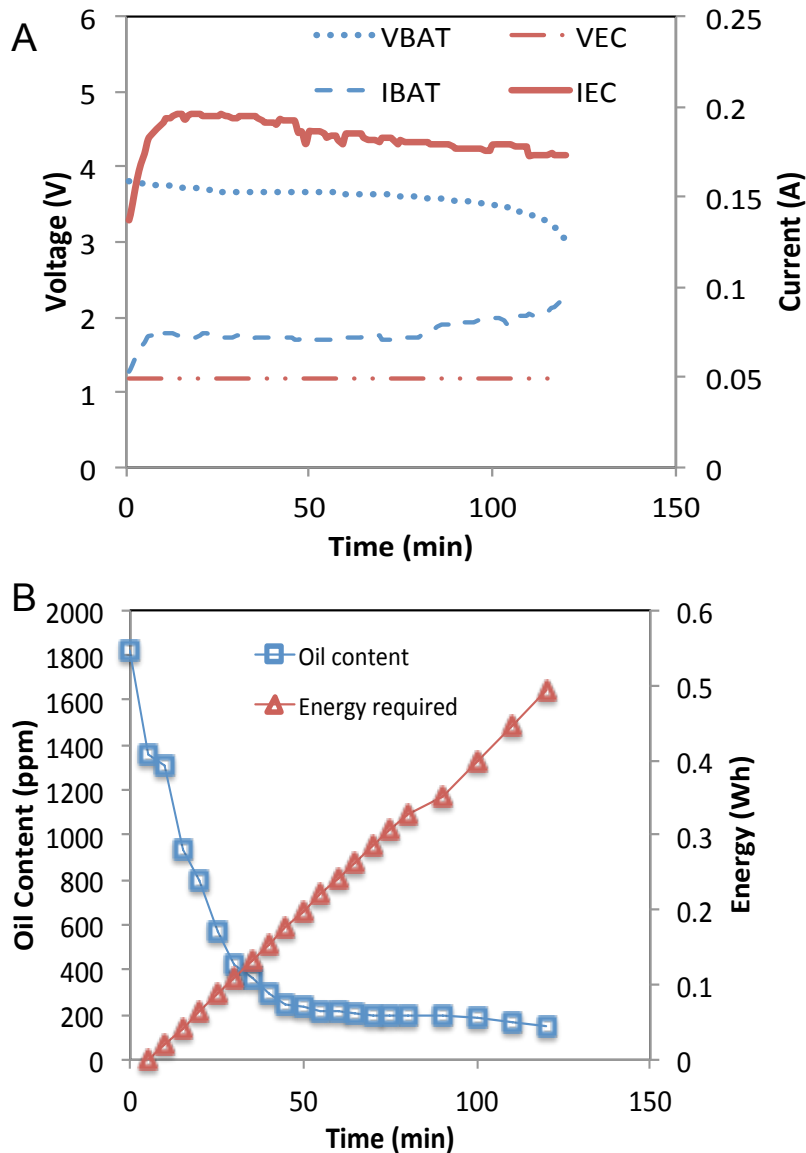


Figure 29 (A) Battery and electrocoagulation voltage and current profile, (B) oil content and energy consumption during bilge water treatment by electrocoagulation.

After the first hour of EC treatment, the bilge water oil content reduced to 214 ppm, which corresponds to 88% oil removal with an energy requirement of 0.26 Wh. After the second hour of EC treatment, oil content was reduced to 150 ppm, which correspond to 92% oil removal with an energy requirement of 0.54 Wh.

Energy flow Sankey diagram (Figure 30) shows that the energy produced in one batch cycle by the 5L-MFC is more than enough to power EC to remove oil from 500 mL of bilge water. Achieving 92% oil removal EC requires only 34% of the energy produced by the MFC. We have energy losses in both DC-DC converters to charge and discharge the battery. Even though there is an energy loss of 32%, the electronic circuit makes it possible to use the energy harvested from the MFC for a practical application. The remaining energy can be used to maintain the 5-L MFC running with no external energy necessary. Using a 5W air pump, oxygen is bubbled for 30 seconds each day, creating an energy demand of 0.125 Wh per batch cycle. After the batch cycle there still is 0.848 Wh of remaining energy that can be used in other controls of the system or to increase the volume of bilge water to be treated.

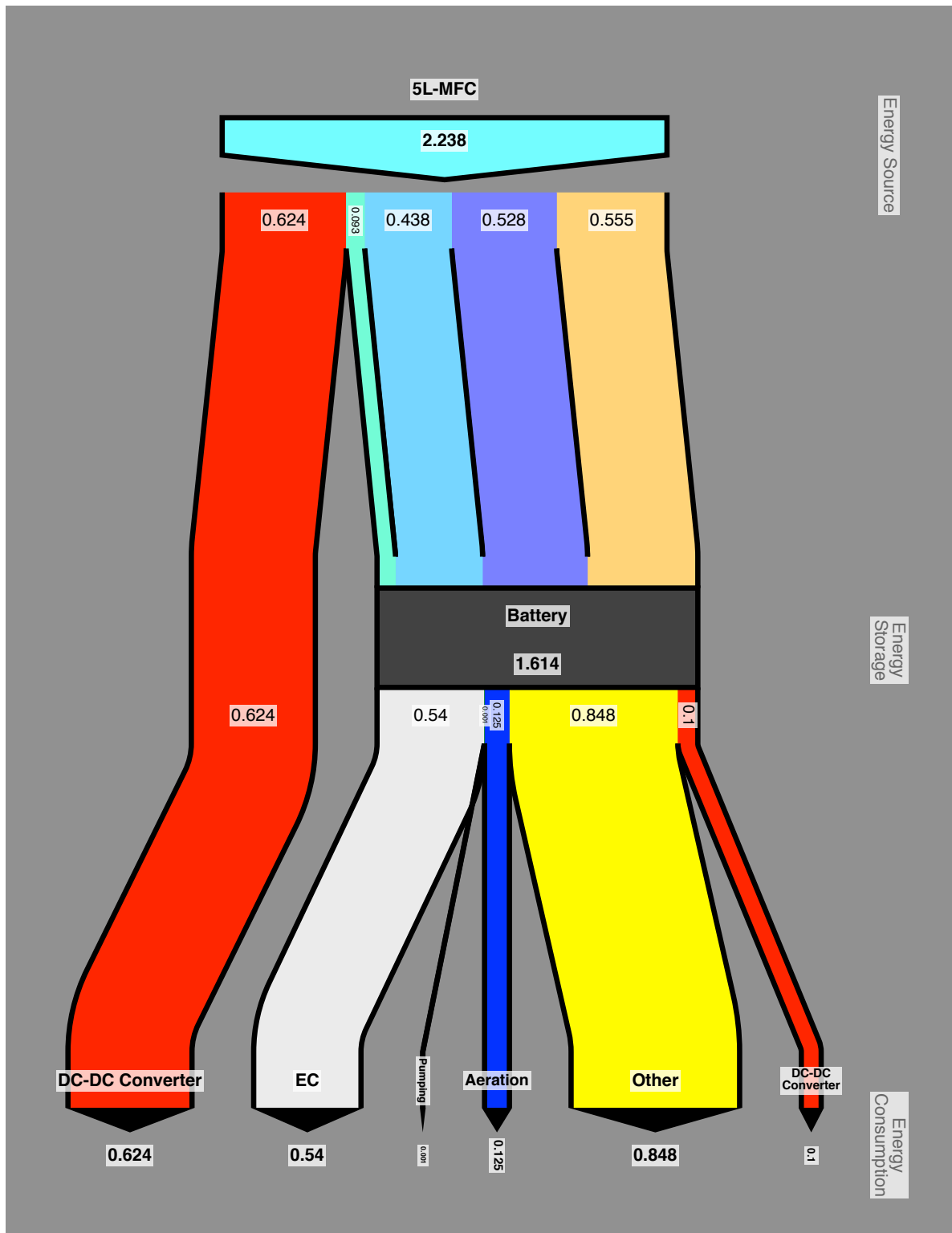


Figure 30 Energy Flow (Wh) Sankey Diagram of integrated MFC-EC system.

Based on the results and analysis, the integration of MFC and EC is considered feasible for concurrent bilge water and wastewater treatment. This brings a good synergy for shipboard wastewater treatment, where EC can be used to treat the non-biodegradable oily bilge water using the energy generated from MFCs, which MFCs can be used to treat the combined black and gray water and provide electricity for EC and other devices. Even though the energy production of MFC requires more time and wastewater volume to match EC energy consumption, electrical control and energy storage can be a key solution to make this system integration work, because EC doesn't need to be operated continuously as the bilge water is generally connected only once a week. The ratio of volumes of domestic wastewater and bilge water treatment in the preliminary test was 10:1, but since the unused energy showed as 'other' in the energy flow Sankey diagram (Figure 30) is enough to power another EC, this ratio can be changed to 5:1 at least. Further experiments are necessary to evaluate if real domestic wastewater can achieve similar power production and COD removal similar as sodium acetate with buffer solution. In addition, EC performance can be improved by AC power supply instead of DC, reducing electrode passivation and energy consumption¹³⁴. Another improvement to the system can be the use of biochar instead of GAC in the construction of the MFC, being a cheaper and more sustainable alternative.

BIBLIOGRAPHY

- (1) Correia, J. C. Atendimento energético a pequenas comunidades isoladas: barreiras e possibilidades. *T&C Amaz.* **2005**, *6*, 30–35.
- (2) Velázquez, S. M. S. G.; Santos, S. M. A.; Moreira, J. R.; Coelho. A Geração de Energia Elétrica em Comunidades Isoladas na Amazônia a partir de Biomassa Sustentável: Projeto ENERMAD. *XIII Congr. Bras. Energ. - XIII CBE* **2010**, *14*.
- (3) Hanna, R.; Oliva, P. Implications of Climate Change for Children in Developing Countries. **2016**, *26*, 115–132.
- (4) WHO. WHO| Sanitation, Fact Sheet N 392
<http://www.who.int/mediacentre/factsheets/fs392/en/>.
- (5) Logan, B.; Rabaey, K. Conversion of wastes into bioelectricity and chemicals by using microbial electrochemical technologies. *Science (80-)*. **2012**, *337*, 686–690.
- (6) Wang, H.; Ren, Z. J. A comprehensive review of microbial electrochemical systems as a platform technology. *Biotechnol. Adv.* **2013**, *31*, 1796–1807.
- (7) Logan, B. E. *Microbial Fuel Cells*; John Wiley & Sons: Hoboken, NJ, 2008.
- (8) Lovley, D. R. Bug juice: harvesting electricity with microorganisms. *Nat. Rev. Microbiol.* **2006**, *4*, 497–508.
- (9) Rozendal, R. a; Hamelers, H. V. M.; Rabaey, K.; Keller, J.; Buisman, C. J. N. Towards practical implementation of bioelectrochemical wastewater treatment. *Trends Biotechnol.* **2008**, *26*, 450–459.
- (10) Wang, H.; Luo, H.; Fallgren, P. H.; Jin, S.; Ren, Z. J. Bioelectrochemical system platform for sustainable environmental remediation and energy generation. *Biotechnol. Adv.* **2015**, *33*, 317–334.
- (11) Sleutels, T. H. J. A.; Ter Heijne, A.; Buisman, C. J. N.; Hamelers, H. V. M. Bioelectrochemical systems: An outlook for practical applications. *ChemSusChem*, 2012, *5*, 1012–1019.
- (12) Wang, H.; Park, J.; Ren, Z. J. Practical Energy Harvesting for Microbial Fuel Cells: A Review. *Environ. Sci. Technol.* **2015**, *49*, 3267–3277.
- (13) Park, J. Do; Ren, Z. Hysteresis-controller-based energy harvesting scheme for microbial fuel cells with parallel operation capability. *IEEE Trans. Energy Convers.* **2012**, *27*, 715–724.
- (14) Park, J.-D.; Ren, Z. Hysteresis controller based maximum power point tracking energy harvesting system for microbial fuel cells. *J. Power Sources* **2012**, *205*, 151–156.
- (15) Alaraj, M.; Ren, Z. J.; Park, J.-D. Microbial fuel cell energy harvesting using synchronous flyback converter. *J. Power Sources* **2014**, *247*, 636–642.
- (16) Wang, H.; Ren, Z. J. Bioelectrochemical metal recovery from wastewater: a review. *Water Res.* **2014**, *66*, 219–232.
- (17) Hamelers, H. V. M.; Ter Heijne, A.; Sleutels, T. H. J. A.; Jeremiasse, A. W.; Strik, D. P. B. T. B.; Buisman, C. J. N. New applications and performance of bioelectrochemical systems. *Applied Microbiology and Biotechnology*, 2010, *85*, 1673–1685.
- (18) Logan, B. E. Scaling up microbial fuel cells and other bioelectrochemical systems. *Applied Microbiology and Biotechnology*, 2010, *85*, 1665–1671.
- (19) Wang, H.; Park, J.-D.; Ren, Z. J. Pratical energy harvesting for microbial fuel cells: a review. *Submitted*.

- (20) Degrenne, N.; Allard, B.; Buret, F.; Adami, S.-E.; Labrousse, D.; Vollaïre, C.; Morel, F. A 140 mV Self-Starting 10 mW DC/DC Converter for Powering Low-Power Electronic Devices from Low-Voltage Microbial Fuel Cells. *J. Low Power Electron.* **2012**, *8*, 13.
- (21) Adami, S.-E.; Degrenne, N.; Vollaïre, C.; Allard, B.; Buret, F.; Costa, F. Autonomous ultra-low power DC/DC converter for Microbial Fuel Cells. *2011 18th IEEE Int. Conf. Electron. Circuits, Syst.* **2011**, 398–401.
- (22) Degrenne, N.; Buret, F.; Morel, F.; Adami, S. E.; Labrousse, D.; Allard, B.; Zaoui, A. Self-starting DC:DC boost converter for low-power and low-voltage microbial electric generators. In *IEEE Energy Conversion Congress and Exposition: Energy Conversion Innovation for a Clean Energy Future, ECCE 2011, Proceedings*; 2011; pp. 889–896.
- (23) Dewan, A.; Beyenal, H.; Lewandowski, Z. Intermittent energy harvesting improves the performance of microbial fuel cells. *Environ. Sci. Technol.* **2009**, *43*, 4600–4605.
- (24) Liang, P.; Wu, W.; Wei, J.; Yuan, L.; Xia, X.; Huang, X. Alternate charging and discharging of capacitor to enhance the electron production of bioelectrochemical systems. *Environ. Sci. Technol.* **2011**, *45*, 6647–6653.
- (25) Kim, Y.; Hatzell, M. C.; Hutchinson, A. J.; Logan, B. E. Capturing power at higher voltages from arrays of microbial fuel cells without voltage reversal. *Energy Environ. Sci.* **2011**, *4*, 4662.
- (26) Ren, S.; Xia, X.; Yuan, L.; Liang, P.; Huang, X. Enhancing charge harvest from microbial fuel cells by controlling the charging and discharging frequency of capacitors. *Bioresour. Technol.* **2013**, *146*, 812–815.
- (27) Donovan, C.; Dewan, A.; Heo, D.; Beyenal, H. Batteryless, wireless sensor powered by a sediment microbial fuel cell. *Environ. Sci. Technol.* **2008**, *42*, 8591–8596.
- (28) Meehan, A. Energy harvesting with microbial fuel cell and power management system. *Power Electron. IEEE ...* **2011**, *26*, 176–181.
- (29) Donovan, C.; Dewan, A.; Peng, H.; Heo, D.; Beyenal, H. Power management system for a 2.5W remote sensor powered by a sediment microbial fuel cell. *J. Power Sources* **2011**, *196*, 1171–1177.
- (30) Gong, Y.; Radachowsky, S. E.; Wolf, M.; Nielsen, M. E.; Girguis, P. R.; Reimers, C. E. Benthic microbial fuel cell as direct power source for an acoustic modem and seawater oxygen/temperature sensor system. *Environ. Sci. Technol.* **2011**, *45*, 5047–5053.
- (31) Shantaram, A.; Beyenal, H.; Raajan, R.; Veluchamy, A.; Lewandowski, Z. Wireless sensors powered by microbial fuel cells. *Environ. Sci. Technol.* **2005**, *39*, 5037–5042.
- (32) ABB micro inverter system
[http://www05.abb.com/global/scot/scot232.nsf/veritydisplay/7efd88eadc51c585257dc5006e334e/\\$file/MICRO-0.25-0.3-0.3HV-Rev1.6.pdf](http://www05.abb.com/global/scot/scot232.nsf/veritydisplay/7efd88eadc51c585257dc5006e334e/$file/MICRO-0.25-0.3-0.3HV-Rev1.6.pdf)
- (33) Wang, H.; Heil, D.; Ren, Z. J.; Xu, P. Removal and fate of trace organic compounds in microbial fuel cells. *Chemosphere* **2015**, *125*, 94–101.
- (34) Zhu, H.; Wang, H.; Li, Y.; Bao, W.; Fang, Z.; Preston, C.; Vaaland, O.; Ren, Z.; Hu, L. Lightweight, conductive hollow fibers from nature as sustainable electrode materials for microbial energy harvesting. *Nano Energy* **2014**, *10*, 268–276.
- (35) Erickson, R. W.; Maksimovic, D. *Fundamentals of Power Electronics*; Second Edi.; Kluwer Academic Publishers: New York, Boston, Dordrecht, London, Moscow, 2001.
- (36) Logan, B. E.; Hamelers, B.; Rozendal, R.; Schroder, U. Microbial Fuel Cells : Methodology and Technology †. *Environ. Sci. Technol.* **2006**, *40*, 5181–5192.
- (37) Wang, H.; Ren, Z.; Park, J.-D. Power electronic converters for microbial fuel cell energy

- extraction: Effects of inductance, duty ratio, and switching frequency. *J. Power Sources* **2012**, *220*, 89–94.
- (38) Lu, Z.; Girguis, P.; Liang, P.; Shi, H.; Huang, G.; Cai, L.; Zhang, L. Biological capacitance studies of anodes in microbial fuel cells using electrochemical impedance spectroscopy. *Bioprocess Biosyst. Eng.* **2015**.
- (39) Wang, X.; Feng, C.; Ding, N.; Zhang, Q. Accelerated OH–Transport in Activated Carbon Air Cathode by Modification of Quaternary Ammonium for Microbial Fuel Cells. ... *Sci. Technol.* **2014**, *48*, 4191–4198.
- (40) Alexander, C. K.; Sadiku, M. N. O. *Fundamentals of Electric Circuit*, Fifth Edit.; McGraw-Hill: New York, 2013.
- (41) Henderson, R. D.; Rose, P. J. Harmonics: The Effects on Power Quality and Transformers. *IEEE Trans. Ind. Appl.* **1994**, *30*.
- (42) Committee, D.; Power, I.; Society, E. IEEE Recommended Practice and Requirements for Harmonic Control in Electric Power Systems IEEE Power and Energy Society. **2014**, *2014*.
- (43) Wang, H.; Park, J.-D.; Ren, Z. Active energy harvesting from microbial fuel cells at the maximum power point without using resistors. *Environ. Sci. Technol.* **2012**, *46*, 5247–5252.
- (44) Erbay, C.; Carreon-Bautista, S.; Sanchez-Sinencio, E.; Han, A. High performance monolithic power management system with dynamic maximum power point tracking for microbial fuel cells. *Environ. Sci. Technol.* **2014**, *48*, 13992–13999.
- (45) Boghani, H. C.; Papaharalabos, G.; Michie, I.; Fradler, K. R.; Dinsdale, R. M.; Guwy, A. J.; Ieropoulos, I.; Greenman, J.; Premier, G. C. Controlling for peak power extraction from microbial fuel cells can increase stack voltage and avoid cell reversal. *J. Power Sources* **2014**, *269*, 363–369.
- (46) Park, J.-D.; Ren, Z. High efficiency energy harvesting from microbial fuel cells using a synchronous boost converter. *J. Power Sources* **2012**, *208*, 322–327.
- (47) Li, W.; Yu, H.; He, Z. Environmental Science Towards sustainable wastewater treatment by using microbial fuel cells-centered technologies. **2014**, 911–924.
- (48) Dewan, A.; Ay, S. U.; Karim, M. N.; Beyenal, H. Alternative power sources for remote sensors: A review. *J. Power Sources* **2014**, *245*, 129–143.
- (49) Logan, B. Exoelectrogenic bacteria that power microbial fuel cells. *Nat. Rev. Microbiol.* **2009**, *7*, 375–381.
- (50) Winfield, J.; Chambers, L. D.; Stinchcombe, A.; Rossiter, J.; Ieropoulos, I. The power of glove: Soft microbial fuel cell for low-power electronics. *J. Power Sources* **2014**, *249*, 327–332.
- (51) He, W.; Liu, J.; Li, D.; Wang, H.; Qu, Y.; Wang, X.; Feng, Y. The electrochemical behavior of three air cathodes for microbial electrochemical system (MES) under meter scale water pressure. *J. Power Sources* **2014**, *267*, 219–226.
- (52) Degrenne, N.; Buret, F.; Allard, B.; Bevilacqua, P. Electrical energy generation from a large number of microbial fuel cells operating at maximum power point electrical load. *J. Power Sources* **2012**, *205*, 188–193.
- (53) Pinto, R. P.; Srinivasan, B.; Uiot, S. R.; Tartakovsky, B. The effect of real-time external resistance optimization on microbial fuel cell performance. *Water Res.* **2011**, *45*, 1571–1578.
- (54) Lu, L.; Ren, Z. J. Microbial electrolysis cells for waste biorefinery: A state of the art

- review. *Bioresour. Technol.* **2016**, *215*, 254–264.
- (55) Jacobson, K. S.; Drew, D. M.; He, Z. Use of a liter-scale microbial desalination cell as a platform to study bioelectrochemical desalination with salt solution or artificial seawater. *Environ. Sci. Technol.* **2011**, *45*, 4652–4657.
- (56) Ren, Z.; Yan, H.; Wang, W.; Mench, M. M.; Regan, J. M. Characterization of microbial fuel cells at microbially and electrochemically meaningful time scales. *Environ. Sci. Technol.* **2011**, *45*, 2435–2441.
- (57) Lyon, D. Y.; Buret, F.; Vogel, T. M.; Monier, J. M. Is resistance futile? Changing external resistance does not improve microbial fuel cell performance. *Bioelectrochemistry* **2010**, *78*, 2–7.
- (58) Cheng, S.; Liu, H.; Logan, B. E. Increased performance of single-chamber microbial fuel cells using an improved cathode structure. *Electrochem. Commun.* **2006**, *8*, 489–494.
- (59) Lu, L.; Yazdi, H.; Jin, S.; Zuo, Y.; Fallgren, P. H.; Ren, Z. J. Enhanced bioremediation of hydrocarbon-contaminated soil using pilot-scale bioelectrochemical systems. *J. Hazard. Mater.* **2014**, *274*, 8–15.
- (60) Lu, L.; Hou, D.; Fang, Y.; Huang, Y.; Ren, Z. J. Nickel based catalysts for highly efficient H₂ evolution from wastewater in microbial electrolysis cells. *Electrochim. Acta* **2016**, *206*, 381–387.
- (61) Wang, X.; Zhou, L.; Lu, L.; Lobo, F. L.; Li, N.; Wang, H.; Park, J.; Ren, Z. J. Alternating Current Influences Anaerobic Electroactive Biofilm Activity. *Environ. Sci. Technol.* **2016**, *50*, 9169–9176.
- (62) Chookaew, T.; Prasertsan, P.; Ren, Z. J. Two-stage conversion of crude glycerol to energy using dark fermentation linked with microbial fuel cell or microbial electrolysis cell. *N. Biotechnol.* **2014**, *31*, 179–184.
- (63) Zhi, W.; Ge, Z.; He, Z.; Zhang, H. Methods for understanding microbial community structures and functions in microbial fuel cells: A review. *Bioresour. Technol.* **2014**, *171*, 461–468.
- (64) Labelle, E.; Bond, D. R. *Cyclic voltammetry for the study of microbial electron transfer at electrodes*; Rabaey, K.; Angenent, L. T.; Schröder, U.; Keller, J., Eds.; IWA Publishing: London, New York, 2010.
- (65) Hong, Y.; Call, D. F.; Werner, C. M.; Logan, B. E. Adaptation to high current using low external resistances eliminates power overshoot in microbial fuel cells. *Biosens. Bioelectron.* **2011**, *28*, 71–76.
- (66) Commault, A. S.; Lear, G.; Packer, M. A.; Weld, R. J. Influence of anode potentials on selection of *Geobacter* strains in microbial electrolysis cells. *Bioresour. Technol.* **2013**, *139*, 226–234.
- (67) Logan, B. E.; Wallack, M. J.; Kim, K. Y.; He, W.; Feng, Y.; Saikaly, P. E. Assessment of Microbial Fuel Cell Configurations and Power Densities. *Environ. Sci. Technol. Lett.* **2015**, *2*, 206–214.
- (68) Santoro, C.; Arbizzani, C.; Erable, B.; Ieropoulos, I. Special Section: “Microbial fuel cells: From fundamentals to applications”: Guest Editors’ note. *J. Power Sources* **2017**, *356*, 223–224.
- (69) Malvankar, N. S.; Tuominen, M. T.; Lovley, D. R. Biofilm conductivity is a decisive variable for high-current-density *Geobacter sulfurreducens* microbial fuel cells. *Energy Environ. Sci.* **2012**, *5*, 5790.
- (70) Yang, W.; Kim, K.-Y.; Saikaly, P. E.; Logan, B. E. The impact of new cathode materials

- relative to baseline performance of microbial fuel cells all with the same architecture and solution chemistry. *Energy Environ. Sci.* **2017**, 29–31.
- (71) Zhu, X.; Yates, M. D.; Hatzell, M. C.; Rao, H. A.; Saikaly, P. E.; Logan, B. E. Microbial Community Composition Is Unaffected by Anode Potential. *Environ. Sci. Technol.* **2014**, *48*, 1352–1358.
- (72) Stratford, J. P.; Beecroft, N. J.; Slade, R. C. T.; Grüning, A.; Avignone-Rossa, C. Anodic microbial community diversity as a predictor of the power output of microbial fuel cells. *Bioresour. Technol.* **2014**, *156*, 84–91.
- (73) Lobo, F. L.; Wang, X.; Ren, Z. J. Energy harvesting influences electrochemical performance of microbial fuel cells. *J. Power Sources* **2017**, *356*, 356–364.
- (74) Lu, L.; Huggins, T.; Jin, S.; Zuo, Y.; Ren, Z. J. Microbial metabolism and community structure in response to bioelectrochemically enhanced remediation of petroleum hydrocarbon-contaminated soil. *Environ. Sci. Technol.* **2014**, *48*, 4021–4029.
- (75) Lu, L.; Xing, D.; Ren, N. Bioreactor performance and quantitative analysis of methanogenic and bacterial community dynamics in microbial electrolysis cells during large temperature fluctuations. *Environ. Sci. Technol.* **2012**, *46*, 6874–6881.
- (76) Lu, L.; Xing, D.; Ren, Z. J. Microbial community structure accompanied with electricity production in a constructed wetland plant microbial fuel cell. *Bioresour. Technol.* **2015**, *195*, 115–121.
- (77) Ahn, Y.; Zhang, F.; Logan, B. E. Air humidity and water pressure effects on the performance of air-cathode microbial fuel cell cathodes. *J. Power Sources* **2014**, *247*, 655–659.
- (78) Lobo, F. L.; Wang, X.; Ren, Z. J. Energy harvesting influences electrochemical performance of microbial fuel cells. *J. Power Sources* **2017**, 1–9.
- (79) Liu, Y.; Kim, H.; Franklin, R. R.; Bond, D. R. Linking spectral and electrochemical analysis to monitor c-type cytochrome redox status in living geobacter sulfurreducens biofilms. *ChemPhysChem* **2011**, *12*, 2235–2241.
- (80) Freguia, S. Organics oxidation. In *Bioelectrochemical systems: From extracellular electron transfer to biotechnological application*; Rabaey, K.; Angenent, L. T.; Schröder, U.; Keller, J., Eds.; IWA Publishing: London, New York, 2010; pp. 226–242.
- (81) Torres, C. I.; Krajmalnik-Brown, R.; Parameswaran, P.; Marcus, A. K.; Wanger, G.; Gorby, Y. A.; Rittmann, B. E. Selecting Anode-Respiring Bacteria Based on Anode Potential: Phylogenetic, Electrochemical, and Microscopic Characterization. *Environ. Sci. Technol.* **2009**, *43*, 9519–9524.
- (82) Wang, H.; Qu, Y.; Li, D.; Ambuchi, J. J.; He, W.; Zhou, X.; Liu, J.; Feng, Y. Cascade degradation of organic matters in brewery wastewater using a continuous stirred microbial electrochemical reactor and analysis of microbial communities. *Sci. Rep.* **2016**, *6*, 27023.
- (83) Miran, W.; Nawaz, M.; Kadam, A.; Shin, S.; Heo, J.; Jang, J.; Lee, D. S. Microbial community structure in a dual chamber microbial fuel cell fed with brewery waste for azo dye degradation and electricity generation. *Environ. Sci. Pollut. Res.* **2015**, *22*, 13477–13485.
- (84) Wrighton, K. C.; Agbo, P.; Warnecke, F.; Weber, K. a; Brodie, E. L.; DeSantis, T. Z.; Hugenholtz, P.; Andersen, G. L.; Coates, J. D. A novel ecological role of the Firmicutes identified in thermophilic microbial fuel cells. *ISME J.* **2008**, *2*, 1146–1156.
- (85) Ren, Z.; Ward, T. E.; Regan, J. M. Electricity Production from Cellulose in a Microbial Fuel Cell Using a Defined Binary Culture Electricity Production from Cellulose in a

- Microbial Fuel Cell Using a Defined Binary Culture. *Environ. Sci. Technol.* **2007**, *41*, 4781–4786.
- (86) Lu, L.; Xing, D.; Ren, N.; Logan, B. E. Syntrophic interactions drive the hydrogen production from glucose at low temperature in microbial electrolysis cells. *Bioresour. Technol.* **2012**, *124*, 68–76.
- (87) Fritz, G.; Griesshaber, D.; Seth, O.; Kroneck, P. M. H. Nonheme Cytochrome *c*, a New Physiological Electron Acceptor for [Ni , Fe] Hydrogenase in the Sulfate-Reducing Bacterium *Desulfovibrio desulfuricans* Essex : Primary Sequence , Molecular Parameters , and Redox Properties †. *Biochemistry* **2001**, *40*, 1317–1324.
- (88) Kang, C. S.; Eaktasang, N.; Kwon, D. Y.; Kim, H. S. Enhanced current production by *Desulfovibrio desulfuricans* biofilm in a mediator-less microbial fuel cell. *Bioresour. Technol.* **2014**, *165*, 27–30.
- (89) Wang, K.; Sheng, Y.; Cao, H.; Yan, K.; Zhang, Y. Impact of applied current on sulfate-rich wastewater treatment and microbial biodiversity in the cathode chamber of microbial electrolysis cell (MEC) reactor. *Chem. Eng. J.* **2017**, *307*, 150–158.
- (90) Yang, Y.; Xu, M.; Guo, J.; Sun, G. Bacterial extracellular electron transfer in bioelectrochemical systems. *Process Biochem.* **2012**, *47*, 1707–1714.
- (91) Kumar, A.; Hsu, L. H.-H.; Kavanagh, P.; Barrière, F.; Lens, P. N. L.; Lapinsonnière, L.; Lienhard V, J. H.; Schröder, U.; Jiang, X.; Leech, D. The ins and outs of microorganism–electrode electron transfer reactions. *Nat. Rev. Chem.* **2017**, *1*, 24.
- (92) Sydow, A.; Krieg, T.; Mayer, F.; Schrader, J.; Holtmann, D. Electroactive bacteria molecular mechanisms and genetic tools. *Appl. Microbiol. Biotechnol.* **2014**, *98*, 8481–8495.
- (93) Yu, J.; Park, Y.; Cho, H.; Chun, J.; Seon, J.; Cho, S.; Lee, T. Variations of electron flux and microbial community in air-cathode microbial fuel cells fed with different substrates. *Water Sci. Technol.* **2012**, *66*, 748–753.
- (94) Hodgson, D. M.; Smith, A.; Dahale, S.; Stratford, J. P.; Li, J. V.; Grüning, A.; Bushell, M. E.; Marchesi, J. R.; Avignone Rossa, C. Segregation of the anodic microbial communities in a microbial fuel cell cascade. *Front. Microbiol.* **2016**, *7*, 1–11.
- (95) Kiely, P. D.; Call, D. F.; Yates, M. D.; Regan, J. M.; Logan, B. E. Anodic biofilms in microbial fuel cells harbor low numbers of higher-power-producing bacteria than abundant genera. *Appl. Microbiol. Biotechnol.* **2010**, *88*, 371–380.
- (96) Clark, C. E.; Veil, J. A. *Produced water volumes and management practices in the United States*; 2009.
- (97) Vasudevan, S.; Oturan, M. a. Electrochemistry: as cause and cure in water pollution—an overview. *Environ. Chem. Lett.* **2013**, *12*, 97–108.
- (98) Vasudevan, S.; Lakshmi, J.; Sozhan, G. Studies on the Al–Zn–In-alloy as anode material for the removal of chromium from drinking water in electrocoagulation process. *Desalination* **2011**, *275*, 260–268.
- (99) Vasudevan, S.; Lakshmi, J.; Sozhan, G. Electrocoagulation Studies on the Removal of Copper from Water Using Mild Steel Electrode. *Water Environ. Res.* **2012**, *84*, 209–219.
- (100) Vasudevan, S.; Epron, F.; Lakshmi, J.; Ravichandran, S.; Mohan, S.; Sozhan, G. Removal of NO₃- from Drinking Water by Electrocoagulation - An Alternate Approach. *CLEAN - Soil, Air, Water* **2010**, *38*, 225–229.
- (101) Kuokkanen, V.; Kuokkanen, T.; Rämö, J.; Lassi, U. Recent Applications of Electrocoagulation in Treatment of Water and Wastewater—A Review. *Green Sustain.*

- Chem.* **2013**, 3, 89–121.
- (102) Rubach, S.; Saur, I. Onshore testing of produced water by electroflocculation. *Filtr. Sep.* **1997**.
- (103) Vasudevan, S.; Lakshmi, J.; Sozhan, G. Effects of alternating and direct current in electrocoagulation process on the removal of cadmium from water. *J. Hazard. Mater.* **2011**, 192, 26–34.
- (104) Kamaraj, R.; Ganesan, P.; Lakshmi, J.; Vasudevan, S. Removal of copper from water by electrocoagulation process--effect of alternating current (AC) and direct current (DC). *Environ. Sci. Pollut. Res. Int.* **2013**, 20, 399–412.
- (105) Vasudevan, S.; Lakshmi, J.; Sozhan, G. Studies on the removal of arsenate from water through electrocoagulation using direct and alternating current. *Desalin. Water Treat.* **2012**, 48, 163–173.
- (106) Vasudevan, S. Effects of alternating current (AC) and direct current (DC) in electrocoagulation process for the removal of iron from water. *Can. J. Chem. Eng.* **2012**, 90, 1160–1169.
- (107) Vasudevan, S.; Kannan, B. S.; Lakshmi, J.; Mohanraj, S.; Sozhan, G. Effects of alternating and direct current in electrocoagulation process on the removal of fluoride from water. *J. Chem. Technol. Biotechnol.* **2011**, 86, 428–436.
- (108) Mollah, M. Y. a; Schennach, R.; Parga, J. R.; Cocke, D. L. Electrocoagulation (EC) — science and applications. *J. Hazard. Mater.* **2001**, 84, 29–41.
- (109) Secula, M. S.; Cagnon, B.; de Oliveira, T. F.; Chedeville, O.; Fauduet, H. Removal of acid dye from aqueous solutions by electrocoagulation/GAC adsorption coupling: Kinetics and electrical operating costs. *J. Taiwan Inst. Chem. Eng.* **2012**, 43, 767–775.
- (110) Secula, M.; Cretescu, I.; Cagnon, B.; Manea, L.; Stan, C.; Breaban, I. Fractional Factorial Design Study on the Performance of GAC-Enhanced Electrocoagulation Process Involved in Color Removal from Dye Solutions. *Materials (Basel)*. **2013**, 6, 2723–2746.
- (111) Vivek Narayanan, N.; Ganesan, M. Use of adsorption using granular activated carbon (GAC) for the enhancement of removal of chromium from synthetic wastewater by electrocoagulation. *J. Hazard. Mater.* **2009**, 161, 575–580.
- (112) Huggins, T.; Wang, H.; Kearns, J.; Jenkins, P.; Ren, Z. J. Biochar as a sustainable electrode material for electricity production in microbial fuel cells. *Bioresour. Technol.* **2014**, 157, 114–119.
- (113) Kołodyńska, D.; Wnętrzak, R.; Leahy, J. J.; Hayes, M. H. B.; Kwapiński, W.; Hubicki, Z. Kinetic and adsorptive characterization of biochar in metal ions removal. *Chem. Eng. J.* **2012**, 197, 295–305.
- (114) Tan, X.; Liu, Y.; Zeng, G.; Wang, X.; Hu, X.; Gu, Y.; Yang, Z. Application of biochar for the removal of pollutants from aqueous solutions. *Chemosphere* **2015**, 125, 70–85.
- (115) Huggins, T. M.; Pietron, J. J.; Wang, H.; Ren, Z. J.; Biffinger, J. C. Graphitic biochar as a cathode electrocatalyst support for microbial fuel cells. *Bioresour. Technol.* **2015**, 195, 147–153.
- (116) Ni'am, M. F.; Othman, F.; Sohaili, J.; Fauzia, Z. Electrocoagulation technique in enhancing COD and suspended solids removal to improve wastewater quality. *Water Sci. Technol.* **2007**, 56, 47–53.
- (117) Kobya, M.; Demirbas, E.; Dedeli, a; Sensoy, M. T. Treatment of rinse water from zinc phosphate coating by batch and continuous electrocoagulation processes. *J. Hazard. Mater.* **2010**, 173, 326–334.

- (118) Xu, L.; Sheldon, B.; Larick, D.; Carawan, R. Recovery and utilization of useful by-products from egg processing wastewater by electrocoagulation. *Poult. Sci.* **2002**, *81*, 785–792.
- (119) Barkley, N. P.; Farrell, C. W.; Gardner-Clayson, T. W. Alternating Current Electrocoagulation for Superfund Site Remediation. *Air Waste* **1993**, *43*, 784–789.
- (120) Asselin, M.; Drogui, P.; Brar, S. K.; Benmoussa, H.; Blais, J.-F. Organics removal in oily bilgewater by electrocoagulation process. *J. Hazard. Mater.* **2008**, *151*, 446–455.
- (121) Valero, D.; Ortiz, J. M.; García, V.; Expósito, E.; Montiel, V.; Aldaz, A. Electrocoagulation of wastewater from almond industry. *Chemosphere* **2011**, *84*, 1290–1295.
- (122) Kongjao, S.; Damronglerd, S.; Hunsom, M. Simultaneous removal of organic and inorganic pollutants in tannery wastewater using electrocoagulation technique. *Korean J. Chem. Eng.* **2008**, *25*, 703–709.
- (123) Esmaeilirad, N.; Carlson, K.; Omur Ozbek, P. Influence of softening sequencing on electrocoagulation treatment of produced water. *J. Hazard. Mater.* **2015**, *283*, 721–729.
- (124) Zhao, S.; Huang, G.; Cheng, G.; Wang, Y.; Fu, H. Hardness, COD and turbidity removals from produced water by electrocoagulation pretreatment prior to Reverse Osmosis membranes. *Desalination* **2014**, *344*, 454–462.
- (125) Thiel, G. P.; Tow, E. W.; Banchik, L. D.; Chung, H. W.; Lienhard, J. H. Energy consumption in desalinating produced water from shale oil and gas extraction. *Desalination* **2015**, *366*, 94–112.
- (126) Forrestal, C.; Xu, P.; Ren, Z. Sustainable desalination using a microbial capacitive desalination cell. *Energy Environ. Sci.* **2012**, *5*, 7161.
- (127) Forrestal, C.; Stoll, Z.; Xu, P.; Ren, Z. J. Microbial capacitive desalination for integrated organic matter and salt removal and energy production from unconventional natural gas produced water. *Environ. Sci. Water Res. Technol.* **2015**, *1*, 47–55.
- (128) Lobo, F. L.; Wang, H.; Forrestal, C.; Ren, Z. J. AC power generation from microbial fuel cells. *J. Power Sources* **2015**, *297*, 252–259.
- (129) Wu, S.; Li, H.; Zhou, X.; Liang, P.; Zhang, X.; Jiang, Y.; Huang, X. A novel pilot-scale stacked microbial fuel cell for efficient electricity generation and wastewater treatment. *Water Res.* **2016**, *98*, 396–403.
- (130) Akarsu, C.; Ozay, Y.; Dizge, N.; Gulsen, H. E.; Ates, H.; Gozmen, B.; Turabik, M. Electrocoagulation and nanofiltration integrated process application in purification of bilge water using response surface methodology. *Water Sci. Technol.* **2016**, *74*, 564–579.
- (131) Tiselius, P.; Magnusson, K. Toxicity of treated bilge water: The need for revised regulatory control. *Mar. Pollut. Bull.* **2017**, *114*, 860–866.
- (132) Siringi, D. O.; Home, P.; Chacha, J. S.; Koehn, E. Is electrocoagulation (EC) a solution to the treatment of wastewater and providing clean water for daily use. *ARPN J. Eng. Appl. Sci.* **2012**, *7*, 197–204.
- (133) Ulucan, K.; Kabuk, H. A.; Ilhan, F.; Kurt, U. Electrocoagulation Process Application in Bilge Water Treatment Using Response Surface Methodology. *Int. J. Electrochem. Sci.* **2014**, *9*, 2316–2326.
- (134) Lobo, F. L.; Wang, H.; Huggins, T.; Rosenblum, J.; Linden, K. G.; Ren, Z. J. Low-energy Hydraulic Fracturing Wastewater Treatment via AC Powered Electrocoagulation with Biochar. *J. Hazard. Mater.* **2016**, *309*, 180–184.

APPENDIX A

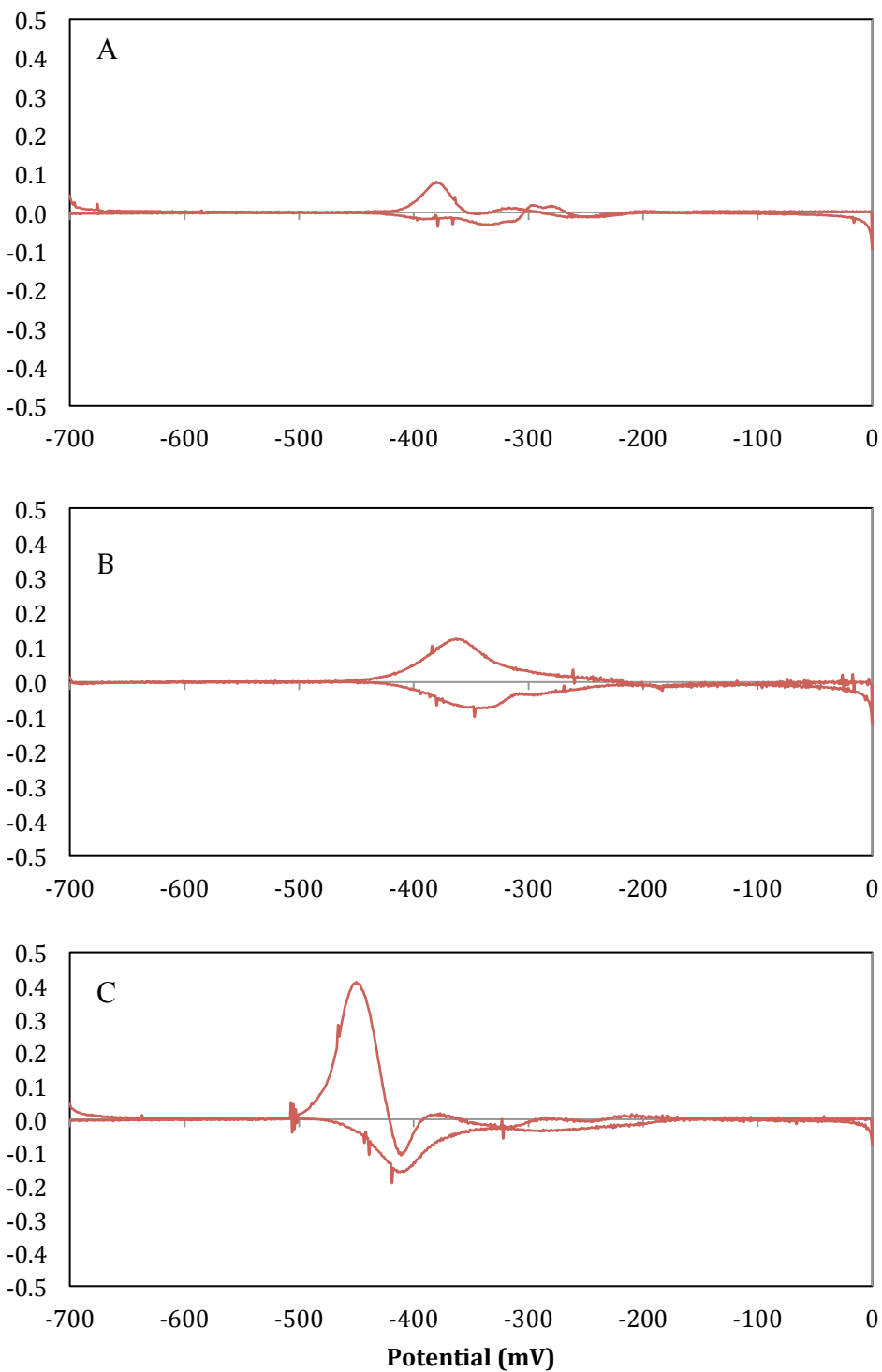


Figure A1 First derivative over the potential of the voltammetric curve of MPP-H (A) 60 days (stage I), (B), 90 days (30 days of stage II) and 114 days (54 days of stage II).

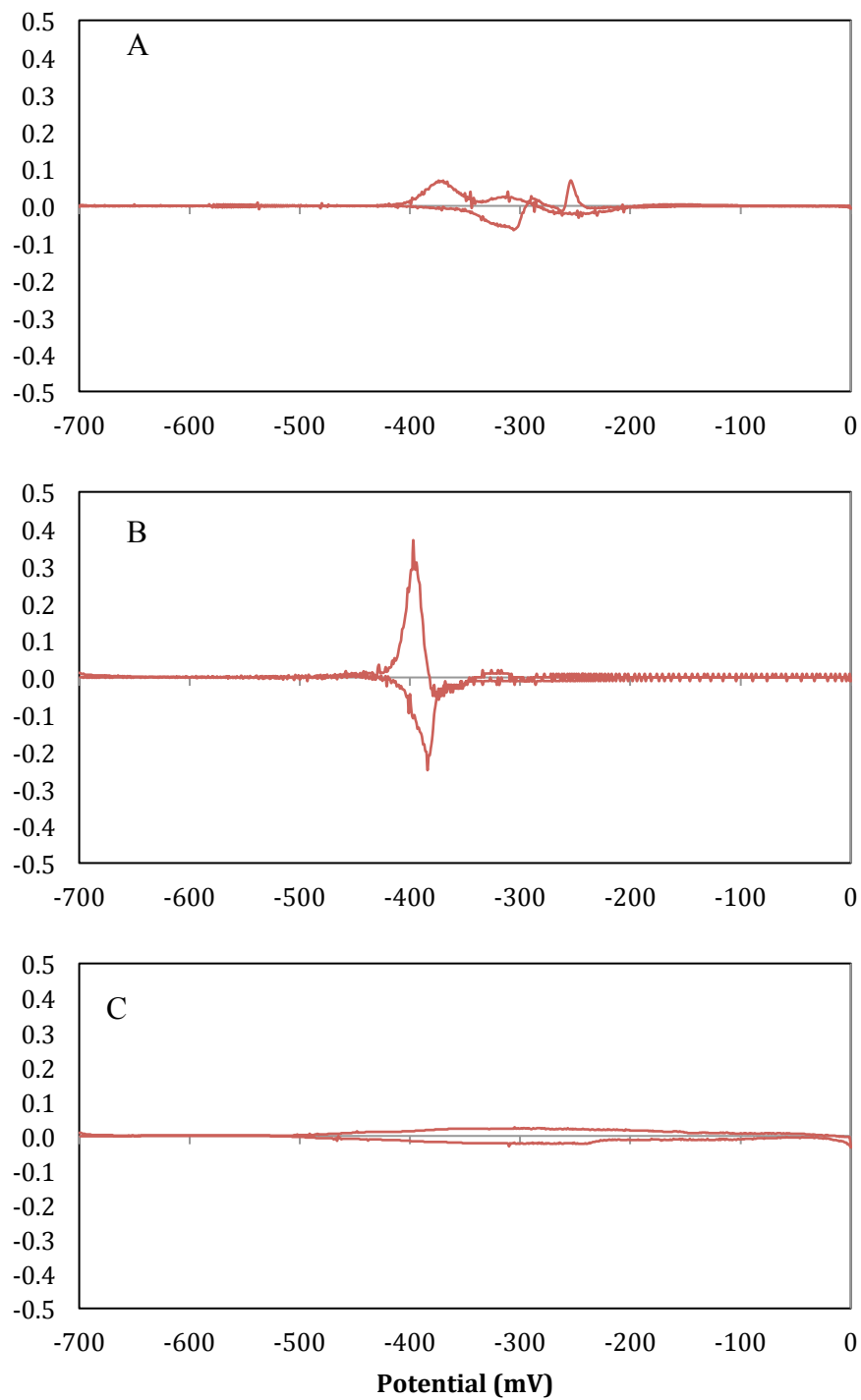


Figure A2 First derivative over the potential of the voltammetric curve of MPP-R (A) 60 days (stage I), (B), 90 days (30 days of stage II) and 114 days (54 days of stage II).

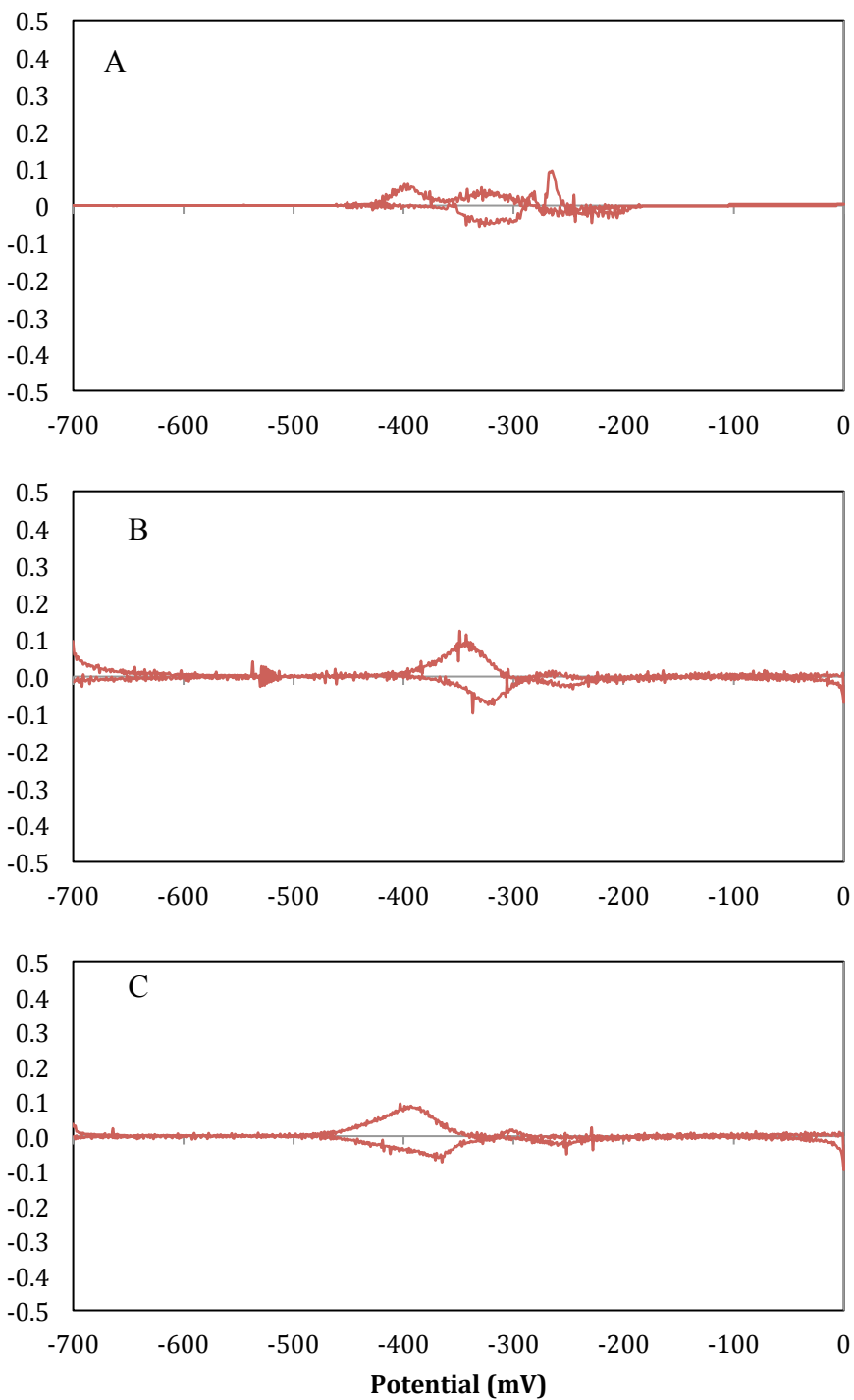


Figure A3 First derivative over the potential of the voltammetric curve of MCP-EH (A) 60 days (stage I), (B), 90 days (30 days of stage II) and 114 days (54 days of stage II).

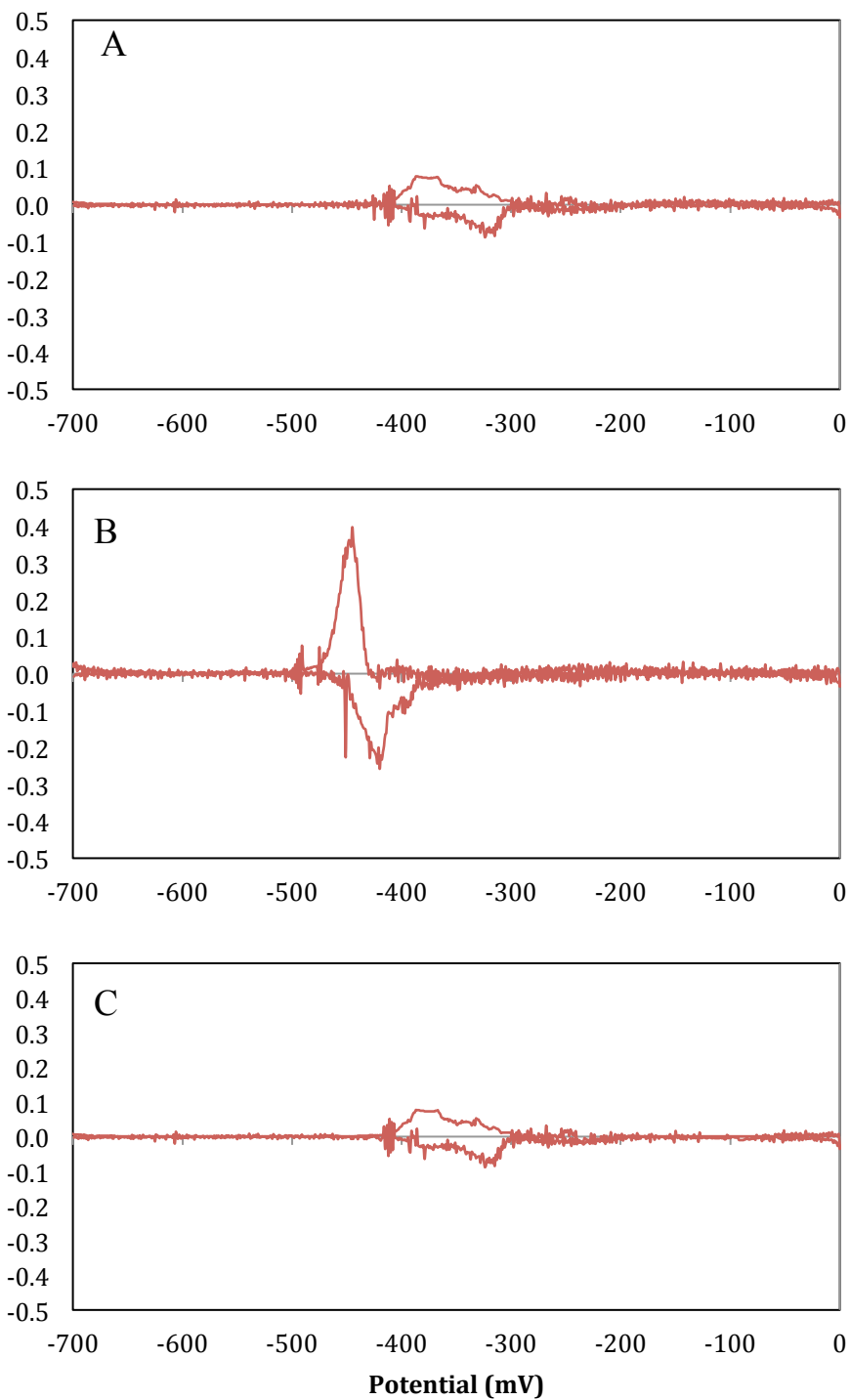


Figure A4 First derivative over the potential of the voltammetric curve of MCP-R (A) 60 days (stage I), (B), 90 days (30 days of stage II) and 114 days (54 days of stage II).

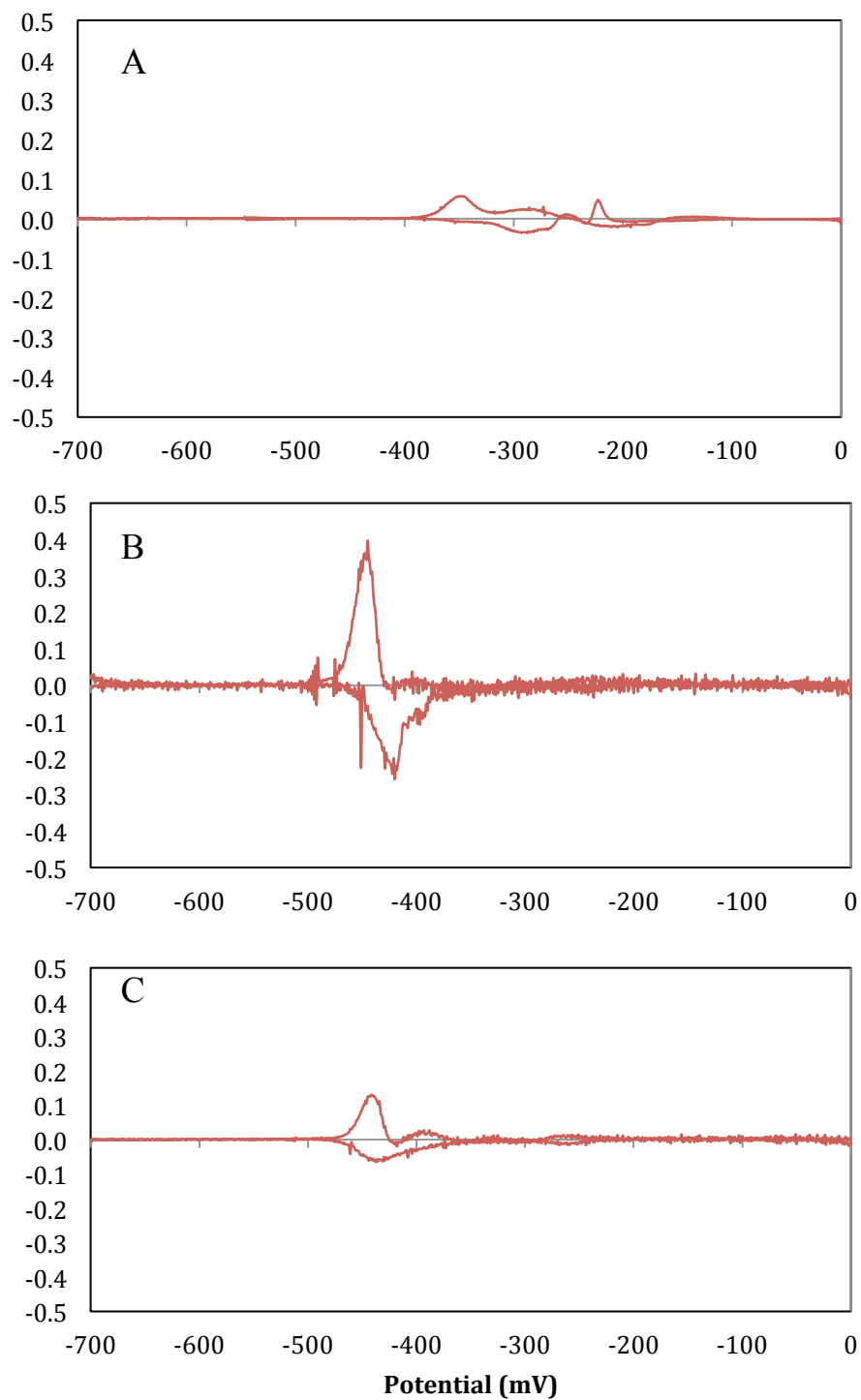
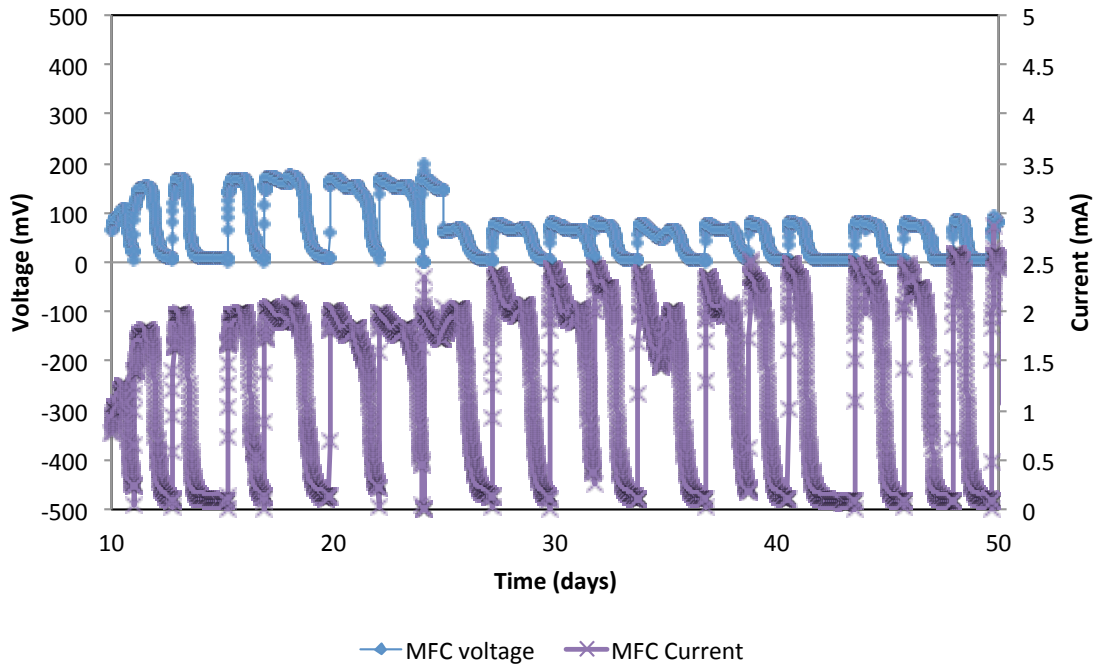


Figure A5 First derivative over the potential of the voltammetric curve of MVP-R (A) 60 days (stage I), (B), 90 days (30 days of stage II) and 114 days (54 days of stage II).

A



B

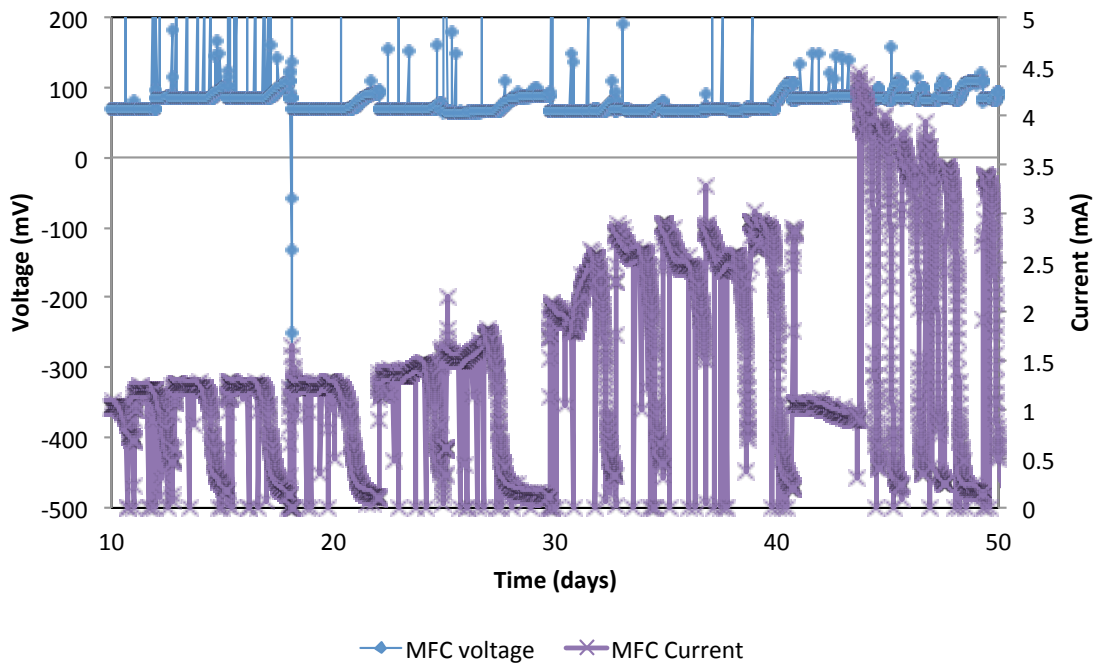
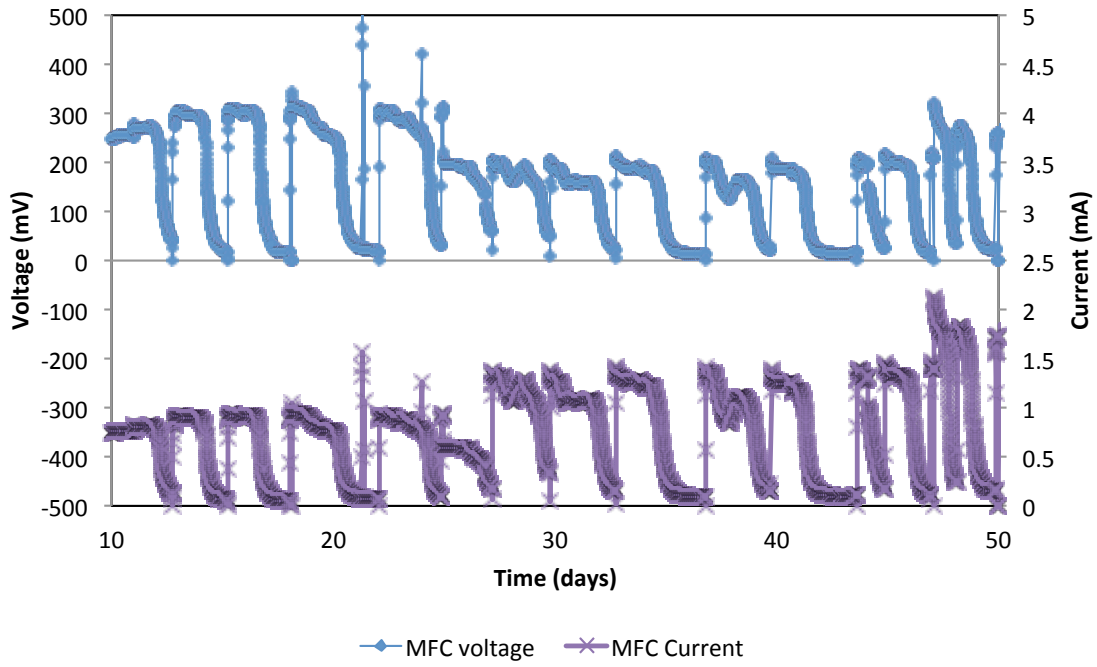


Figure A6 – Voltage and current profile on MFCs on scenarios CR (A) and CH (B).

A



B

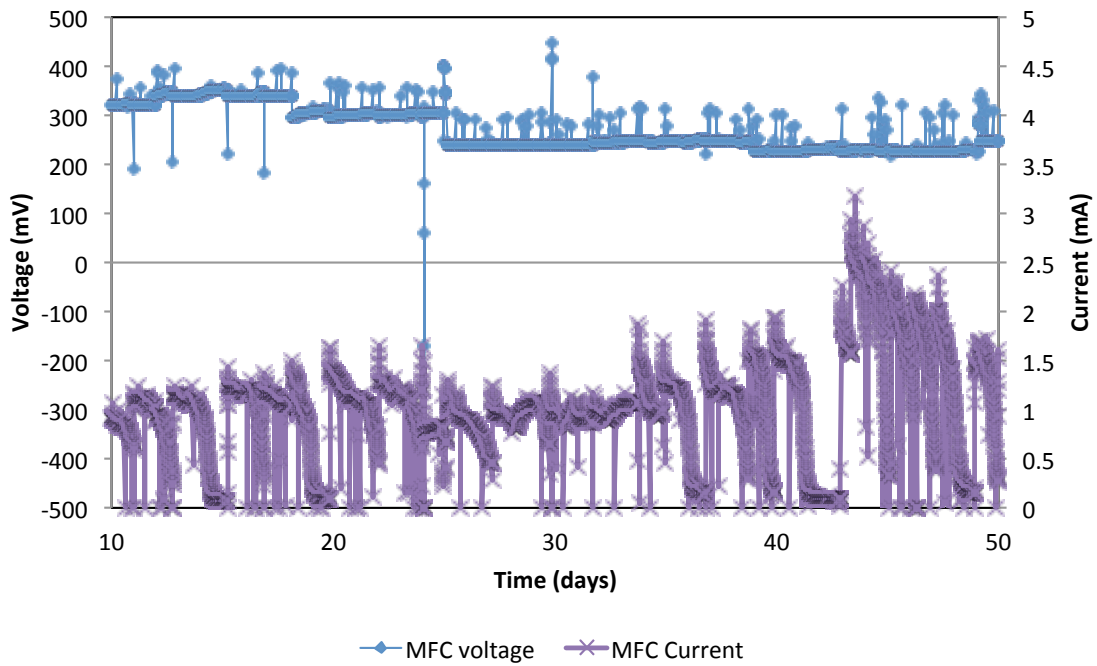


Figure A7 – Voltage and current profile on MFCs on scenarios PR (A) and PH (B).

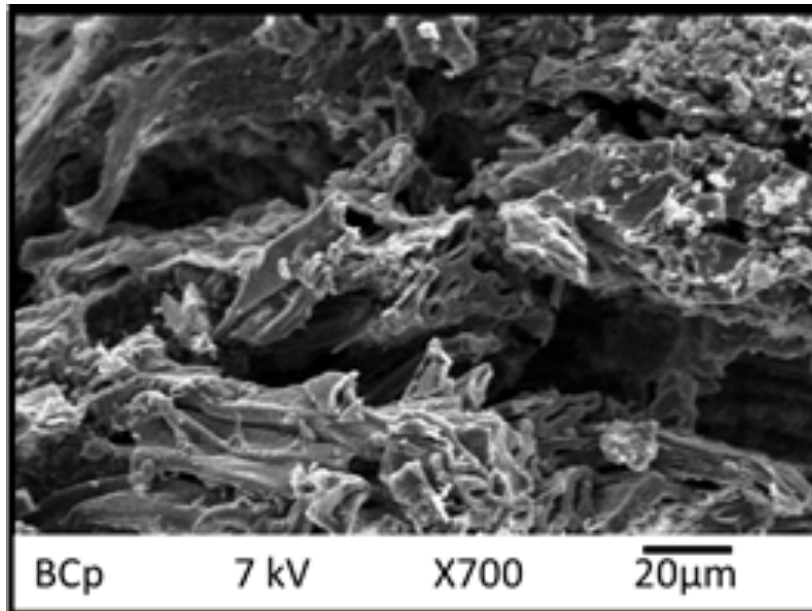


Figure A8 – Images of the biochar used in this study.